Monopile Installation Using a Motion-Compensated Gripper Frame on a DP Vessel

Thijs van Essen

TU Delft
NTNU
EWEM

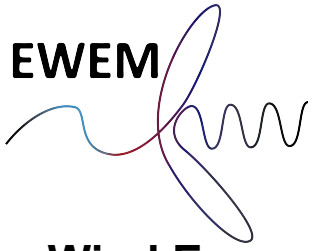

European Wind Energy Master

Offshore Engineering

Monopile Installation Using a Motion-Compensated Gripper Frame on a DP vessel

Master of Science Thesis
To be defended 7 October 2020

Thijs van Essen
October 5, 2020

To obtain the degree of

Norwegian University of Science and Technology

Department of Marine Technology
Master of Science
Technology - Wind Energy

Delft University of Technology

Faculty of 3mE
Master of Science
Offshore Engineering

Student number

517533

4371623

Supervisors

Prof. Dr. A. Metrikine
Prof. Dr. Z. Gao
Dr. J.M. Barbosa

Ir. I. van Winsen
Ir. J. ter Braak

An electronic version of this thesis is available at `http://repository.tudelft.nl/`

Preface

This MSc. thesis is the final step in finishing the Offshore Track of the European Wind Energy Master (EWEM). It serves as the last deliverable to obtain both a degree in Offshore Engineering from Delft University of Technology and a degree in Technology - Wind Energy from the Norwegian University of Science and Technology. This thesis has been written in collaboration with Heerema Engineering Solutions (HES).

Writing the final words of this thesis marks the end of an amazing two years as an EWEM student. I am grateful for the experience of studying at three different universities during these two years, the knowlegde I have gained, and for the opportunity to meet so many other students. I would like to thank my fellow EWEM students for making the past two years unforgettable.

Furthermore, I would like to thank Zhen Gao and João Barbosa for supervising me. Your comprehensive feedback during the writing of this thesis has been very helpful. Furthermore, I would like to thank my colleagues at HES for the great time at the company. I think it is an amazing team and you always made me feel very welcome. Special thanks to Ivan van Winsen and Jelle ter Braak for their supervision and guidance over the past nine months.

Finally, I would like to thank my friends, family and girlfriend for their support, as writing this thesis would have been much harder without it. I am also grateful for the wind, and the waves it generates, enabling me to refresh my mind once in a while.

Delft, September 2020

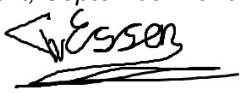

Thijs van Essen

Abstract

Offshore wind energy is one of the solutions to meet the growing demand for renewable energy. The offshore wind turbines producing this energy keep increasing in size and, as a result, the monopile foundations are becoming larger and heavier. The traditional jack-up installation vessels have limited crane capacity and many of these vessels are unable to install the XXL monopiles. Therefore, the offshore industry is currently investigating a new installation method using a motion-compensated gripper frame on floating vessel with a dynamic positioning system. The gripper frame is attached to the vessel and encloses the monopile with a ring to keep it vertical during the installation. In addition, the gripper frame compensates for the vessel motions such that the vessel motions do not influence the monopile motions.

The purpose of this thesis is to investigate the feasibility of such a motion-compensated gripper frame and to determine what control settings minimise the monopile inclination and the force exerted on the monopile. The system is composed of three main bodies: the vessel, the gripper frame and the monopile. The monopile and PID controller, which controls the amount of force exerted on the monopile to keep it vertical, have been modelled in the frequency domain to gain insight in the effect of changing the control parameters. To model the dynamics of the coupled system an OrcaFlex model has been set-up. The system has been tested for various values of proportional and derivative gain, k_P and k_D respectively, in various wave conditions. First the perfect control system is tested, where the force to keep the monopile vertical is applied instantly and the vessel motions are fully compensated. However, as the real world is never perfect, the system tested for sensor lag and imperfect motion compensation as well. The results are judged based on three criteria regarding the maximum monopile inclination, actuator force and actuator stroke.

Resonance is observed in case a value of k_P is selected such that the natural frequency of the monopile and controller matches the wave forcing frequency. Adding derivative gain k_D limits the monopile motions and force exerted in this case. To limit the monopile motion the proportional gain should be selected such that resonance is avoided. Two different control settings are investigated and it has been found that a relatively high value of k_P of 10,000 kN/m in combination with a k_D of 11,000 kNs/m is a suitable setting based on the three criteria. Furthermore, bow quartering waves is the favourable wave direction compared to head waves for the system considered in this thesis, as the force on the monopile is more evenly distributed over the actuator in x- and y-direction. Introducing a sensor lag into the system results in higher monopile motions and forces on the monopile. If the sensor lag exceeds 0.3 s it leads to instability of the monopile for both settings. The effect of not fully compensating the vessel motions is found to be limited due to the fact that these motions are slowly varying.

The results of this work contribute to a better understanding of the dynamics of the system in various wave conditions. Furthermore, it provides insight in the effect of sensor lag and imperfect motions compensation, contributing to the design of a motion-compensated gripper frame for the installation of XXL monopiles.

Contents

List of Figures

List of Tables

List of Abbreviations

2D	two-dimensional
API	application programming interface
CoG	centre of gravity
DOF	degree of freedom
DP	dynamic positioning
EoM	equation of motion
FFT	fast Fourier transform
GF	gripper frame
HES	Heerema Engineering Solutions
HLV	heavy lift vessel
HMC	Heerema Marine Contractors
HTV	heavy transport vessel
KC	Keulegan-Carpenter
MCGF	motion-compensated gripper frame
MP	monopile
PID	proportional–integral–derivative
TP	transition piece

1 Introduction

1.1. Problem Description

The ever increasing energy demand combined with the increasing awareness of the negative effects of fossil fuel such as high carbon dioxide emissions calls for action. A partial solution to this problem is the installation of cleaner, renewable forms of energy. As shown in Figure 1.1, wind energy is one of the fastest growing forms of renewable energy and even is today's second largest form of power generation capacity.

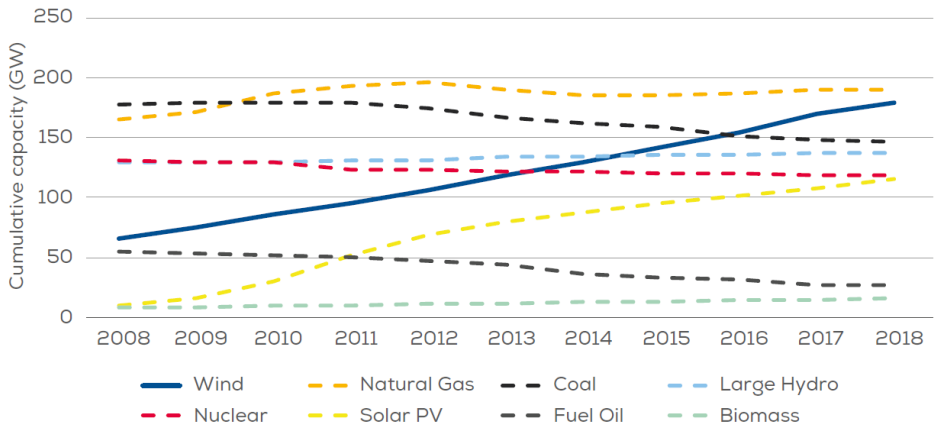

Figure 1.1: An overview of the power generation capacity in the European Union from 2008 to 2018 [17].

With this increase in the amount of wind farms the rated power and, as a result, the size of the wind turbines are increasing as well. This trend of increasing wind turbine sizes is depicted in Figure 1.2. Larger turbines have a higher hub height and, therefore, experience steadier winds. Furthermore, a larger rotor diameter means a larger area to extract energy from. As a result the capacity factor, a measure of how much energy is produced compared to how much energy could have been produced if the wind turbine was always operating at maximum power, is increasing with turbine size [6].

Depending on the water depth and type of soil a certain foundation is selected. With 74.5% of all installed foundations of 2018 being a monopile, it remains the most popular foundation for offshore wind turbines [14]. This popularity is due to the fact that a monopile is relatively easy to manufacture, transport, and has lower maintenance costs [9]. Moreover, it is suited for shallow water depths, with preliminary designs ranging to 50 m water depth, making it ideal for the relatively shallow North Sea [14].

With the size of the turbines increasing, the diameter of the monopiles is increasing as well to compen-

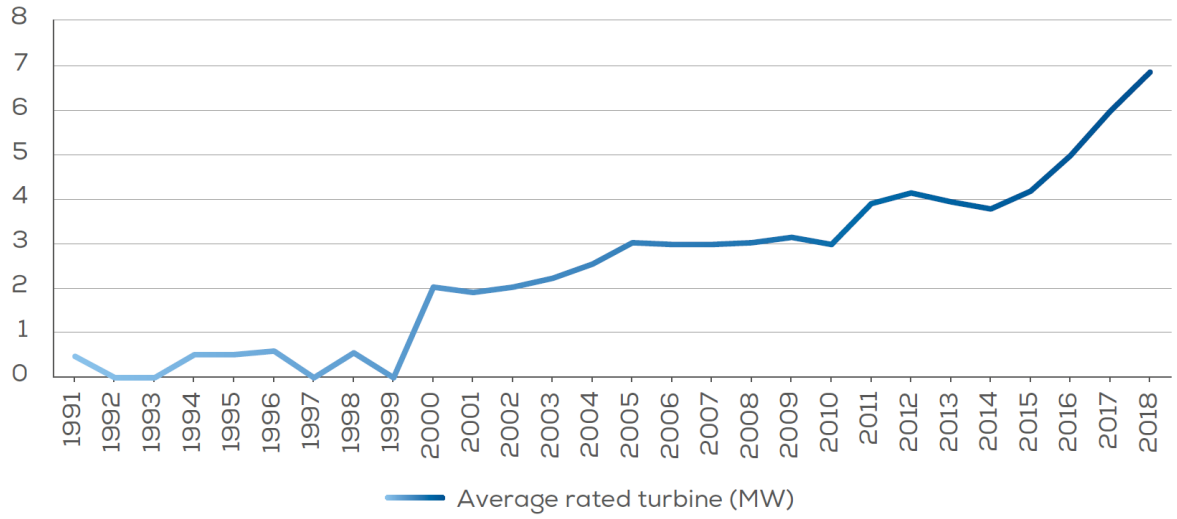

Figure 1.2: The average rated power output of the wind turbines installed in that specific year. There is a steady increase in the installed capacity, reaching 6.8 MW in 2018 [14].

sate for the increasing thrust loads acting on the pile, as indicated in Table 1.1. As a result the lifting operations become more complex and require larger crane capacity, limiting the amount of suitable vessels.

Wind Turbine Particulars					
		2015	2017	2020	
Turbine capacity	P_E	4	8	12	MW
Rotor diameter	D_R	130	165	200	m
Water depth	WD	32	40	50	m
Monopile dimensions					
Length	L_P	65	80	90	m
Diameter	D_P	7	8	10	m
Weight	W_P	800	1300	2200	ton

Table 1.1: With the increasing size of the wind turbines its foundations are increasing in size and weight [4].

Currently, the conventional installation method of offshore wind turbine foundations is using jack-up barges. A jack-up is a vessel which sails to its destination where it then extends its legs all the way to the seabed, lifting itself above the water level. An example of a jack-up vessel is depicted in Figure 1.3. Due to relatively small wave loads on the legs a jack-up provides a stable working platform and is therefore often used for monopile installations. The monopile is held vertical in a gripper frame and can be lowered to the seabed; the gripper frame is also depicted in Figure 1.3. After the monopile has reached the seabed, it is hammered to the required penetration depth. A more detailed overview of these steps is given in section 2.1. The major disadvantage of this type of installation vessel is that jacking up the vessel takes a significant amount of the total installation time, as this process may take up several hours. Another drawback of using a jack-up is the limited allowable sea state for a safe transfer from floating vessel to lifting itself outside the water, which is generally up to significant wave heights of 1.5 m [28]. This low transfer sea state limits the operational window of the installation. Moreover, the crane capacity of the current jack-up vessel is limited and hardly any jack-up vessel is able to install XL monopiles that weigh over 1000 tonnes.

Another method of monopile installation is the use of floating vessels. Floating vessel are considerably more sensitive to wave loads compared to the jack-up and, as a result, the waves induce significant

[1] `https://twd-uk.com/solutions/pile-handling-tools/` [Last Accessed: 21-11-2019]

Figure 1.3: A jack-up vessel upending a monopile. Note the gripper frame at the side of the vessel.[1]

motions of the vessel. To successfully install the monopile the vessel has to remain at the same position and keep the correct heading over the entire course of the installation. One solution to keep a vessel at its intended position during the installation is using a mooring system. A mooring system anchors the ship to the seabed using multiple mooring lines. Like the jack-up vessel the main drawback of using a moored floating vessel is the time required to moor the vessel, as this takes up a significant portion of the installation time. Reference [1] estimates it takes up to 8 hours to moor a Heavy Lift Vessel (HLV) to the seabed. Furthermore, in Figure 1.4 it is shown that 42% of the installation time of the monopile and the transition piece is used to install the mooring lines [23].

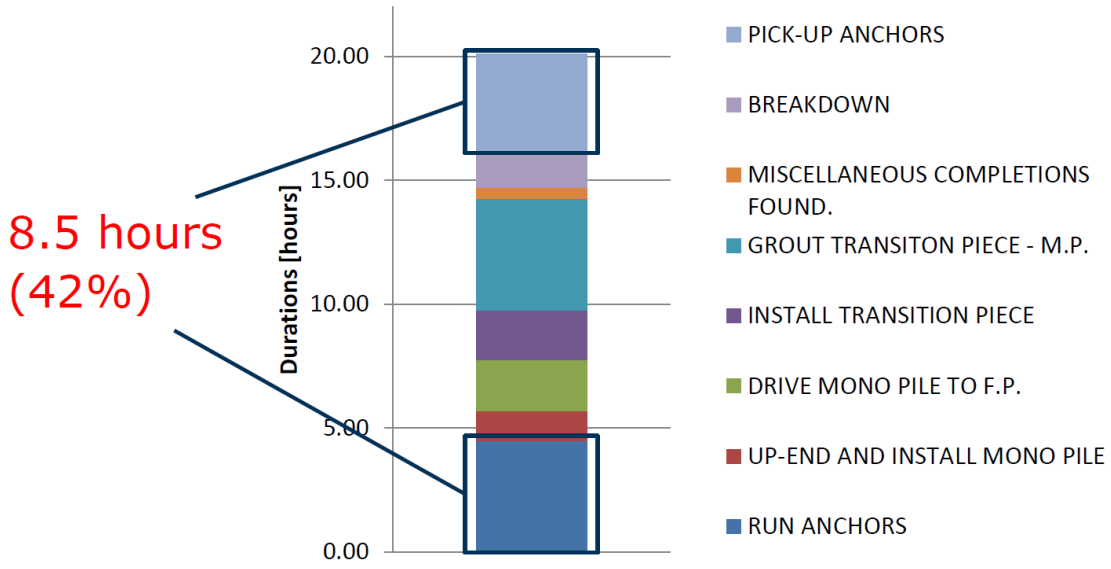

Figure 1.4: Mooring an installation vessel takes up over 40% of the total installation time. Therefore, installing monopiles using a dynamic positioning vessel can significantly decrease the required installation time. [23]

Both the jack-up and the moored floating vessel have proven track records, however, in both cases the preparation of the positioning of the vessel requires a substantial amount of the installation time. Therefore, the offshore industry is investigating other, faster methods of installation. One of the possible solutions to this problem is using a floating vessel equipped with dynamic positioning (DP). A dynamic positioning system automatically keeps the vessel at a predefined position using its thrusters; this is described in more detail in section 2.4. The installation time can be substantially reduced as there is no time required for the mooring or jacking-up of the vessel and once the DP system is engaged, the installation can start right away. However, once the monopile has been lowered to the seabed and penetrates the seabed, the coupling between the vessel and the monopile complicates the use of the DP system.

During the lowering and installation of the monopile, it has to be held stationary in a vertical position by the vessel and, to keep the monopile within the installation tolerances, any undesired inclination of the monopile has to be corrected for. A motion compensating gripper frame holding the monopile is a promising solution, as it can reduce the loads transferred from the vessel to the monopile and vice versa by compensating for the vessel motions. In addition, the gripper frame combined with the use of the thrusters of the vessel can exert a force on the monopile to correct an inclination if necessary. In order to determine the technical feasibility of designing a gripper frame a fundamental model of the dynamic behaviour of the installation configuration is required. The installation configuration is comprised of a coupled system including the vessel, gripper frame and monopile.

1.2. Thesis Scope and Outline

This thesis focuses on the feasibility of a motion-compensated gripper frame for the installation of monopiles using a DP floating vessel. The research question is:

What values of the gripper frame parameters - e.g. control setting: k_P, k_I and k_D – minimise the pile inclination and the GF force exerted on the monopile and are these parameters feasible in practice?

Furthermore, the following sub-question has been defined:

How sensitive is the system to system and sensor inaccuracies such as a delay in the controller or imperfect motion compensation?

Chapter 2 outlines the most important steps of the monopile installation and presents the theoretical background of this work. The set-up of the model is described in chapter 3. This chapter also presents calculations of the motion of the monopile in the frequency domain for various values of proportional and derivative gain. Furthermore, some basic tests are described to determine if the model behaves as expected. Chapter 4 presents the results of the simulations carried out. In chapter 5 the research question and sub-question are answered and recommendations for future work are presented.

2

Theoretical Background

This chapter describes the different steps of a monopile installation. This is a general approach which is very similar for different installation vessels. Furthermore, this chapter provides insight in the systems required for the installation of a monopile such as the dynamic positioning system and the gripper frames. Wave loads and wave theory are discussed as well.

2.1. Overview of monopile installation steps

This section gives an overview of the different steps and challenges that come into play when installing an offshore monopile foundation. A flow diagram of the different installation steps is given in Figure 2.1. The installation of the transition piece is shortly mentioned, but not the primary focus of this study.

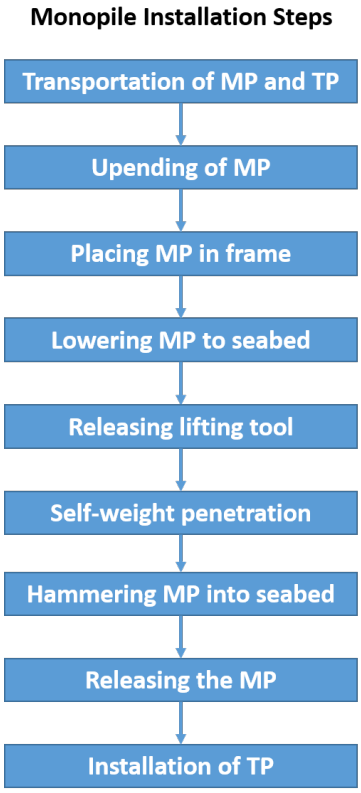

Figure 2.1: An overview of the steps of the installation of a monopile (MP) and transition piece (TP).

1. **Transportation of the monopile and transition piece**:
   The monopile has to be transported from the fabrication site to the location of the offshore wind farm. There are several methods of transportation depending on the installation strategy. There are many types of transportation vessels available. Some (heavy lift) vessels can transport the monopiles on deck and can install the monopiles without another vessel supplying the vessel. Another option is to transport the monopiles on barges or heavy transport vessels (HTVs) which bring the monopiles to the installation vessel, as shown in Figure 2.2. This does require an additional installation vessel to install the monopiles as the HTV is unable to perform this part of the operation itself. The latter strategy usually applies to smaller installation vessels due to the limited deck loads and lower capacity cranes [22].

Figure 2.2: A transportation vessel transporting the monopiles to the wind farm location. Some HLVs can carry the monopiles on deck. Other means of transportation are using barges or wet-towing the monopiles.[0]

The choice of installation vessel depends on the size and weight of the monopiles, the deck load and crane capacity, and the distance to shore from the installation site. In addition, the environmental conditions should be taken into account as rough sea states limit the amount of suitable vessels [22].

Another means of transportation is letting the monopiles float by sealing off the ends of the monopile using end-caps and tow it to the desired location using tugboats [16]. At the wind farm location the monopile is flooded again and upended using a crane. The advantage of the floating transportation is that the upending of the monopile can be performed by a crane with a capacity slightly smaller than the self-weight of the monopile, as the buoyancy force on the monopile decreases the weight hanging from the crane [28]. However, a tugboat can usually tow far fewer monopiles compared to the amount a HTV or a barge can carry. Furthermore, the upending of the monopiles in water is more sensitive to rougher sea states.

The transition piece is often manufactured at a different location than the monopile. Therefore, it is usually transported by another vessel than the installation vessel and/or the vessel carrying the monopiles. However, depending on the logistics and the vessel it is possible to carry both the monopile and transition pieces on the same vessel.

[0] http://www.esru.strath.ac.uk/EandE/Web_sites/14-15/XL_Monopiles/technical.html#transport [Last Accessed: 02-08-2020]

2. **Upending of the monopile**:
   Once the monopile has been transported to the offshore wind farm site, the monopile is upended. This step of the installation usually defines the required crane capacity [22], as there is no buoyant forces yet when the monopile is suspended in the air. Upending is not required in case the monopiles are transported vertically, however, this is usually not the case. The upending is performed by hooking the monopile onto the crane and slowly lifting it with one or two cranes until it is perpendicular to the seabed. The monopile can be lifted by hooking the monopile onto the crane using pre-installed lifting anchors on the monopile. Alternatively, there are lifting tools that hold the monopile by clamping it at the top, one of these upending tools is displayed in Figure 2.3.

   The critical parts of this operation are the maximum lifting wire force, which may not be exceeded to guarantee a safe operation. Furthermore, the motions of the monopile should be limited as there is a slamming hazard which may cause damage to the ship, the monopile itself or jeopardise the safety of the personnel. Furthermore, if there is any support from a gripper frame during the upending, like the one shown in Figure 2.3, the maximum contact force between the MP and the tool may not be exceeded.

Figure 2.3: An example of an upending tool with a capacity of 1,400 tonnes that clamps the monopile at the top.[1]

3. **Placing the monopile in a frame to keep it upright**:
   There are multiple methods to keep the monopile stationary during the lowering of the monopile to the seabed. First of all, a jack-up vessel usually has a gripper frame at one of the sides of the vessel. Once the monopile has been upended, it is placed in the frame to keep the monopile from falling over under the influence of wave and wind forces. A floating vessel can be equipped with a similar frame. However, the increased vessel motions of the HLV complicate holding the monopile steady compared to the jack-up vessel. The type of coupling between the monopile and gripper frame is of major importance for the dynamics between the vessel and the monopile, as it determines how the motions of the vessel are transferred to the monopile and vice versa.

   Another option currently researched in industry is using a subsea template, where a frame is placed on the seabed and the monopile is lowered into the frame. The frame supports the monopile and avoids it falls over. In addition, the frame is able to correct the inclination of the monopile. The gripper frame and the subsea template are described in more detail in section 2.2.

[1] https://www.ihciqip.com/en/news/ihc-iqip-delivers-new-1400t-upending-tool-to-seaway-heavy-lifting [Last Accessed: 05-12-2019]

Critical parts of this installation are the envelope of the gripper frame combined with the motions of the monopile, as the reach of the gripper frame should be far enough. Furthermore, the contact force between the monopile with the gripper frame or the subsea template has to be within the maximum.

4. **Lowering the monopile to the seabed**:
   Once the monopile has been placed into the gripper frame, the monopile can be lowered to the seabed. For the subsea template case the lowering would have happened earlier, as the monopile needs to be lowered towards the seabed to reach the subsea template. During the lowering process wave loads are introduced onto the monopile and the constantly changing draft of the monopile leads to varying properties of the dynamic system. The length of the lift wire changes, which affects the total restoring stiffness of the monopile. Furthermore, the added mass of the monopile and wave loads on the monopile increase with the increase of the submerged length. All of these effects influence the natural period of the vessel and monopile system [21].

5. **Self-weight penetration of the monopile**:
   After the monopile has reached the seabed, it sinks down into the soil due to its own weight. Generally the self-weight penetration depth is equal to half of the diameter of the pile [34]. However, this is strongly dependent on the type of soil.

6. **Releasing lifting tool**:
   When the monopile has been lowered to the seabed the lifting tool is disconnected from the monopile and put back onto the deck of the vessel. The monopile is no longer connected to the crane and only connected to the vessel through the gripper frame. As the monopile has hardly penetrate the soil it is standing onto the seabed like a hinged inverted pendulum. The movement of the monopile due to environmental loading should be limited by the gripper frame or the subsea template such that it does not fall over.

7. **Installing hammer**:
   When the lifting tool has been placed back onto the deck and released from the crane, the hammer should be connected to the crane. The hammer is then place on top of the monopile. During this step the monopile motions should be limited by the gripper frame or template, as the hammer cannot be connected to the monopile in case of large motions.

8. **Hammering the monopile into the seabed**:
   Once the hammer has been connected the weight of the hammer slightly increases the self-weight penetration depth. There are two different methods of hammering: impact hammering vs. vibro-hammering. The main difference is that during impact hammering a weight is dropped on top of the monopile and the monopile is hammered in, whereas with vibro-hammering the pile is driven into the soil by generating vibrations in the soil particles resulting in a decrease of the soil resistance. Impact hammering is based on dropping a relatively high load with a low frequency, vibro-hammering is based on a relatively low and steady load at a high frequency. An example of an impact hammering connected to the top of the monopile is given in Figure 2.4.

   The hammering process has been accurately described in [1] and is summarised in this section. First of all, there is generally an initial inclination of the monopile which has to be corrected for, as this inclination angle would become worse as the penetration depth increases. The inclination angle has to remain below a certain tolerance value to have a successful installation. These tolerances of the inclination angle are becoming even smaller as the size of the turbines and its foundations increases and the maximum allowable values for the inclination angles can even be as small as 0.25° [7]. The inclination angle can be measured using a handheld inclinometer or using high resolution cameras [24]. Adequately monitoring the inclination angle of the monopile for such small tolerance values remains challenging still today. The inclination angle can be corrected for using the gripper frame and the thrusters/mooring of the vessel, which can apply a force in the direction opposing the inclination.

   Once the inclination angle has been corrected for, the monopile is hammered/vibrated into the seabed.The penetration rate of the monopile during hammering depends on the soil type and

[2] http://www.offshorewindenergy.org/EUROS/projects/p2/wp2/

Figure 2.4: An example of an monopile and hydraulic hammer at the top. The monopiles are hit with the hammer and driven into the seabed. [2]

the diameter of the monopile. Larger diameter monopiles have greater soil resistance leading to smaller penetration depths per hammering sequence. Due to an increasing soil resistance the penetration rate decreases for an increasing penetration depth. For many hammering processes with an impact hammer, there is a time interval between every few blows of the hammer during which the movement of the vessel and monopile can create a new inclination angle. If this is the case the monopile inclination angle has to be corrected for again after each hammering sequence. The effect of the ship motions on a new inclination angle could be less if the gripper frame is able to compensate for the vessel motions. This process of correcting the inclination angle and hammering is repeated until the desired penetration depth is reached, which depends on the diameter of the monopile, the soil type and the loads on the turbine. Note that it requires more and more force to correct for the inclination angle of the monopile at greater penetration depths due to the larger soil resistance. Once the monopile has reached the desired penetration depth, the hammer is released and placed back on the deck.

Critical parameters during the hammering phase are the maximum hammering force that the hammer can deliver and that the monopile can withstand. The hammering force should always be larger than the soil resistance before the minimum penetration depth is reached. Furthermore, the maximum force between the gripper frame and the monopile should be higher than the required correction force before the minimum penetration depth is reached. Moreover, the thruster force of the vessel should be large enough to provide the required correction force in case of a monopile installation vessel using DP for station-keeping. Another critical parameter is the inclination angle of the monopile.

9. **Releasing the gripper frame**:
   It has not been established in current literature and industry practise at what stage the gripper frame should be released, when using a motion compensating gripper frame. Reference [1] suggests two critical penetrations depths for the installation of a monopile with a gripper frame and a moored floating vessel:

- $d_{crit,1}$ is the depth at which the monopile has penetrated the seabed to such an extent that it can stand alone without support of the vessel. This means the bearing capacity is large enough to withstand the external loads at the time of installation.
- $d_{crit,2}$ is the depth at which the (hydraulic) cylinders of the gripper frame and/or the thruster/mooring forces are not able to provide enough force to correct for the inclination of the monopile.

It is paramount that the first critical depth $d_{crit,1}$ is reached before $d_{crit,2}$ for a safe and successful hammering operation. In other words, the gripper frame should be able to support the monopile until it can stand alone in the soil and before it is retracted [1]. At which depth $d_{crit,1}$ is reached and the extreme forces acting on the frame should be planned in advance to guarantee the gripper frame is able to correct the inclinations until the first critical depth is reached. Note that this critical depth depends on the sea state.

Analysis performed by Reference [1] suggests that the force exerted on the hydraulic cylinder increases as the penetration depth of the monopile increases. For this case it is assumed that the gripper frame is used in combination with the mooring lines to correct for the inclination of the monopile. Due to this increase in required correction force it is suggested that the monopile is released by the gripper frame as soon as the monopile can stand alone in the soil in the installation sea state, which is defined as $d_{crit,1}$.

If the gripper frame is able to correct for the vessel motions, the inclination angle is likely to be less compared to the installation with a non-compensating gripper frame used in the analysis above. However, the approach mentioned above still applies.

10. **Install the transition piece**:
The transition piece is a tubular steel part that connects the monopile foundation and the tower of the turbine. Figure 2.5 shows a transition piece that together with the monopile forms the foundation of the wind turbine. It has various purposes such as access to the wind turbine (for maintenance) and corrosion protection for the foundation and tower [9]. Moreover, the transition piece can correct for a slight undesired inclination of monopile to ensure tower supporting the turbine is straight. All secondary steel such as boat landings and ladders can already be installed on the mainland, speeding up the offshore installation of the turbine. Depending on the installation plan the transition pieces are installed immediately after the installation of the monopile by the same vessel or installed at a later stage. The transition piece is commonly connected through a grouted connection. However, there is ongoing research [29] into the possibility of using a slip joint as a connection between the monopile and tower of the turbine is. The slip joint is a friction-based connection achieved by matching the conical shape of the monopile with the conical shape of the tower of the turbine. The tower is slid onto the monopile without using any bolted or grouted connections.

2.2. Keeping monopile upright

Once the monopile has been upended it has to be stabilised in order to keep it from falling over due to the environmental loads. Two examples of solutions to keep the monopile vertical investigated by offshore companies are a subsea monopile installation template and a gripper frame attached to the installation vessel. Both the solutions are described in this section.

Subsea Template

The monopile installation template is a steel frame that is installed at the seabed prior to the installation of the monopile. During the lowering of the monopile to the seabed it is placed in the template. It is then clamped by the frame at the seabed. Subsea templates have proven to be successful in the pre-piling of jacket foundation. Reference [28] proposes a new method of monopile installation using a subsea structure. The proposed structure is shown in Figure 2.6 and is composed of a structure with a gripper that laterally supports the monopile.The gripper is able to correct for any undesired inclination of the monopile by using a rack and pinion system. The advantage of this structure is that the vessel motions hardly influence the motions of the monopile compared to an installation with a gripper frame attached

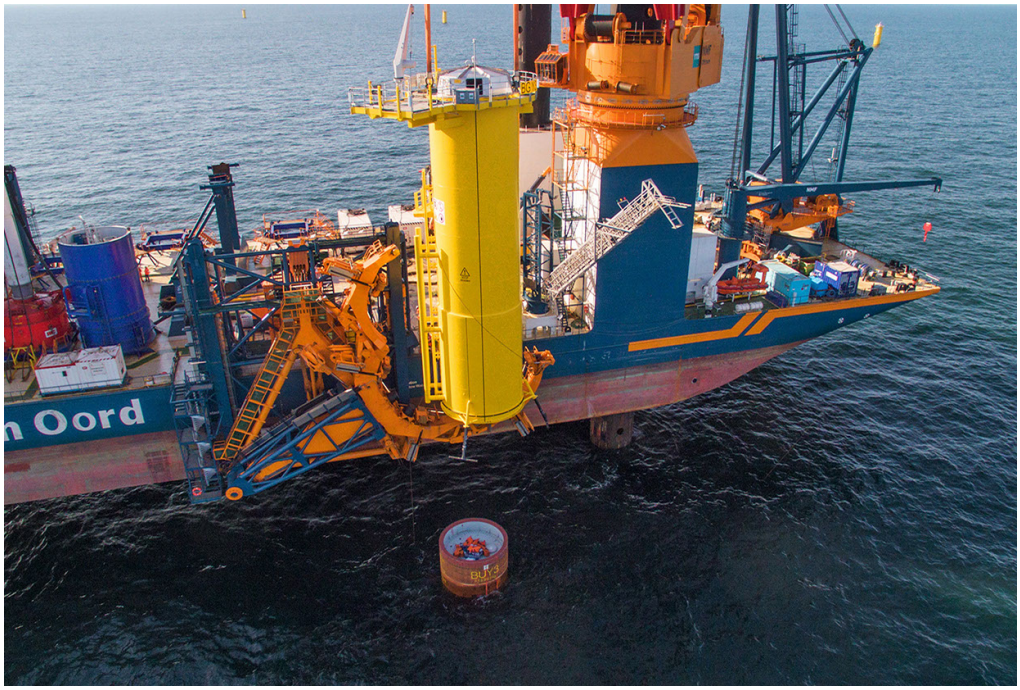

Figure 2.5: A transition piece being installed onto the monopile. [9]

to the vessel (unless the gripper frame is able to fully compensate for any vessel motions). However, currently there are no reports of an installation of a XL monopile using subsea templates that have been successfully carried out.

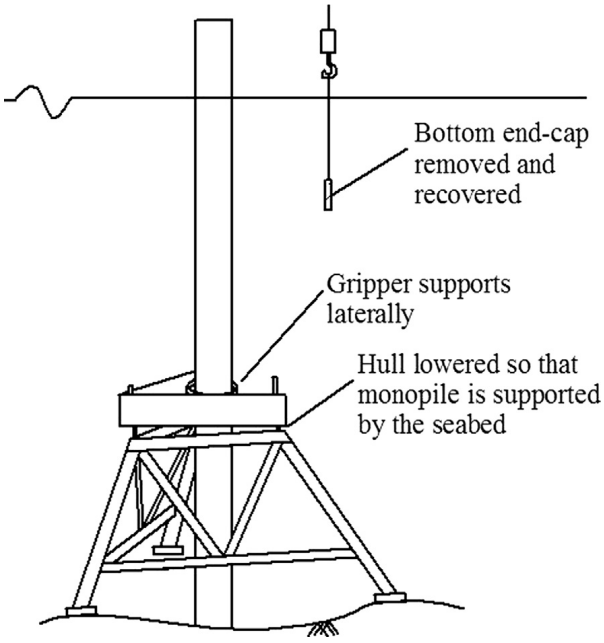

Figure 2.6: A concept of a monopile installation subsea template [28].

Gripper Frame

Next to the subsea template there is the gripper frame solution to keep the monopile stable during the monopile installation. The gripper frame not only keeps the monopile upright, it can also correct undesired inclinations of the monopile to ensure the monopile angle is within the installation tolerances.

Figure 2.7 shows an example of a gripper frame. This gripper frame is also shown in Figure 1.3 installed at the side of the jack-up vessel Aeolus. The gripper frame is composed of a ring-shaped steel frame with a hydraulic system holding the monopile during the lowering and hammering phase of the installation. Depending on the design there is a number of hydraulic cylinders exerting force on the monopile to keep it clamped in the gripper frame [24]. The gripper frame in Figure 2.7 has four hydraulic cylinders. When the monopile has the tendency to fall over or move due the wave forcing, the gripper frame can limit and/or correct this movement by exerting a force on the monopile. As described in [24] the gripper frame uses a hydraulic system which includes actuators, an electric motor, pump, control system and a support structure. When the gripper frame is installed on a jack-up it is usually a passive system which does not compensate for any vessel motions. However, for the use of a gripper frame on a floating vessel it is desirable to compensate the motions of the vessel with the gripper frame. This is a much more complicated process and requires an active control system. The gripper frame shown in Figure 2.8 has active motion compensation and the ring holding the monopile can move with respect to the vessel. The motion of the ring is actively controlled and moved by the actuators shown in the picture.

Figure 2.7: An example of a gripper frame holding the monopile upright during the hammering phase of the monopile installation [33]. This gripper frame has been used on van Oord's jack-up vessel Aeolus.

One of the limiting parameters during the monopile installation is the maximum force in the hydraulic cylinder(s) of the gripper frame. Research suggests that the contact force increases as the penetration depth of the monopile increases and the peak period of the waves increases [19]. Therefore, the design of the gripper frame actuators strongly influences the operational weather window of the monopile installation. Moreover, the stiffness of the gripper frame is an important parameter in the design of the gripper frame as well. Research suggests that the relative motion and contact force between the monopile and the vessel are sensitive to the gripper frame stiffness during the lowering process. A higher stiffness of the gripper frame results in a better control of the horizontal motions of the monopile. On the other hand, a higher stiffness results in higher contact forces which might damage the structure [20]. Furthermore, a higher contact force requires a more robust design and increasing the costs of the gripper frame.

The motions of the vessel are transferred onto the monopile through the gripper frame, if it does not perfectly compensate for the vessel motions. The hydraulic system of the gripper frame must be able to cope with the induced loads or the gripper frame should have a motion compensation system which compensates for the motion of the vessel which decouples the vessel motions from the gripper frame.

In addition, it is important to incorporate failure of the station-keeping systems, such as breakage of mooring lines or failure of the DP system, into the design. Failure of these components or an sudden increase in environmental conditions may lead to an increase in contact forces. It is important to establish the magnitude of these loads for this scenario and to have a safe solution in case of an emergency scenario. Reference [24] proposes the use of a control barrier like a pressure relief valve or pressure switch on the supply of the hydraulic cylinder to protect it from forces exceeding the structural limit. Another option is using structural elements in the support structure to protect the hydraulic actuators.

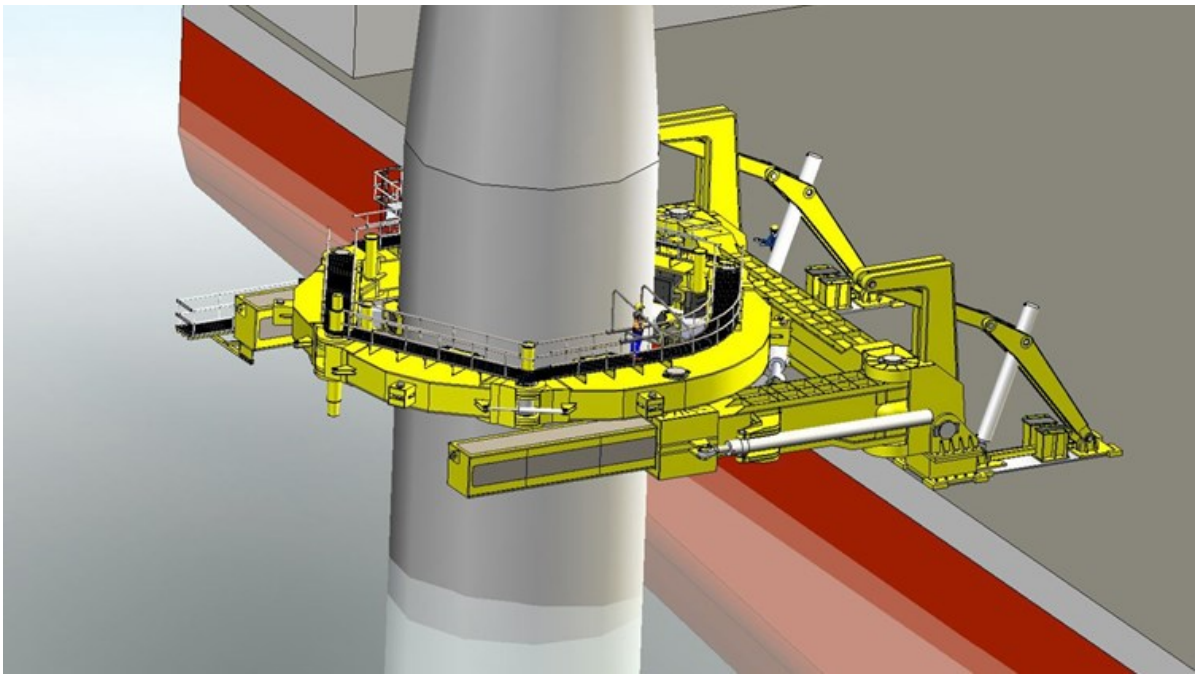

Figure 2.8: An example of an actively controlled gripper frame holding the monopile upright during the hammering phase of the monopile installation. [3]

2.3. Existing Motion Compensation Systems

Currently there are several motion compensating systems used in the offshore industry to increase the operational window of the vessels or to increase the safety of the operation. A well-known example of a motion compensating platform is the system designed by Ampelmann shown in Figure 2.9, which is able to compensate the vessel motions in all the 6 DOFs. Due to its motion compensating ability the platform is providing a stable gangway for the transfer of personnel from the moving vessel to the (stationary) offshore structure. Comparable to the motion compensating gripper frame, the motions of the vessel are measured and based on these measurements the hydraulic cylinders at the base of the platform are adjusted in length. Due to slight inaccuracies and delays there is always some residual motion in reality [13]. Using the same principle the Ampelmann created systems that keep loads of up to 65 tonnes stationary on a platform. Current gangway systems, similar to the one shown in Figure 2.9, are able to compensate motions of the vessel in waves with a significant wave height H_s of up to 4.5 m and can transfer cargo loads up to 5 tonnes with a crane [3], significantly increasing the operational window.

[3] https://www.macgregor.com/news-insights/news-articles/2018/combined-expertise-cuts-wind-turbine-installation-t
Accessed: 13-12-2019]

Figure 2.9: An example of a motion compensating platform 'The Ampelmann' used to safely transfer personnel from a vessel to an offshore structure. The platform is able to compensate for all 6 degrees of freedom of the vessel, meaning the platform does not move during transfer [3].

Another example of existing motion compensating systems is the heave compensating crane, schematically represented in Figure 2.10 [27]. The heave motion of the vessel induces a motion of the cargo hanging from the crane, resulting in high loads in the lifting wire and potential slamming hazard when the cargo is close to an object. The heave motion of the vessel can be compensated for by actively adjusting the length of the lift wire with a cylinder. The controller input is the data of the sensor measuring the motion of the ship and the current position of the hydraulic cylinder. Based on the input the lift wire is adjusted to keep the cargo stable. The lift wire runs over a pulley which is supported by the cylinder as depicted in Figure 2.10. Suppose the crane tip moves 1 m upwards due heave motion of the vessel, the cylinder moves 0.5 m downwards to lower the load by 1 m. This yields a total displacement of 0 m of the cargo and the heave motion has been compensated for.

Furthermore, there are several passive compensation systems that combine cylinder and gas systems to create a system that acts like a spring of which the pre-tension and stiffness can be adjusted [2]. However, this is outside the scope of this work.

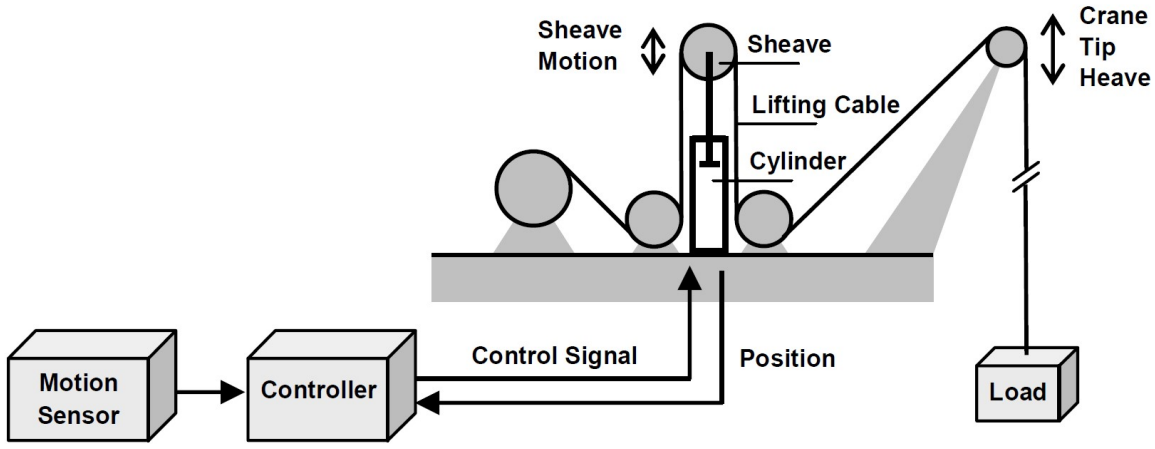

Figure 2.10: Schematic overview of a heave compensating crane based on the adjustment of the length of the lift wire [27].

All of the systems mentioned above use hydraulic cylinders to compensate for the vessel motion, which is similar to a motion compensating gripper frame. However, it should be noted that the masses in the

systems above are relatively low compared to the mass of the monopile, which can easily be larger than 1000 tonnes for a XL monopile.lid for the Ampelmann system. Besides, the gripper frame is attached at the side of the vessel and the large mass influences the roll motion of the vessel. Furthermore, the hydrodynamic loads on the monopile are significant for large diameters and are not comparable to the wind forces acting on the cargo hanging from a crane.

2.4. Dynamic Positioning (DP)

A dynamic positioning (DP) system is a system that automatically keeps the vessel at the intended position and it is widely used in the offshore industry for numerous applications such as installation vessels, HLV, cable and pipe laying vessels and FPSO's [34]. Next to keeping the vessel at a certain position, the DP system can be used to keep a vessel on a certain track or follow another moving object as well. In addition, DP may be used for weathervaning, meaning adjusting the heading of the ship to minimise the environmental loading on the ship.

Figure 2.11 depicts an overview of the working of a DP system. Multiple sensors like wind sensors, gyro's and motion sensors combined with position reference sensors obtain information about the positioning of the vessel and the environmental forces acting on the vessel [32]. Using the (hydrodynamic) vessel model the response of the vessel due to the environmental forcing is estimated. An extensive control system measures the position error based on the data of the sensors and the vessel model and adjusts the thruster force and direction accordingly.

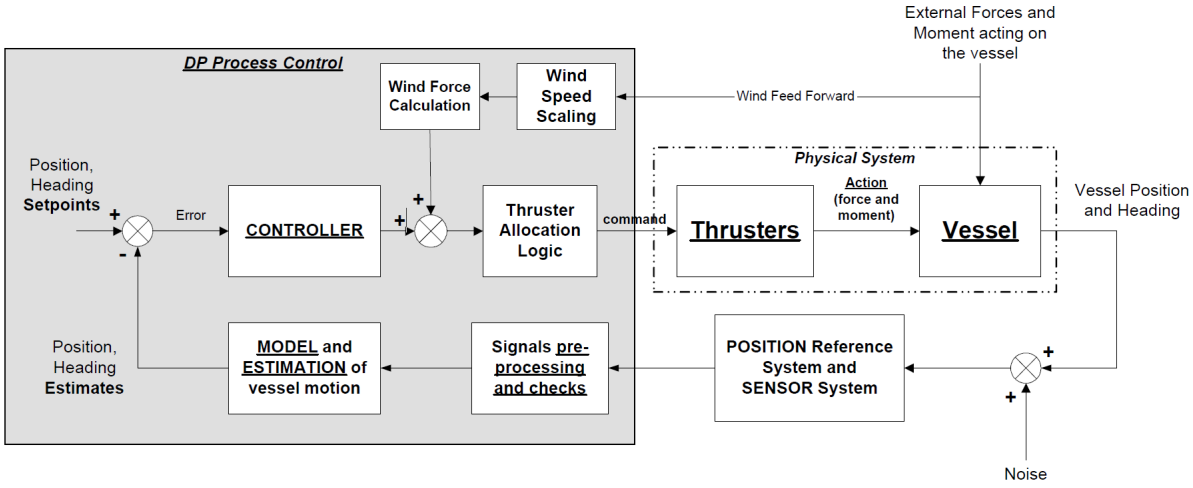

Figure 2.11: An overview of the working of a dynamic positioning (DP) system [5].

The DP system is not able to counteract the higher frequency environmental forces such as the first-order wave motions because the thrusters cannot react quick enough to these forces. Furthermore, these forces have a zero mean and introduce relatively little drift to the system. These first-order wave motions are filtered from the signal by a filter, usually a Kalman filter. The low frequency environmental forces of currents, wind and second-order wave forcing on the other hand can be corrected for by the DP system. For the proper working of a DP system the hydrodynamic model of the vessel should be as detailed as possible. The model can be tuned by verifying the model parameters during sea trials [5]. However, it is virtually impossible to capture all dynamics of the vessel and, as a result, the DP system is never perfect. Therefore, the DP system always has a certain footprint.

The smaller the footprint of the DP system, the higher the DP capability, which is defined as the station-keeping ability of the vessel under certain environmental loads. This can be expressed in a DP capability plot, an example of which is shown in Figure 2.12. This plot is created by assessing all the external loads such as wind, waves and current for every angle of attack, assuming the forces are all acting in the same direction. Figure 2.12 shows the maximum wind speed for which the DP system can keep the vessel stationary for every wind direction. Note that the plot is usually symmetrical due to the symmetry

of the vessel. As shown in this figure the wind speed can be substantially higher when it is blowing parallel to the heading of the vessel (0° or 180°) compared to a wind direction ranging from 30° - 150 ° or 210° - 330 °. This difference in wind speed is a result of the surface area of the vessel exposed to the wind for both directions, as the frontal area is much smaller than the area of the side of the vessel.

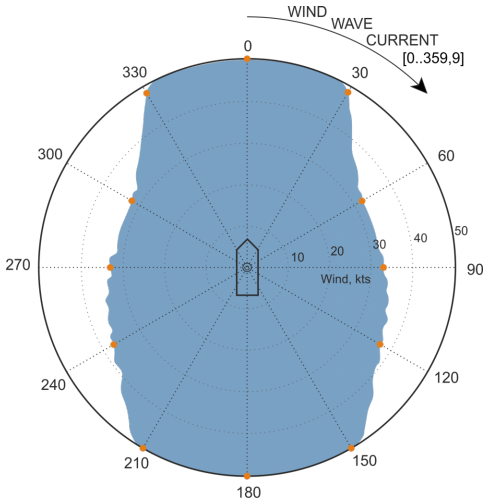

Figure 2.12: An example of a DP capability plot. The blue shading indicates the limiting wind speed from a certain direction during which the DP system can still ensure station-keeping of the vessel. [4]

2.5. Environmental Conditions and Loads

The dynamic behaviour of the vessel and monopile configuration is strongly dependent on the loads imposed on both objects. The three main environmental loads acting on the vessel and monopile are wind, waves and current loads, as shown in Figure 2.13. In order to adequately model these loads the environmental conditions at a certain site, such as probabilities of wave height, peak periods, wind and current speeds, should be known. In addition, the directions of wind, waves and currents can be important. Once the environment is known, the loads resulting from this type of wave or wind speed can be calculated.

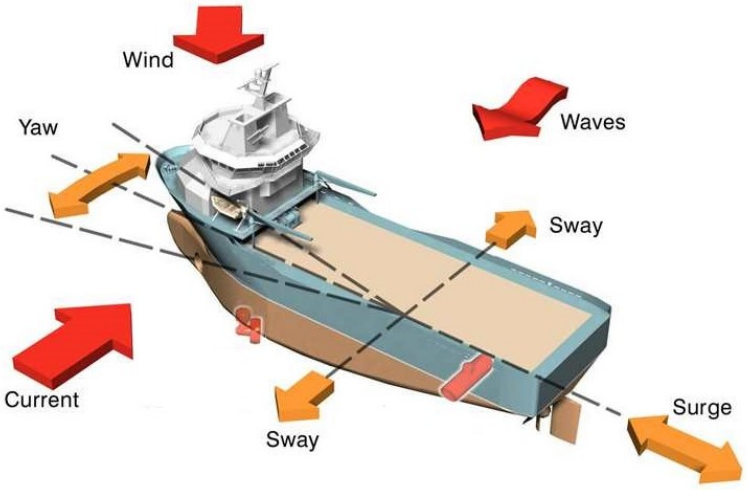

Figure 2.13: Environmental forces acting on a vessel such as wind, wave and current loads. The orange arrows represent the degrees of freedom in the horizontal plane, which are surge, sway and yaw, this is described in more detail in **??**. [5]

[4] `https://navisincontrol.com/CP_NEOY.php` [Last accessed 18-12-2019]

2.5.1. Waves

To model the wave loads on an offshore structure such as a monopile or a floating vessel requires two different steps. The first step is determining the wave environment for a particular location and deciding how to model this wave. The second step is translating this particular wave motion to a force on the structure.

Wave environment
The wave loads experienced by the structure depend on the sea state, in particular the significant wave height H_s and peak period T_p. There are several ways of modelling wave loads ranging from regular waves, which are represented by a simple sinusoidal function, to modelling of irregular waves using wave spectra, which may be uni-directional or taking into account wave spreading. In reality a sea state is comprised of a mix of many waves of different periods. The summation of all these regular waves forms the 'realistic' irregular wave. This summation of regular waves is depicted in Figure 2.14. An approximation of describing a sea surface in a certain state is the wave spectrum. This spectrum gives the wave energy distribution for different wave frequencies [30]. This wave spectrum is shown on the left in Figure 2.14 for increasing wave frequency ω.

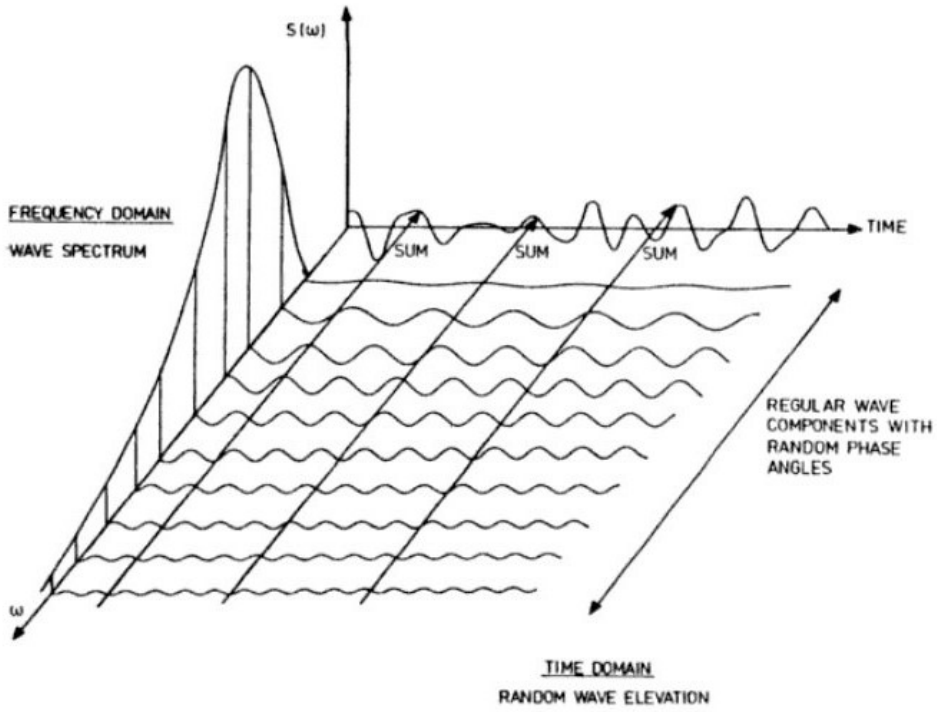

Figure 2.14: An irregular wave can be represented as a summation of regular waves. The wave spectrum on the left axis displays the wave energy distribution over the wave frequency. [10].

An example of such a wave spectrum is the JONSWAP spectrum, which describes the waves characterising the North Sea and is based on data analysis during the Joint North Sea Wave Observation Project [**?**]. It uses linear theory and is used to simulate irregular wave assuming that a long-crested irregular wave can be written as the sum of a large number of regular waves. From this spectrum a wave elevation plot of an irregular wave in the time domain can be created by applying inverse Fast Fourier Transform (FFT) on the wave spectrum and applying superposition of the regular waves resulting from the FFT. This is displayed in Figure 2.15. Figure 2.15a shows the JONSWAP wave spectrum and Figure 2.15b displays the resulting time series when FFT is applied.

The peak period and the significant wave height are related and according to [18] the JONSWAP spectrum is expected to be reasonable if the ratio falls between the value given in Equation 2.1.

[5] https://www.researchgate.net/figure/Forces-acting-on-vessel_fig1_279460235

$$3.6 < \frac{T_p}{\sqrt{H_s}} < 5 \tag{2.1}$$

The peak shape parameter determines the height of the peak of the spectrum. As the area under the curve should be equal, increasing the value of gamma leads to a higher, but narrower peak. γ depends on the ratio of the peak period T_p and the significant wave height H_s and is determined according to Equation 3.7 (see chapter 3) [18]. Furthermore, it should be noted that the JONSWAP spectrum reduces to a Pierson-Moskowitz spectrum for a γ = 1. As shown in Equation 3.7 this happens for increasing peak periods for a constant wave height due to the fact that the JONSWAP spectrum represents a wind generated sea state in a fetch-limited area [15], whereas the Pierson-Moskowitz wave spectrum represents a fully developed sea where waves with higher periods are more often encountered. It is possible to select a different combination of H_s and T_p but for larger periods with the same significant wave height the JONSWAP spectrum is then reduced to the Pierson-Moskowitz spectrum.

$$\begin{gathered}\gamma = 5 \text{ for } T_P/\sqrt{H_S} \leq 3.6 \\ \gamma = \exp\left(5.75 - 1.15\frac{P}{\sqrt{H}}\right) \text{ for } 3.6 < T_P/\sqrt{H_S} < 5 \\ \gamma = 1 \text{ for } 5 \leq T_P/\sqrt{H_S}\end{gathered} \tag{2.2}$$

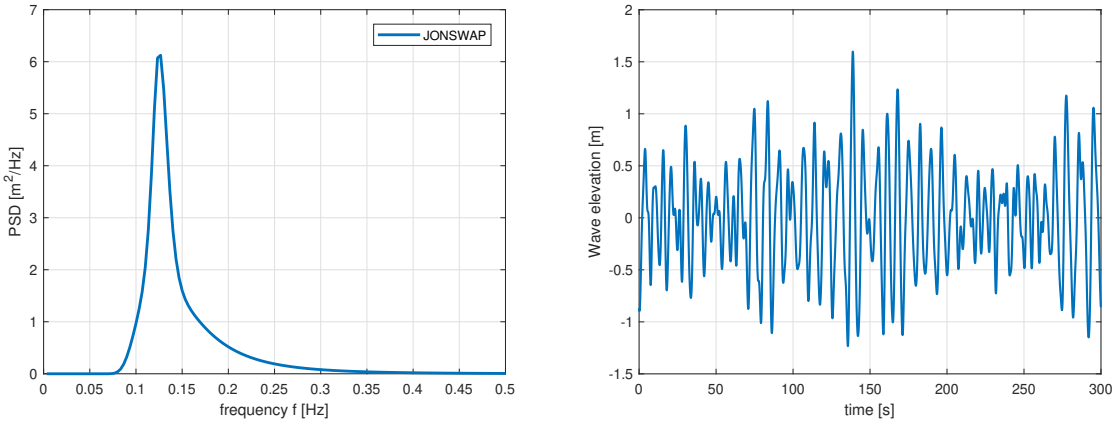

(a) The JONSWAP wave spectrum for a wave with an 2 m significant wave H_s and a peak period T_p of 8 s.

(b) A time series of the random irregular waves resulting from the inverse FFT of the JONSWAP wave spectrum shown on the left hand side.

Figure 2.15: A wave spectrum shown in Figure 2.15a can be converted in a time series of the wave elevation shown in Figure 2.15b.

Wave loads: the Morison equation

There are many methods to obtain the resulting load from an incoming wave, ranging from a more simple linear approach to complex non-linear methods. The non-linear methods provide more accurate results, but at the same time require much more computational power and are therefore much slower. A relatively simple and good approximation of the wave loads on the monopile can be obtained by using the well-known Morison equation for slender fixed bodies shown in Equation 2.3. This equation holds for slender bodies with a diameter to wave length ratio $\frac{D}{\lambda}$ smaller than 0.2, for which effects of diffraction and radiation are assumed to be insignificant [21]. Note that for decreasing wave frequency, so for increasing wave length, the effects of diffraction and radiation decrease.

The body is split up into multiple sections and the wave forcing per section is integrated over the entire length of the body. Equation 2.3 gives the wave load on one section and the total hydrodynamic load and overturning moment can be determined by integrating the distributed loads acting on every section along the length of the monopile. This equation has an inertia component f_i, related to the particle acceleration, and a drag component f_d related to the particle velocity. C_m and C_d are the mass

coefficient and the drag coefficient, which depend on the Reynolds number. $\dot{u}$ and u represent the wave particle acceleration and velocity, respectively. D is the diameter of the structure and ρ is the density of the (sea)water.

$$f(t) = f_i + f_d = C_m \frac{1}{4}\rho\pi D^2 \dot{u} + C_d \frac{1}{2}\rho D|u|u \tag{2.3}$$

Note that Equation 2.3 is limited to linear wave theory and does not incorporate any higher-order wave forcing. Furthermore, the structure should be slender, as the Morison equation assumes a uniform flow acceleration at the location of the body. For larger structures or shorter wave lengths diffraction effects should be taken into account. The MacCamy-Fuchs correction for diffraction can be applied, modifying the acceleration term to ensure inertia force is not overestimated.

The Morison equation above assumes a stationary rigid body. During the monopile installation, however, the body is moving. Therefore, the expression for the velocity u and acceleration $\dot{u}$ of the wave particles in Equation 2.3 can be replaced by the relative velocity of the wave particles compared to the structure, as shown in Equation 2.4 [21]. $\ddot{\zeta}_s$ and $\dot{\zeta}_s$ represent the acceleration and velocity of the particles. The motion of the monopile is described by $\ddot{x}_s$ and $\dot{x}_s$. The terms C_m, C_a and C_d represent the mass, added mass and the drag coefficient.

$$f_{w,s} = \rho_w C_m \frac{\pi D^2}{4} \cdot \ddot{\zeta}_s - \rho_w C_a \frac{\pi D^2}{4} \cdot \ddot{x}_s + \frac{1}{2}\rho_w C_d D \left|\dot{\zeta}_s - \dot{x}_s\right| \cdot \left(\dot{\zeta}_s - \dot{x}_s\right) \tag{2.4}$$

The first term of Equation 2.4 accounts for the non-viscous wave excitation forces using the diffraction and Froude-Krylov force. The second term represents inertia and is characterised by the added mass C_a and the third term represents the drag force [21]. The drag coefficient depends both on the Reynolds and the KC number. For a monopile the KC number is relatively small, meaning the inertia force is dominant over the drag force. Figure 2.16 shows the regimes expressing the dominant force depending on the wave height H, cross sectional diameter D and wave length λ [8].

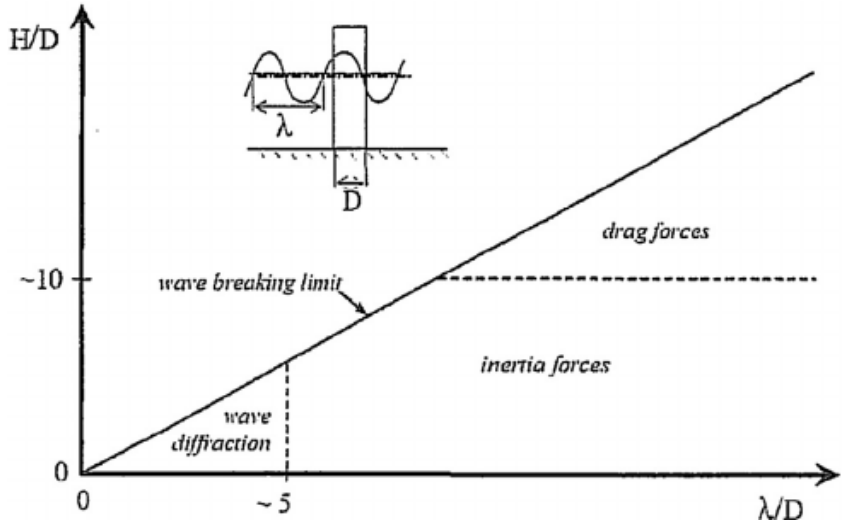

Figure 2.16: Relationship between wave height H, wave length λ and diameter of the structure D and the regime in which the drag, inertia or wave diffraction forces are dominant. [8]

As depicted in Figure 2.16, with the increasing diameter the effects of diffraction (and radiation) become more significant, especially in short wave lengths (as the diameter to wave length ratio $\frac{D}{\lambda}$ should be smaller than 0.2). Furthermore, a larger diameter structure (like a vessel) generally has a more inertia dominated than drag dominated wave load. Due to the significance of diffraction and radiation for an increasing diameter, reference [21] suggests combining the Morison equation with viscous damping by adding a retardation function. The radiation force is then calculated by a convolution integral, which represents the memory effect. Incorporating the effects of damping results in a smaller response both

at the resonance frequency and at the wave frequency, especially at the resonance frequency and the wave frequency. The disadvantage of adding the potential damping effects is the calculation should be performed in the time domain, which slows down the calculation.

To calculate the loads on the ship in regular waves the hydrodynamic problem can be split in two separate problems [10]. First of all, there is the wave excitation load on the body when the vessel is restrained from moving and there are incoming waves. These wave excitation loads are composed of Froude-Krylov and diffraction forces and moments. Furthermore, there are forces and moments acting on the body when the structure is forced to oscillate in the undisturbed surface of the fluid [15]. These loads are known as hydrodynamic loads and are composed of added mass, damping and restoring terms. As both the wave excitation loads and the other hydrodynamic loads are assumed to be linear, these can be summed to calculate the total hydrodynamic loads.

Wave loads: potential flow theory
As an alternative to the Morison equation one can use potential flow theory, which is more widely applicable. Potential flow theory can be used to calculate the hydrodynamic loads on the installation vessel. For potential flow it is assumed the flow is inviscid (frictionless), irrotational and incompressible [26]. Applying the assumption of irrotational flow in the continuity equation yields the Laplace's equation for the velocity potential ϕ, see Equation 2.5. Furthermore, the momentum equation is reduced to Bernoulli's equation shown in Equation 2.6.

$$\frac{\partial^2 \Phi}{\partial x^2} + \frac{\partial^2 \Phi}{\partial y^2} + \frac{\partial^2 \Phi}{\partial z^2} = 0 \tag{2.5}$$

$$\left(\frac{\partial \Phi}{\partial t} + \frac{\nabla \Phi \bullet \nabla \Phi}{2} + \frac{p}{\rho} + gz \right) = const. \tag{2.6}$$

where ϕ is the velocity potential, ρ is the density of the fluid, p is the pressure, g is the gravitational acceleration and z is the elevation from the reference plane with the axis pointing upwards. These two equations are the governing equations for nonlinear waves. Solving these equations using valid boundary conditions can give the first-order velocity potential $\phi^{(1)}$ [11]. These boundary conditions can for example be dynamic conditions at the free surface conditions, such as assuming the pressure p is equal to zero at the ocean surface, and kinematic conditions at the bottom and surface. This is described in more detail in [31]. Once the velocity potential has been determined, the frequency-dependent added mass, linear damping and wave excitation can be solved for by using Equation 2.7. The problem may be solved for a rigid body influenced by small-amplitude harmonic waves or for small rigid body motions in still water.

$$\Phi^{(1)}(x,t) = \mathrm{Re} \sum_j \phi_j^{(1)}(x) e^{i\omega_j t} \tag{2.7}$$

Note that this is the first-order potential theory, or linear wave theory. Often linear wave theory, or first-order potential flow, is sufficient to describe the dominant loads on a structure [10]. However, potential flow is not limited by nonlinear terms and second-order potential flow theory can be useful for structures with natural frequencies outside the range of the wave excitation [11]. Excitation at frequencies that lie outside the wave excitation range may result from the interaction of two waves.

2.6. Control theory

2.6.1. PID-control

A PID-controller is a widely industry applied form of feedback control, meaning the controlled output is measured and fed back into the system as input to adjust the controlled variable(s) accordingly. PID stands for Proportional, Integral and Derivative. The output $u(t)$ of the controller in the time domain is given by Equation 2.8 and is a function of the control parameters and the error. The error is the offset of the desired value of the controlled variable.

The first controller variable k_P is the **proportional gain** and, as suggested by its name, the output signal is directly proportional to the error in proportional feedback. In its simplest form the proportional gain can be compared to a spring, where k_P is the spring constant. A higher proportional gain increases the speed at the response. However, this increased speed of the response comes at a price of increased overshoot and damping in the system [12]. Furthermore, increasing the proportional gain may lead to instability for higher order systems.

The **integral gain** k_I is meant to minimise the steady-state tracking error and the steady-state output response to disturbances, as a proportional controller only always has a nonzero steady-state offset and is not capable of completely rejecting a constant disturbance in the input. As shown in Equation 2.8 the error is integrated, meaning it is a summation of all the past values of the tracking error and the control action is based on the past system errors. Therefore, it corrects for the accumulation of error. The disadvantage of integral control is the increased complexity of the system and the contribution to the overshoot of the response.

The **derivative gain** k_D is meant to speed up the transient response, reduce the overshoot and improve the closed-loop stability of the system. The k_D control action is comparable to that of a dashpot, as the response depends on the value of k_D and the rate (speed) at which the error changes. As the k_D term is multiplied with the derivative of the error, the control action is based on the slope of the error and, as a result, it has anticipatory behaviour. The disadvantage of derivative control is that it tends to amplify noise.

$$u(t) = K_p e(t) + K_i \int e(t)dt + K_d \frac{de}{dt} \tag{2.8}$$

3

Model set-up and verification

This chapter describes the physical system to be modelled. Before modelling the complete and coupled system, the monopile motions are studied in the frequency domain to gain insight into the effect of changing settings of the PID controller that keeps the monopile vertical. Then, the monopile model is set-up in OrcaFlex, a widely used dynamic analysis software package for offshore marine systems, and compared to the frequency domain results. The model is set-up using a Python application programming interface (API), as this gives a clear overview of the parameters and allows for efficient data processing. Afterwards, the coupled system, composed of the monopile, gripper frame and vessel, is modelled in OrcaFlex and tested by performing certain basic tests.

3.1. Model overview

An example of the physical system is shown in Figure 3.1. The fixed component of the gripper frame, which is the base of the x-y table and denoted as number 5 in Figure 3.1, is installed on the deck of the vessel (number 4 in the latter figure). The monopile, see number 1, is enclosed by the gripper frame ring, which is the moving part of the gripper frame and indicated with number 3 in Figure 3.1. The ring can move relatively to the base of the x-y table on the vessel. Actuators (not visible in Figure 3.1) move the ring with respect to the vessel in order to compensate for the horizontal vessel motions. If the vessel, for instance, moves 1 meter in positive sway-direction, the ring should move 1 meter in opposite direction to ensure a net zero displacement of the pile. Inside the ring the monopile is clamped using actuators with rollers, depicted in Figure 3.1 as number 2, constraining movement of the pile within in the horizontal plane. If the pile moves due to external (environmental) loads the gripper frame should exert a force to limit pile movement and keep it from falling over. The rollers do not constrain movement of the pile along its length, meaning that the pile is free to slide up and down within the ring.

In order to model the system shown in Figure 3.1, it is simplified and reduced to a model with three main bodies. The simplified, 2D representation of the model is shown in Figure 3.2. The three main bodies of the model are the monopile, gripper frame and vessel. The monopile is a thin-walled, steel cylinder with a diameter of 10 m and a length l_{mp} of approximately 100 m, weighing over 1600 tonnes. Details of the monopile are provided in Table 3.1. It is assumed that the monopile is in the early phase of the installation and still hinged at the seabed with zero soil stiffness. At a certain height above the water level, denoted as l_{gf}, the monopile is held by the gripper frame ring. The gripper frame ring is modelled as a point mass connected to the monopile with a translational spring and damper. The stiffness and damping between the ring and the monopile is denoted as k_{ring} and d_{ring}, respectively. The actuators moving the ring are modelled as winches that can exert a force on the pile in both the positive and negative direction. This is described in more detail in section 3.4. The force exerted on the monopile in order to keep it vertical is controlled by a PID-controller, see subsection 2.6.1, and depends on the

[1] https://ocean-energyresources.com/2019/01/16/ihc-introduces-new-dynamic-outrigger-frame/ [Last accessed 30-07-2020]

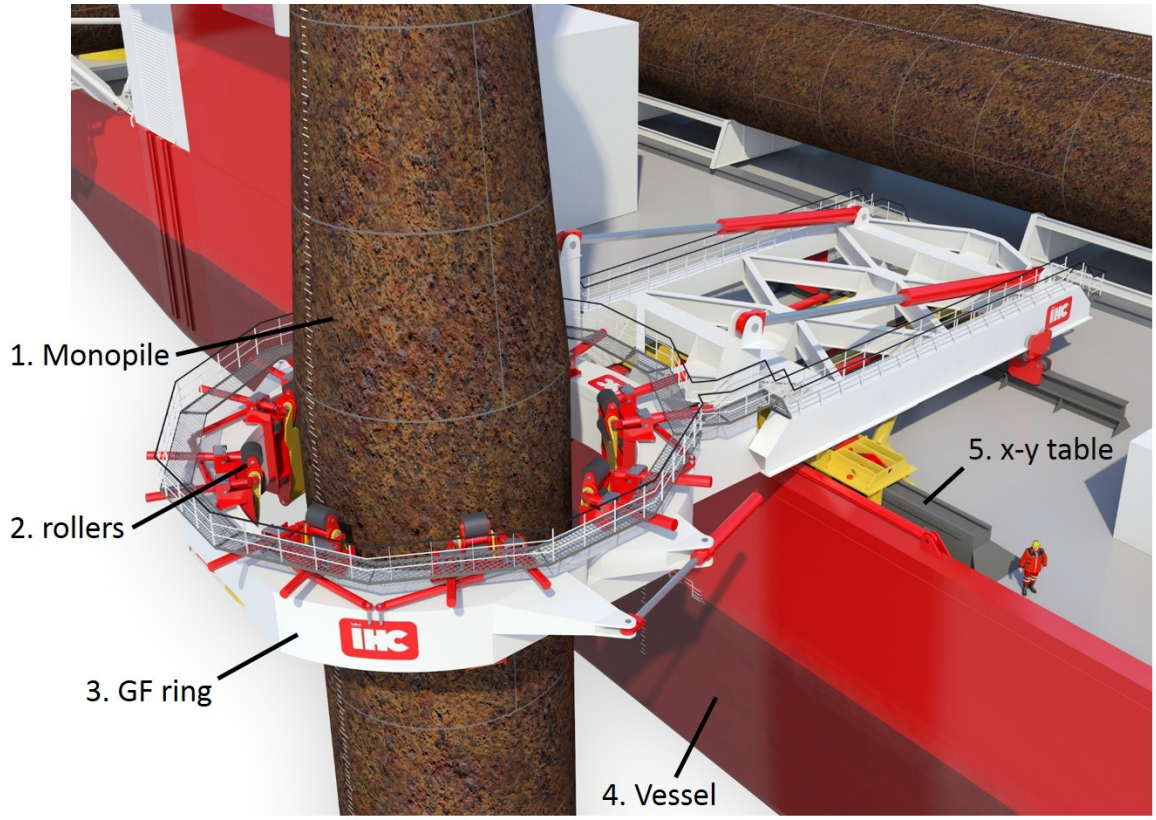

Figure 3.1: An example of a gripper frame developed by Royal IHC [1].

offset of the monopile.

The vessel modelled is the DP crane vessel 'Aegir' of HMC, details of which are given in Table 3.2. The vessel is suited to install and decommission many offshore structures like monopiles, transformer stations or jackets. With its crane capacity of 4000 mT and lifting height of 96 m above deck it is well suited for the installation of large monopiles.

As a start, the behaviour of only the monopile is modelled, instead of the fully coupled system, to gain insight into the behaviour of the pile when subject to different control settings. The monopile motions are initially calculated in the frequency domain, which is described in section 3.2. Then the monopile is modelled in OrcaFlex, see section 3.3. In the latter section the results of the frequency domain calculations obtained in section 3.2 are compared to time domain simulations resulting from the OrcaFlex model. Once the monopile motions have been investigated and the results of the OrcaFlex model and frequency domain have been compared, the fully coupled model shown in Figure 3.2 is modelled in OrcaFlex. This is described in section 3.4.

3.2. Frequency Domain Calculations of Monopile Motions for Various Control Settings and Forcing Frequencies

In this section, the monopile is modelled without the vessel and gripper frame ring in order to investigate the monopile behaviour for various controller settings and forcing frequencies. For the frequency domain calculations it is assumed that the pile is subject to a harmonic force of various forcing frequencies, comparable to a regular wave. In addition, the control parameters k_P and k_D of the PID controller, determining the force exerted on the monopile to keep it vertical, are adjusted. In consultation with HES the early installation phase is modelled where the pile has just been lowered to the seabed and self-penetrated the soil. During this early hammering phase of the installation, the monopile can be approximated by a rigid body hinged at the seabed without any rotational soil stiffness. A sketch of 2D

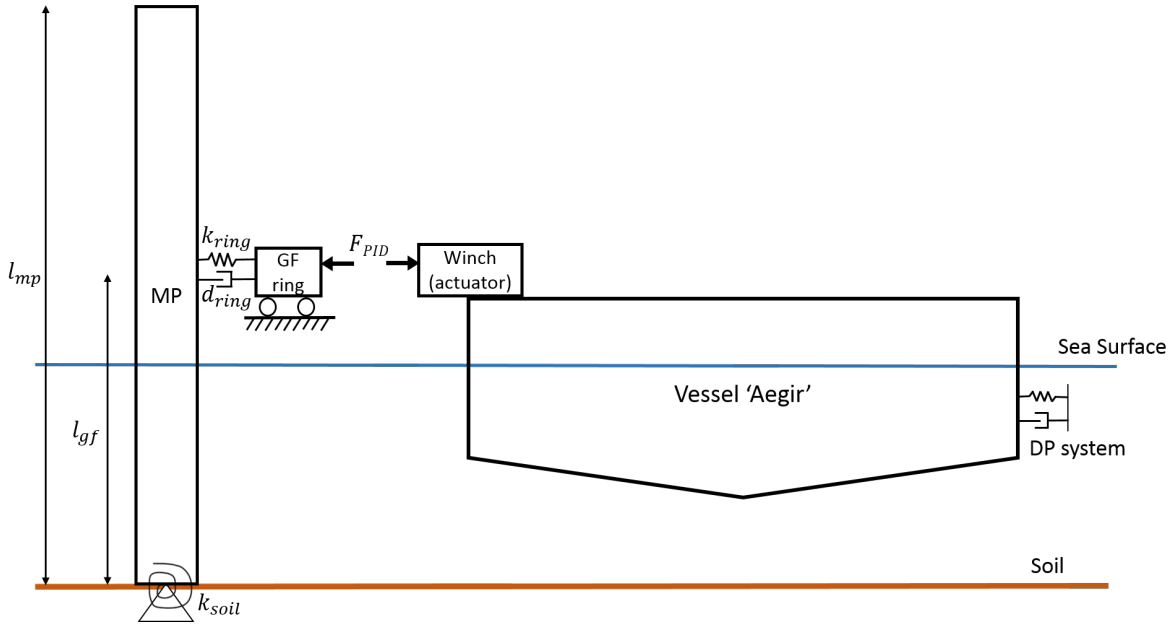

Figure 3.2: Simplified 2D representation of the model.

rigid body representation is shown in Figure 3.3. As described in section subsection 2.6.1, the proportional (k_P) and derivative (k_D) term of the PID controller in its simplest form can be represented by a spring and damper, respectively.

The following assumptions are made:

- The monopile is a homogeneous rigid body with a length of 97 m and a mass of 1653 tonnes.
- The monopile is hinged at the seabed with zero soil stiffness.
- The control parameters k_P and k_D are represented by a spring and damper at a gripper frame height l_{gf} of 60 m. This force is directly applied to the monopile and presence of the gripper frame ring is ignored in this case.
- The monopile is subject to a harmonic force, e.g. a regular wave.

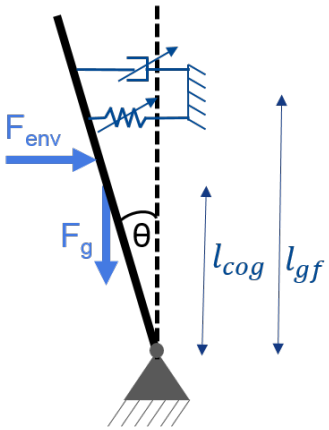

Figure 3.3: Simplified 2D representation of the monopile to perform .

The equation of motion of the system describing the angle of the monopile under harmonic (wave) forcing is shown in Equation 3.1. It is assumed that the hydrodynamic damping is negligible since the drag force on the pile depends on the velocity squared and it is assumed the monopile velocity is small. Therefore, it is assumed that the total damping of the pile c_{tot} only depends on the derivative gain k_D. The total stiffness k_{tot} in the equation of motion depends on the proportional gain k_P, the soil stiffness

and the gravitational force acting on the pile. As the pile is still hinged at the seabed, it is assumed that the rotational soil stiffness is equal to zero. It is assumed that the centre of gravity is exactly in the middle of the pile, neglecting any buoyancy effects. The equation of motion with the expanded stiffness and damping term is given in Equation 3.2.

$$I_{tot}\ddot{\theta}(t) + c_{tot}\dot{\theta}(t) + k_{tot}\theta(t) = M_{env}\cos(\omega_f t) \tag{3.1}$$

$$I_{tot}\ddot{\theta}(t) + k_D l_{gf}^2\dot{\theta}(t) + \left(k_P l_{gf}^2 + \cancelto{0}{k_{soil}} - mgl_{cog}\right)\theta(t) = M_{env}\cos(\omega_f t) \tag{3.2}$$

The total moment of inertia is given by the inertia due to the mass of the pile, the mass of the trapped water and the added mass can be approximated using the following equation:

$$I_{tot} = I_{mp} + I_{tw} + I_{\text{am}} = \frac{1}{3}\left(m_{mp}l_{mp}^2 + m_{tw}l_{water}^2 + m_a l_{water}^2\right) \tag{3.3}$$

The amplitude-frequency characteristic of the monopile under a harmonic force is:

$$|\theta(\omega_f)| = \frac{M_{env}}{k_{tot}}\frac{1}{\sqrt{\left(1 - \frac{\omega_f^2}{\omega_n^2}\right)^2 + \gamma^2\frac{\omega_f^2}{\omega_n^2}}} \tag{3.4}$$

where M_{env} is the magnitude of overturning moment at the point of rotation of the pile due to the external environmental forcing. ω_f represents the forcing frequency. The natural frequency of the system ω_n is obtained by dividing the total rotational stiffness by the total inertia, as shown in Equation 3.5. The amount of damping is represented by γ and given in Equation 3.7, where $2n$ is the ratio between the damping in the system and the total inertia as shown in Equation 3.6.

$$\omega_n^2 = \frac{k_{tot}}{I_{tot}} = \frac{k_P l_{gf}^2 - mgl_{cog} + \cancelto{0}{k_{soil}}}{I_{tot}} \tag{3.5}$$

$$2n = \frac{c}{I_{tot}} = \frac{k_D l_{gf}^2}{I_{tot}} \tag{3.6}$$

$$\gamma = \frac{2n}{\omega_n} = \frac{c_{tot}}{I_{tot}\omega_n} = \frac{k_D l_{gf}^2}{\omega_n I_{tot}} \tag{3.7}$$

Assuming the motion of the monopile in the horizontal plane at gripper level can be measured and is the limiting parameter, it is useful to convert the monopile angle to this variable. The amplitude-frequency characteristic of the motion of the monopile at gripper frame level is then given as:

$$|X(\omega_f)| = \sin(|\theta(\omega_f)|)l_{gf} \tag{3.8}$$

Using the equations above the effect of changing the control parameters k_P and k_D, meaning changing the values of the spring stiffness and damping term shown in Figure 3.3, is discussed in the next paragraphs. The function of the separate controller gains is discussed in subsection 2.6.1.

Changing the proportional gain k_P

The system is only stable if the total stiffness $k_{tot} > 0$. Therefore, there is a minimum value of k_P required to avoid the monopile falling over. The minimum value of k_P is given by Equation 3.9 and is approximately 219 kN/m. Note that this is at the verge of instability and that a disturbance easily leads to an unstable situation. Therefore, the actual value of k_P should be higher in order to provide sufficient stability margin and keep the pile from falling over if parameters are slightly different than anticipated, such as a higher environmental forcing.

$$k_{P,min} = \frac{mgl_{cog} + k_{soil}}{l_{gf}^2} \tag{3.9}$$

As shown in Equation 3.5, increasing the k_P (meaning increasing the stiffness of the system) leads to a higher natural frequency. This is represented in Figure 3.4 as well, where then natural period is plotted as function of k_P. As expected, the natural period decreases for increasing k_P. This means that the monopile can be excited by a certain wave period depending on the proportional gain of the controller. In ordinary installation sea states with wave periods typically ranging from 4 - 10 seconds, resonance is expected for values of k_P ranging from approximately 900 to 6300 kN/m. Therefore, choosing a k_P outside this range reduces the monopile motions.

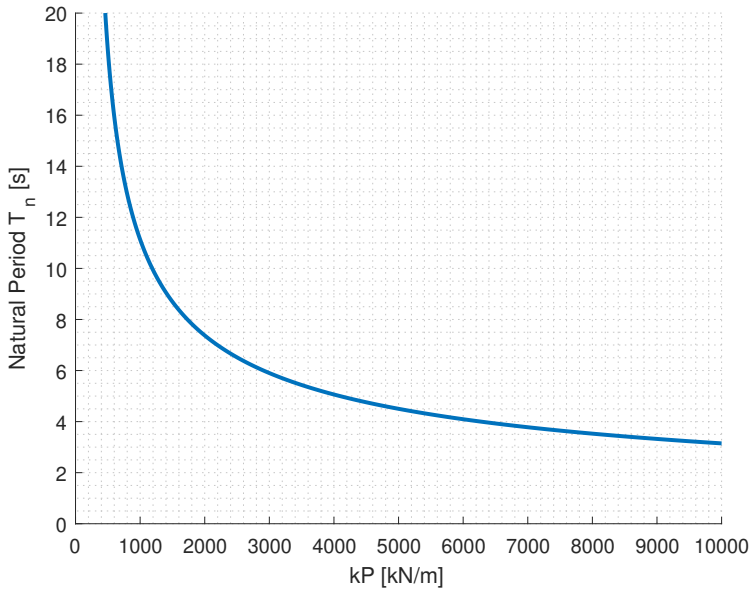

Figure 3.4: The natural period of the monopile for increasing function of k_P. Increasing the k_P results in a higher total stiffness, increasing the natural frequency and, in turn, decreasing the natural period

.

The effects of changing k_P is displayed in Figure 3.5 as well. The amplitude frequency characteristic, see Equation 3.8, is plotted as a function of the proportional gain k_P for two different wave periods (or forcing frequencies) and for different values of k_D. Figure 3.5a and Figure 3.5b show the response of the monopile subject to a harmonic force with a period of 7 and 10 seconds respectively. The amplitude of the moment M_{env} corresponds to an Airy waves with a wave height of 1 meter obtained from the OrcaFlex model described in section 3.4. As shown in Figure 3.4, for increasing k_P the natural period becomes lower. This is illustrated in Figure 3.5 as well, since the value of k_P that results in resonance is higher for a wave period T of 7 seconds than for a period of 10 seconds.

The integral gain k_I
Since it is assumed that the monopile is subject to a harmonic force (Airy waves) in this case, the forcing has a zero mean. Furthermore, it is assumed there are no disturbances or constant forces in the system. Consequently, the integral gain k_I is not required, as it is meant to prevent a steady state tracking error and minimise the effect of disturbances.

Changing the derivative gain k_D
Adding derivative gain decreases the monopile motions, especially in the resonance area. As shown in Figure 3.5, the effect of k_D is only marginal if the forcing frequency is much higher or lower than the natural frequency as the three lines almost coincide in this case. However, if resonance occurs, then adding damping has a substantial effect on the maximum motion of the monopile.

In conclusion, there is a minimum value of k_P required to guarantee stability of the monopile. When

increasing the value of k_P there is resonance at some point depending on the forcing frequency. A lower wave period means a higher value of k_P results in resonance. Adding derivative gain k_D is mainly useful near the resonance area, as the effect of damping is only marginal outside these areas.

In the end, the results of the coupled system are of interest. However, the coupled system is much more complicated and, therefore, it is modelled in OrcaFlex to perform time-domain simulations. For verification purposes the monopile motions of the time simulations of the OrcaFlex model are compared to the frequency-domain calculations in section 3.3.

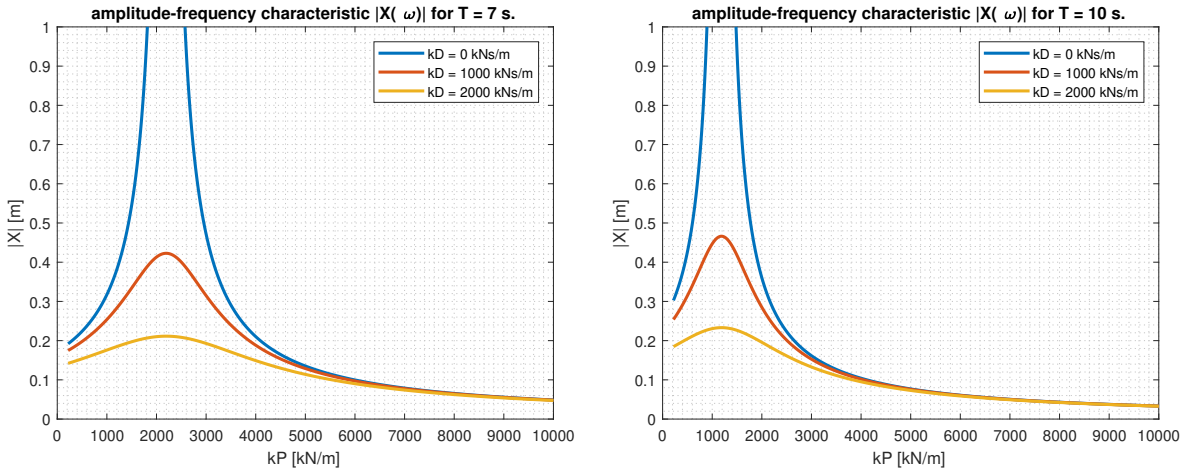

(a) Wave period of 7 s.

(b) Wave period of 10 seconds.

Figure 3.5: The amplitude of the monopile motion at gripper frame level for increasing proportional gain. The increase in proportional gain results in a lower natural frequency. The motion of the monopile decreases if the damping (k_D) is increased.

3.3. Monopile Model in OrcaFlex and Comparison to Frequency Domain Calculations

The monopile is modelled in OrcaFlex for the same case as in the previous section, meaning a 97 m long monopile with a mass of 1653 tonnes hinged at the seabed without any rotational stiffness. At the end of this section, the results of the time domain simulations in OrcaFlex are compared to the results obtained in the frequency domain calculations.

In the OrcaFlex model the monopile is modelled as a homogeneous pipe as this object is the most straightforward representation of the monopile. OrcaFlex automatically calculates the structural properties of the pipe based on the user-specified dimensions of the pipe such as the outer and inner diameter, the Young's modulus and the density of the material. Hydrodynamic loads are applied according to the Morison equation, see subsection 2.5.1.

As mentioned before, the pile remains vertical due to a PID-controlled force which is directly applied to the monopile. In reality the actuators move the gripper frame ring with respect to the vessel, and the movement of the gripper frame ring exerts a force on the monopile. However, in this simplified case, only the monopile itself is modelled and the gripper frame ring is only modelled in the coupled model in section 3.4. Figure 3.6 shows the block diagram of the model. The error e_{mp}, which is the offset of the monopile from the desired position r_{mp}, is fed into the PID controller. This controller is an external function in Python. Every time step the force is determined by this function according to Equation 3.10 and applied to the monopile in OrcaFlex. The total force on the monopile F_{mp} is the sum of the environmental forcing F_{env} and PID force F_{gf}. OrcaFlex then solves the equation of motion to determine the new position of the pile, which is represented by the yellow block in Figure 3.6.

$$F_{gf} = k_P e_n + k_I \frac{1}{2} dt \left(e_n + e_{n,prev}\right) + k_D \frac{\left(e_n - e_{n,prev}\right)}{dt} \tag{3.10}$$

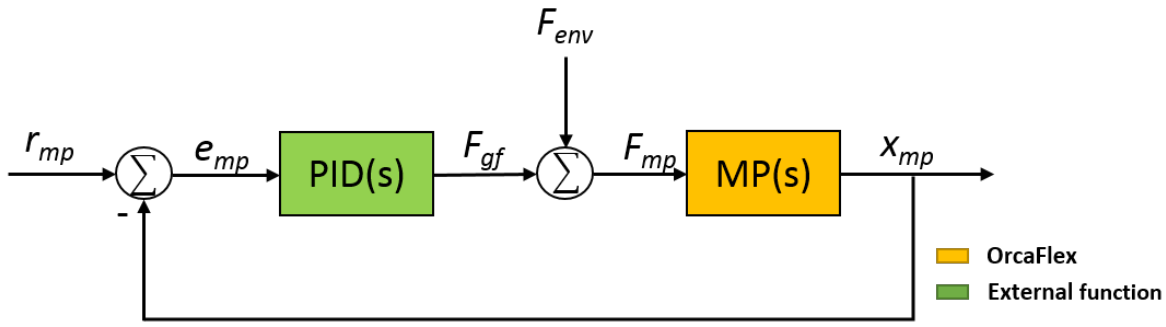

Figure 3.6: A block diagram representing the monopile model including the PID controller. Based on the error of the monopile a force is exerted on the monopile.

Figure 3.7 shows a comparison of the results of OrcaFlex simulations and the amplitude frequency characteristic calculation based on Equation 3.8 for two different wave periods (7 s and 10 s). The monopile response is plotted for various values of k_P and for a k_D of 1000 kNs/m, which is the same case as the red line in Figure 3.5. As mentioned in the previous paragraph, the monopile is subject to a 1 m Airy wave. For the frequency domain calculations the moment due to the waves M_{env} in Equation 3.4 is obtained by calculating the wave force on a fixed pile in OrcaFlex, while the OrcaFlex simulation uses the instantaneous position and wave force on the pile. In addition, OrcaFlex takes sloshing effects into account. Furthermore, the effect of drag is taken into account in the OrcaFlex model. As a result, the pile motions are slightly overestimated in the frequency domain. However, the OrcaFlex model matches the frequency domain calculations sufficiently to conclude that OrcaFlex correctly calculates the monopile motions.

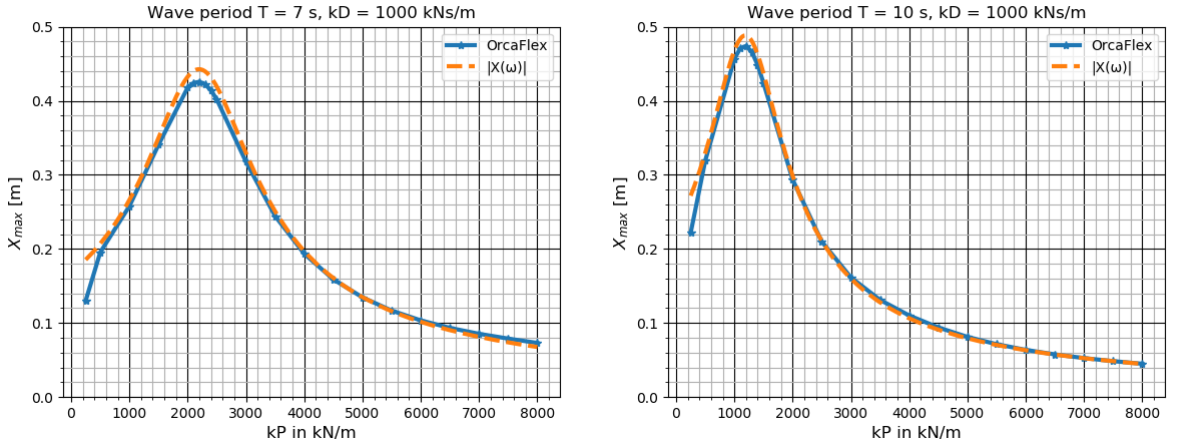

(a) Response of the monopile for a 1 m regular wave with a period of 4 s. (b) Response of the monopile for a 1 m regular wave with a period of 7 seconds.

Figure 3.7: A comparison between the frequency domain calculation and the OrcaFlex simulation of the monopile motion for two different wave periods and various values of k_P. The derivative gain is equal to 1000 kNs/m.

3.4. Coupled Model Set-Up in OrcaFlex

In section 3.2 the effect of changing the proportional and derivative gain on the monopile motions for various wave periods has been studied in the frequency domain. Furthermore, the monopile has been modelled in OrcaFlex and compared to the frequency domain calculations in section 3.3. Now that the motions of only the monopile have been modelled and compared, the coupled model described in section 3.1 is modelled in OrcaFlex. In addition to the monopile modelled in section 3.3 the coupled

model includes a simplified gripper frame and HMC's vessel Aegir. This section describes how the model shown in Figure 3.2 is build up in OrcaFlex. Figure 3.8 shows the model set-up in OrcaFlex.

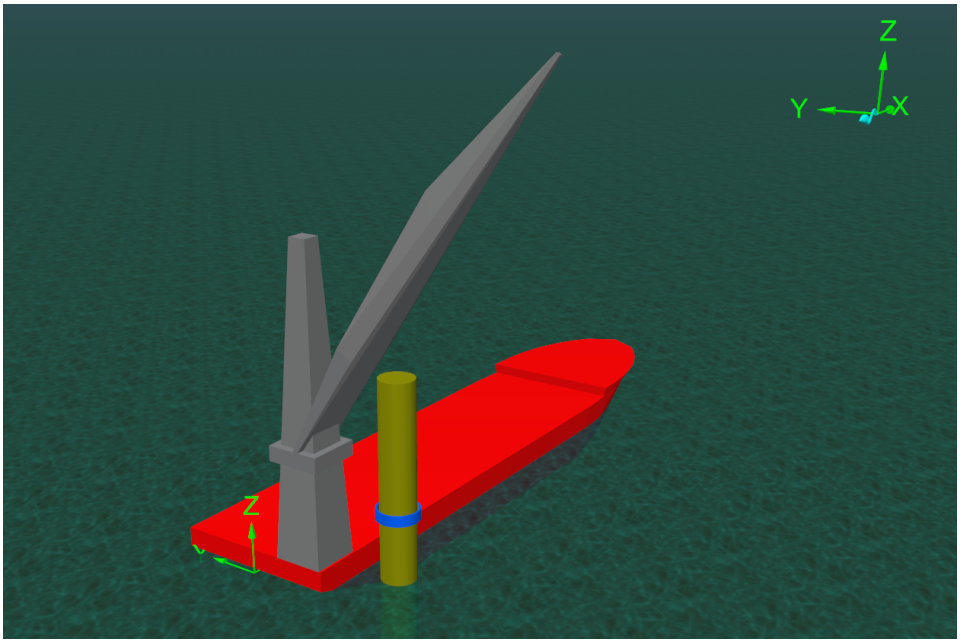

Figure 3.8: The model in OrcaFlex consisting of the vessel, the gripper frame ring and the monopile.

.

3.4.1. Monopile

The monopile is modelled as described in section 3.3. Only the gripper frame height, l_{gf}, is adjusted from 60 to 51 meters to ensure the gripper frame is located at the deck height of the Aegir. The geometry of the monopile is given in Table 3.1 below. The length of the pile depends on the water depth at the installation site. In this case it is assumed the water depth is 41 m and the pile will be driven into the seabed for 50 m.

Monopile parameters	**Symbol**	**Value**	**Unit**
Length	L_{MP}	97	m
Diameter	D_{MP}	10	m
Wall thickness	t	7	mm
Mass	m_{MP}	1653	tonnes
Water depth	l_{water}	41	m

Table 3.1: Parameters of the monopile.

3.4.2. Vessel

A block diagram of the vessel model is provided in Figure 3.9. The two main components of the vessel model are the DP system, implemented in OrcaFlex as an external function, and the vessel model itself. Both components have been provided by HES and are described in this subsection.

The DP system, see section 2.4, is represented by the green block in Figure 3.9. The amount of force applied is determined by a PID controller in an external function and depends on the DP settings and the error of the vessel. The thruster forces keeping the vessel at the intended position are modelled as a two global forces, in x- and y-direction, and a moment around the z-axis (yaw) applied at the centre of gravity of the vessel. A Kalman filter is implemented to filter out the first order wave-motions, since the DP system cannot counteract these forces in real life due to thruster limitations, see section 2.4.

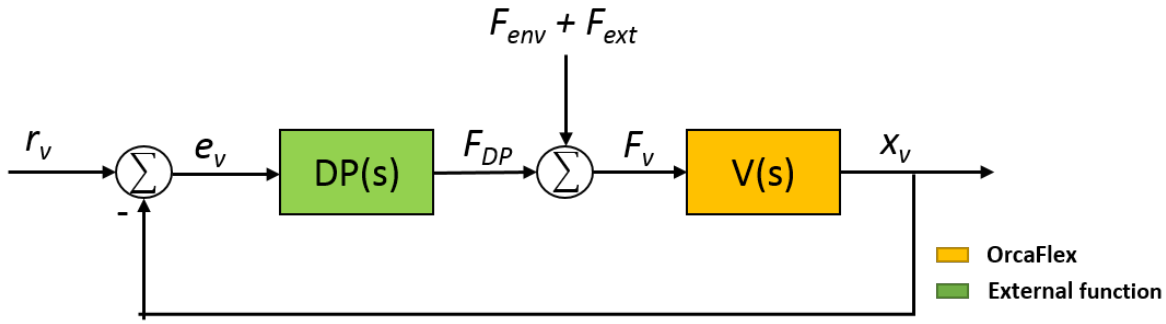

Figure 3.9: A block diagram of the vessel model.

The vessel model in OrcaFlex is represented by the yellow block in Figure 3.9. For each time step OrcaFlex calculates the new position of the vessel by solving the equations of motion. The Aegir is modelled as a vessel in OrcaFlex, meaning it is a rigid body with 6 DOF. OrcaFlex calculates the vessel motion in six DOF based on the first and second order wave loads, the added mass and damping due to wave radiation effects and the applied loads. The applied loads on the vessel F_v are the forces resulting from the DP system F_{DP} and the external loads F_{ext}. The external loads are the environmental loads F_{env} and the force exerted by the gripper frame F_{gf} to correct the pile motion. Furthermore, viscous roll damping is taken into account. The wave load transfer functions determine the first order wave force and moments on the vessel as described in reference [25]. In OrcaFlex the wave load response amplitude operator (RAO) gives the amplitude and phase of the force on the vessel per meter wave amplitude. The RAOs are provided for all six DOFs for different wave periods and wave directions. Whereas displacement RAOs yield the vessel motion per meter wave height, the wave load RAO merely gives the force exerted on the vessel.

The added mass and damping coefficients of the vessel are frequency dependent. Hence, the added mass and damping coefficients are given for different wave period and based on wave period the appropriate coefficients are used to calculate the vessel response. The hydrostatic stiffness of the vessel is given for heave, pitch and roll, and is equal to zero for the remaining three motions. The hydrostatic stiffness determines how the weight an buoyancy load change for small vessel motions (as this is a nonlinear problem that has been linearised). This includes both the effect of the change in submerged volume of the vessel and the varying moment due to the movement of the vessel's centre of buoyancy and centre of gravity as it pitches or rolls. Based on the total force and the vessel properties such as inertia and added mass, the vessel motions are calculated from the equations of motion. Then in the next time step the new vessel position x_v is fed into the DP controller again.

Details Aegir		
Length	210	m
Width	45.2	m
Operating Draft	9	m

Table 3.2: Details of HMC's offshore heavy lift vessel Aegir.

3.4.3. Gripper Frame

A top view of the model is presented in Figure 3.10. The gripper frame ring, shown in Figure 3.1 as number 3, is modelled as a 6D buoy element in OrcaFlex. The mass of the gripper frame ring is estimated to be 500 tonnes based on consultation within the industry. All other properties of the buoy such as buoyancy, added mass and damping are set to negligible. Hence, the buoy is comparable to a point mass connected to the pile. As depicted in Figure 3.2 and Figure 3.10 the interface between the monopile and the ring, resembling the rollers in Figure 3.1, is modelled as springs and dampers with spring stiffness k_{ring} and damping d_{ring}. The translational and rotational stiffness and damping of the constraint can be defined by the user.

The actuators of the gripper frame that move the ring with respect to the vessel are modelled as two winches, see Figure 3.10. One winch to exert a force in the x-direction and another to exert a force in y-direction. The ring of the gripper frame is connected to the vessel by the winch. The winch can either be length or tension-controlled in OrcaFlex. In the case of a length-controlled winch, the length of the winch is adjusted to keep the pile upright and to compensate for the vessel motions. However, the length-controlled winch does not allow compression and, therefore, does not provide a correct representation of the actuator. The tension-controlled winch is able to provide both tension and compression through the winch. Furthermore, all calculations in previous sections were based on a force controlled actuator and not length controlled. Therefore, the tension-controlled winch is selected and the monopile motion is force controlled.

It is assumed that the gripper frame is located 10 m above the water level, which is just above the deck height of the Aegir in case of a operating draft of 9 m. This means l_{gf} shown in Figure 3.2 is equal to 51 m. Furthermore, it is assumed that the gripper frame is located 35 m from the stern at the starboard side of the vessel, such that the crane can easily reach the monopile. The edge of the monopile is located 5 meters from the side of the vessel.

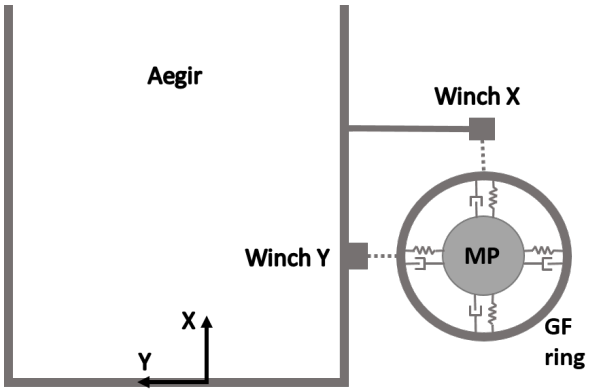

Figure 3.10: Top view of model with winches.

As mentioned in previous chapters, the gripper frame has two functions. First of all, it should compensate the vessel motions. Secondly, the gripper frame should exert a force on the monopile to keep it from falling over due to external loads. The winch compensates for vessel motions by changing the length of the winch, such that no tension is introduced due to the vessel motions. In this chapter, it is assumed that the vessel motions are perfectly compensated and, therefore, the vessel motions do not influence the monopile motions. The effect of imperfect motion compensation is studied in the next chapter.

Due to the fact that the vessel motions are perfectly compensated, tension in the winch is only introduced due to the motion of the monopile. A force is exerted on the pile to keep it vertical and the desired tension is controlled by a PID controller with the x and y position of the MP being the controlled variables, as shown in Equation 3.11.

$$t_{winch} = k_P e_n + k_I \frac{1}{2} dt \left(e_n + e_{n,prev}\right) + k_D \frac{\left(e_n - e_{n,prev}\right)}{dt} \tag{3.11}$$

where the error e_n is given by the offset of the monopile's x and y coordinate at gripper frame level. The subscript n indicates the direction and is either x or y. $e_{n,prev}$ represents the error at the previous time step in x- or y-direction.

To illustrate the functioning of the coupled model a block diagram of the coupled system is shown in Figure 3.6. The two block diagrams of the monopile and vessel, shown in Figure 3.6 and Figure 3.9 respectively, are coupled through the winch. The block diagram of the monopile is the same as in the case of the monopile only, see Figure 3.6. However, in this case the force is applied on the gripper frame ring by adjusting the winch tension, instead of directly applying an external force on the monopile itself. As explained in the previous paragraph, the tension in the winch is adjusted based on Equation 3.11.

The winch is connected to both the gripper frame ring and the vessel and, as a result, a force is exerted on both in opposite direction, see Figure 3.2. This is also illustrated in the block diagram in Figure 3.11, as the tension of the winch t_w resulting from the $PID(s)$ block is going into both the vessel and the monopile. The vessel motions do not influence the monopile motions due to the assumption of perfect motion compensation, so the vessel motion x_v is not fed into the loop of the monopile.

Due to the perfect motion compensation assumption the vessel could theoretically move away from the monopile infinitely far without influencing the monopile motion, which is not a correct representation of reality. Therefore, it is important to check whether the stretched length, which is the actual length between the two objects the winch connects, and the corresponding velocity are realistic requirements for actuators. In addition, the tension of the winch should be compared to the maximum force of actuators in the offshore industry.

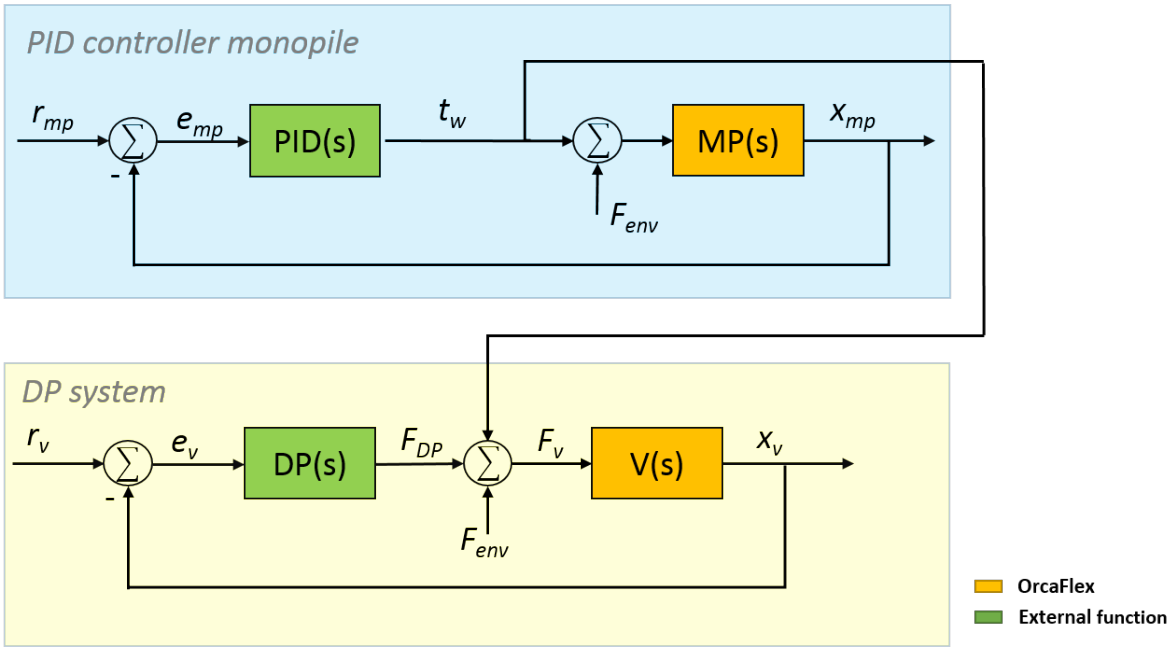

Figure 3.11: A block diagram of the coupled system with perfect motion compensation.

It should be noted that in reality the control system would most likely control the flow of the fluid in the actuators and then the flow in the cylinders would move the actuator. The winches provide a simplified version of these actuators and in the model the required tension is always obtained by the winch, as it is modelled as a 'simple' winch in OrcaFlex. Furthermore, extra tension in the winch may be added to Equation 3.11 to simulate the load resulting from imperfect motion compensation, which is discussed in more detail in subsection 4.3.4.

In this section, the set-up of the coupled model has been described. In the next section some basic tests are performed in order to determine if the model behaves as expected.

3.5. Basic Tests

In order to validate the coupled model described in section 3.4 various basic tests are performed. During the basic tests it is assumed that the ring is rigidly connected to the monopile. The tension in the winch is adjusted based on the motion of the ring and is controlled by a PID controller. The following base cases are tested:

1. Fixed monopile: the monopile is fixed and the Aegir uses the DP system to keep its position. The winch should adjust its length based on the movements of the Aegir only, as perfect motion compensation is assumed.

2. Fixed Aegir: the vessel is fixed and the winch should adjust the tension in the winch to keep the pile upright.

3. No environmental loads: there should be no movement of the Aegir or the monopile.

4. Controls to zero: the monopile should be unstable and fall over.

5. Varying time step: the time step of the model is adjusted.

Fixed monopile: When the monopile is fixed, the controlled variables, the x and y motion of the monopile at gripper frame level, are always equal to the target value, which is the initial position of the monopile. Hence, the error is always zero and the tension in the winch should be equal to zero, as shown in Figure 3.12. Furthermore, in order to have no tension in the winch the length of the winch should be equal to the offset of the Aegir. As illustrated in Figure 3.12 the tension in the winch remains zero and the length of the winch is adjusted based on the motions of the Aegir. Therefore, it can be concluded that the model behaves as expected in this case.

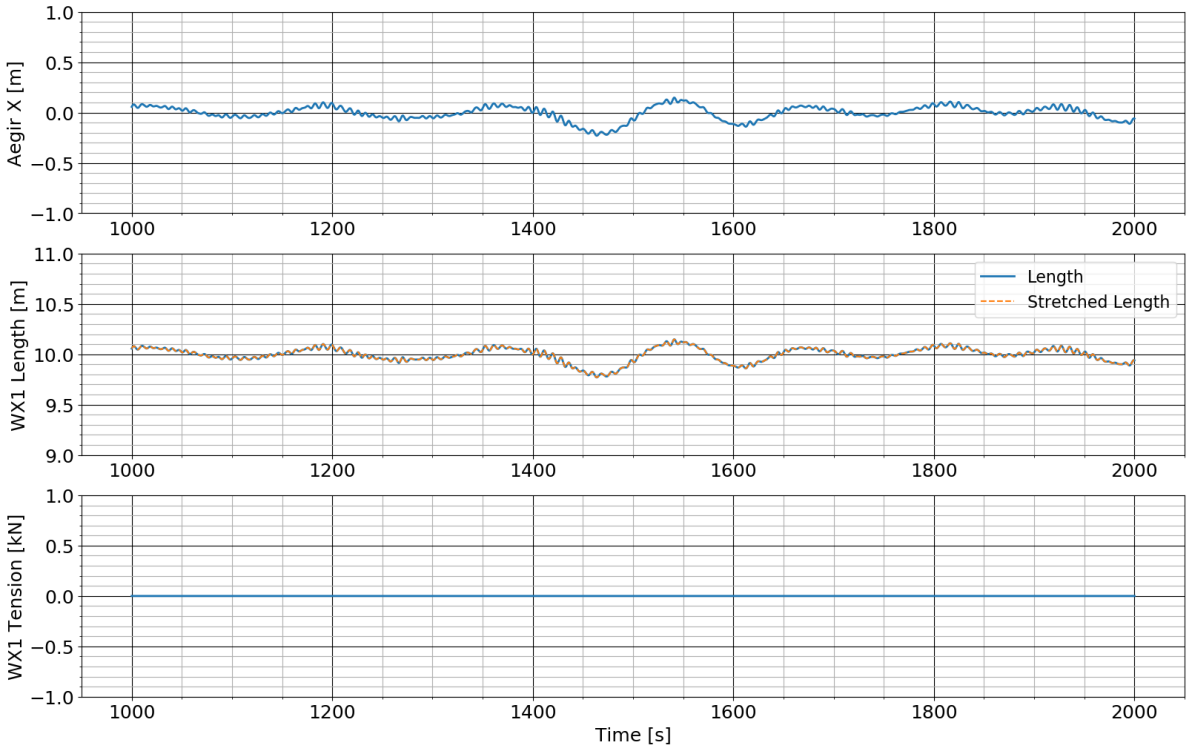

Figure 3.12: Due to the fixed monopile the error is constant and equal to zero. Therefore, the tension in the winch remains equal to zero. The Aegir moves due to the head waves (JONSWAP, H_s = 1 m, T_p = 7 s) and the winch length is adjusted to compensate its motions.

Fixed Aegir: When the Aegir is fixed the winch is only adjusted to provide a certain tension based on the motion of the MP. If the monopile moves in the negative x-direction (as defined in Figure 3.10) the winch should be hauled in and should become smaller than the initial length of 10 m. This is shown in Figure 3.13, where the change in winch length, stretched length and monopile motion are plotted. If the monopile moves in the positive x-direction (towards the winch), then the winch should become longer than the initial length to be in compression, exerting a force on the monopile opposing its motion. This is evident when looking at Figure 3.12 as the tension is negative for a winch length larger than the stretched length and positive for a winch length smaller than the stretched length. For this case it can be concluded that the tension is correctly adjusted based on the monopile motions.

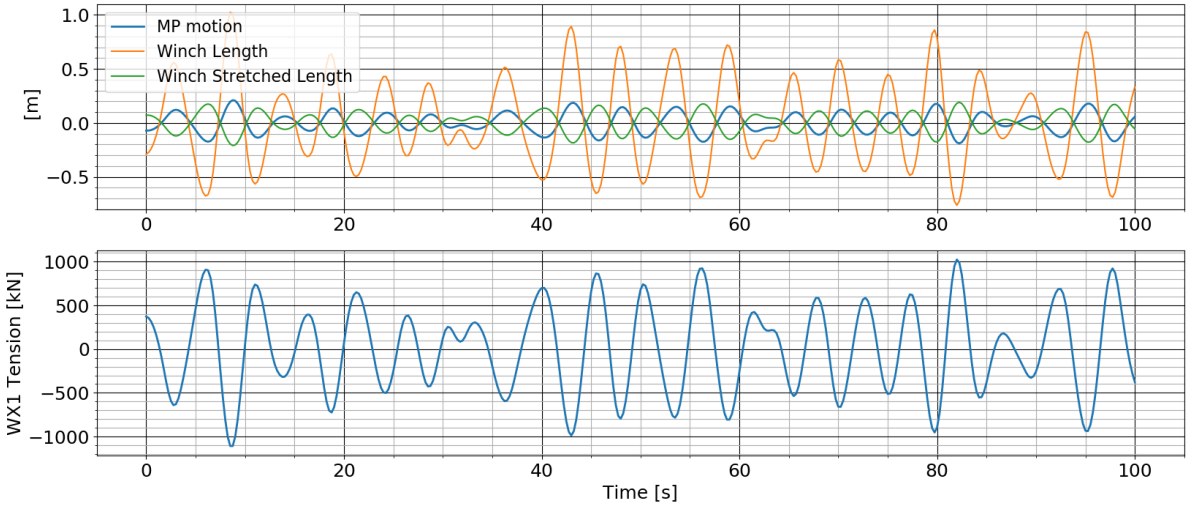

Figure 3.13: Fixed Aegir. The monopile is subject to JONSWAP waves with a H_s of 1 m, T_p of 7 seconds coming from the head direction. The top figure displays to monopile motion and the change in stretched length and change in length of the winch. The bottom graph displays the tension in the winch, which is determined according to **??**.

No control: If the gains of the PID controller are equal to zero the monopile should fall over as the tension in the winch remains equal to zero regardless of the monopile motion. This is depicted in Figure 3.14 where the x-motion of the gripper frame goes to 60 m, which means the gripper frame is parallel to the seabed at this instance. Due to the zero soil stiffness assumption the pile falls through the soil until it is 'hanging' upside down from its hinging connection. As described in section 3.2 there is a minimum value of k_P required for stability, which is higher for the complete model as the mass of the gripper frame ring should be taken into account. In addition, the gripper frame height has been lowered from 60 m in the monopile only model to 51 m in the coupled model. The system is stable for a $k_P \geq$ 392 kN/m, as shown in Figure 3.14. For a k_P of 391 kN/m the monopile is stable in the beginning, but eventually falls over as it is on the verge of instability.

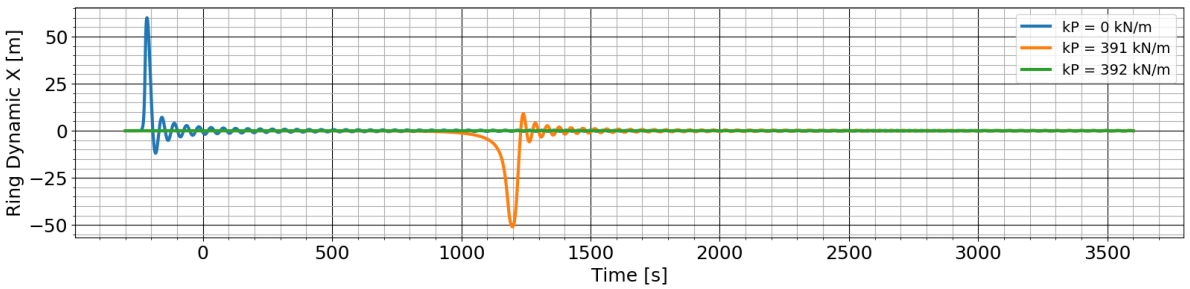

Figure 3.14: The x-motion of the monopile plotted over time for different values of k_P. In case of a k_P of 0 kN/m the monopile falls over, see the blue line. Furthermore, the minimum k_P is equal to 392 kN/m as the monopile falls over for any lower value.

No environmental forces: If there is no environmental forcing the system should remain stable and there should not be any pre-tension in any objects of the model. The results in Figure 3.15 show that the model behaves as expected in this case.

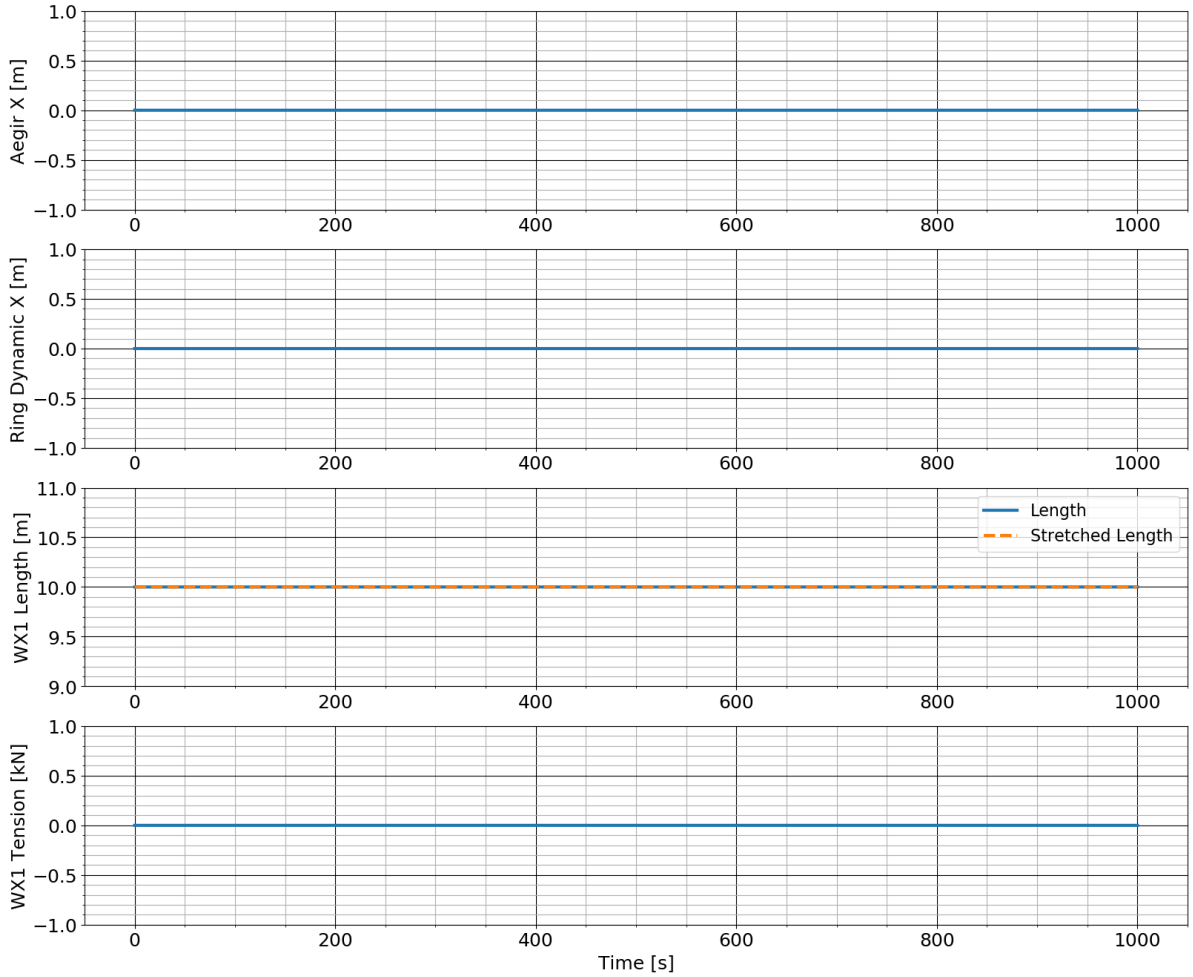

Figure 3.15: Setting environmental forcing is equal to zero yields no displacement of the Aegir, MP ring or change in the length/tension of the winch.

Vary time step: The simulations are run with a time step of 0.1 s and, in order to test if this time step is sufficiently small, the time step of the simulations is varied. When choosing a smaller time step than 0.1 s, the response of the model should not change. Figure 3.16 shows the monopile and vessel response for different time steps. Figure 3.16a shows the response of the monopile and, as shown, the motion is the same for a time step of 0.2 s, 0.1 s or 0.05 s. This means the selected time step of 0.1 s is sufficiently small to correctly model the monopile motions and the PID controller.

Figure 3.16b shows the vessel motions for a simulation that includes only the vessel connected to a spring in an arbitrary sea state. As shown, the vessel motion is identical for all three time steps and the time step is sufficiently small to correctly model the vessel motions. However, when implementing the DP system using the external function, see subsection 3.4.2, the vessel motions do change per time step as indicated in Figure 3.16c. This should not be the case and the error has been reported to HES, as the external function has been provided by the company. The time step of 0.1 s was selected such that the Aegir motions match the data of HMC. Since the vessel motions are not the main focus of this work and the vessel does show realistic behaviour for a time step of 0.1 s, this time step is used in the simulations. In addition, the vessel motions do not influence the monopile motions in case of the perfect system.

Based on the comparison with the frequency domain calculations in section 3.3 it can be concluded that the OrcaFlex model correctly models the motions of the monopile. Furthermore, the basic tests in this section show that the model behaves as expected. Since the monopile motions of the model in OrcaFlex match the frequency domain calculations and the model behaves as expected during the

basic tests described in this section, the simulations of the coupled system can be carried out. This is done in chapter 4, where the various scenarios are tested. First of all, the effect of changing the proportional and derivative control parameters, k_P and k_D, that determine the tension in the winch is simulated. As described in section 3.2 changing the value of the proportional gain k_P leads to resonance of the monopile for some value depending on the forcing period (wave period) and the soil stiffness. Furthermore, increasing the derivative gain k_D leads to a lower response of the monopile close to the resonance area. If the proportional gain is much lower or higher than the value that leads to resonance, adding derivative gain will have virtually no effect on the monopile motions, assuming the controls of the system are perfect. In order to investigate if these findings still hold for the coupled model, simulations are carried out.

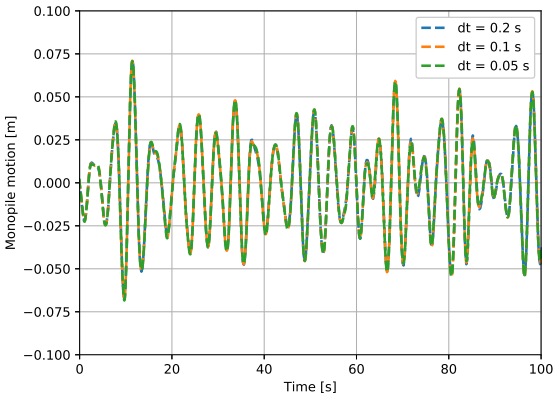

(a) The response of the monopile in x-direction for time steps dt of 0.2 s, 0.1 s and 0.05 s.

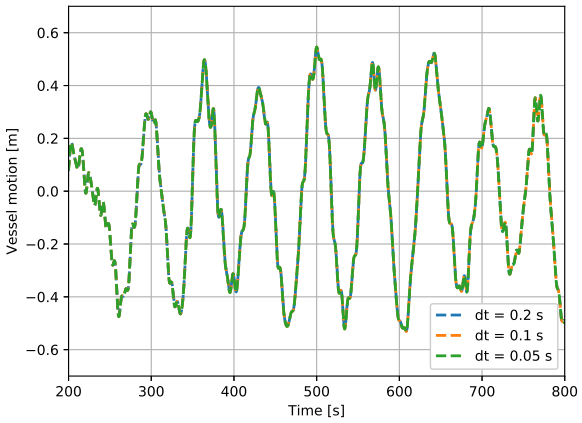

(b) The response of the Aegir in x-direction when connected to a spring for time steps dt of 0.2 s, 0.1 s and 0.05 s.

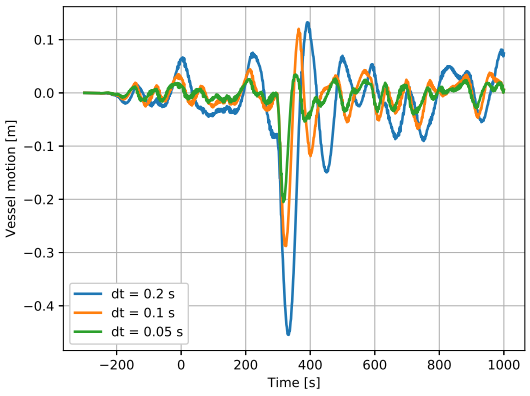

(c) The response of the Aegir when connected to a spring for time steps dt of 0.2 s, 0.1 s and 0.05 s.

Figure 3.16: The response of the monopile and vessel for various time steps dt.

Secondly, the system is tested in case of imperfections in the control system such as a delay in the adjustment of the winch tension. As a base case it is assumed the control system is perfect and the required tension in the winch to keep the monopile stable is instantly reached. However, in the real world a perfect control system does not exist. Therefore, the sensitivity of the system to sensor lag and less efficient motion compensation is modelled as well. When lag is present in the system, the PID controller adjusts the tension based on the error of a few time steps ago.

Another imperfection in the control system is imperfect motion compensation, the scenario where the vessel motions are not perfectly compensated for by the gripper frame. In case of imperfect motion compensation, the winch tension is not only based on the error of the monopile, but on the vessel

motions as well. The efficiency E means to what extent the vessel motions are compensated. In case of an efficiency equal to 1 the motions of the vessel are fully compensated, while an efficiency of 0.7 means the motions of the vessel are compensated for 70 percent only and an additional load is introduced.

4

Results

In the previous chapter the behaviour of only the monopile has been investigated and the set-up of the coupled model has been described. To investigate the behaviour of the coupled system for various values of k_P and k_D, various load cases are simulated. The results of these load cases are presented in this chapter. First of all, the coupled system is tested for various values of k_P for a perfect control system, meaning the required winch wire tension is always obtained instantly and the vessel motions are perfectly compensated, as shown in Figure 3.11. Then the effect of adding a sensor lag in the PID controller is studied, while the motion compensation ability is still perfect. Based on these results a final value of k_P and k_D is selected and simulations are run to determine if these values are suitable. The suitability of these values is based on a few criteria of industry standards for actuators.

The coupled system is simulated for three different cases with respect to controlling the gripper frame ring:

- **Perfect control system**: the required tension in the winch wire based on Equation 3.11 is always obtained instantly. In addition, the vessel motions are fully and instantly compensated and do not influence the monopile motions.
- **Control system with lag**: simulates a time lag τ between the sensor that measures the pile inclination and the movement of the actuators. In the model the tension in the winch wire is based on the monopile motion of a few time steps before. The motion compensation of the vessel is still perfect.
- **Control system with less efficient motion compensation**: it is assumed that the motions of the vessel are not fully compensated, which results in an additional load on the monopile. The efficiency is denoted as E. An efficiency of 0.7 means 70% of the vessel motions are compensated between each time step.

In order to test the behaviour of the coupled system in various sea states and with different control settings and disturbances, the parameters being varied are shown in Table 4.1.

Parameters		Symbol	Values	Units
Wave				
	Wave type	-	JONSWAP	-
	Significant wave height	H_s	1, 2	m
	Peak period	T_p	4, 5, 7	s
	Wave direction	θ	180, 135, 90	°
Gripper Frame				
	Proportional gain	k_P	500 - 100,000	kN/m
	Integral gain	k_I	0	1/s^2
	Derivative gain	k_D	1000 - 11000	kNs/m
Controller				
	Lag	t_{lag}	0.1-0.4	s
	Efficiency	E	0.7-1	-

Table 4.1: Parameters to be varied in the model.

Parameters	Symbol	Unit
Aegir surge at gripper location	x_{Aegir}	m
Aegir sway at gripper location	y_{Aegir}	m
Aegir yaw	$R_{z,Aegir}$	m
x-motion gripper frame ring	x_{ring}	m
y-motion gripper frame ring	y_{ring}	m
x-motion monopile at gf-level	x_{mp}	m
y-motion monopile at gf-level	y_{mp}	m
Winch stretched length	$l_{winch,n}$	m
Winch velocity	$v_{winch,n}$	m/s
Winch tension	$T_{winch,n}$	kN
Winch power	$P_{winch,n}$	kW

Table 4.2: Parameters to be considered in the results.

Figure 4.1 provides a top view of the model to illustrate the different wave directions θ. The directions 180°, 135° and 90° are known as head, bow and beam waves, respectively. Note that 135° is also known as bow quartering, however, this wave direction is hereinafter referred to as bow waves. It is assumed that due to the vessel's symmetry with respect to the x-axis the wave directions between 0-180° yield the same results as the wave directions between 180-360°. Vessel shielding effects are not taken into account, hence, it is assumed the monopile motions are similar for a wave direction of 135° and 45°.

The parameters that will be obtained from the simulations are shown in Table 4.2. The horizontal motions of the vessel are plotted to determine if the gripper frame adequately compensates these motions and to monitor the vessel behaviour during each load case. The motions of the vessel are considered at the gripper frame location, which is the location of Winch Y in Figure 4.1. Secondly, the x- and y-motion at gripper frame level of both the gripper frame ring and the monopile are of interest. Note that the motions of the gripper frame ring and of the monopile are identical, as a rigid connection is assumed. The x- and y-motion of the monopile are chosen instead of the angle of the pile, as this gives more insight in the contributions of Winch X and Winch Y. The force in the actuators is simulated by tension in the winches, so the winch wire tension is obtained as well. The stretched length of the winch gives the distance between the vessel and the gripper frame ring, which would be the required stroke of the actuators moving the gripper frame ring. Furthermore, the velocity of the winch wire is monitored. The product of the velocity and the tension gives the power as shown in Equation 4.1. As mentioned before, in case of the perfect control system the winch tension is only based on the monopile motions and the vessel motions are compensated for perfectly. In subsection 4.3.4 imperfect motion compensation is modelled by adding an additional force to the monopile based on the vessel motions. Note that the winch parameters have a subscript n, since the winch parameters are obtained for both

the x- and y-direction.

$$P_{winch} = T_{winch} v_{winch} \tag{4.1}$$

As a base case for the coupled system simulations a few assumptions are made. First of all, it is assumed that the stiffness of the interface between the monopile and the ring is very high (2 GN/m), resembling the scenario where the monopile is rigidly clamped in the ring with multiple actuators. Furthermore, wind and current forces are not present. Wind loads are neglected, as the motion of the pile is inertia dominated and drag has a negligible effect compared to the inertia forces of the waves. A current merely exerts an additional constant force on the monopile and will not trigger resonance of the coupled system. The constant offset induced by the current is counteracted by enabling the integral gain k_I, but not taken into account in this work.

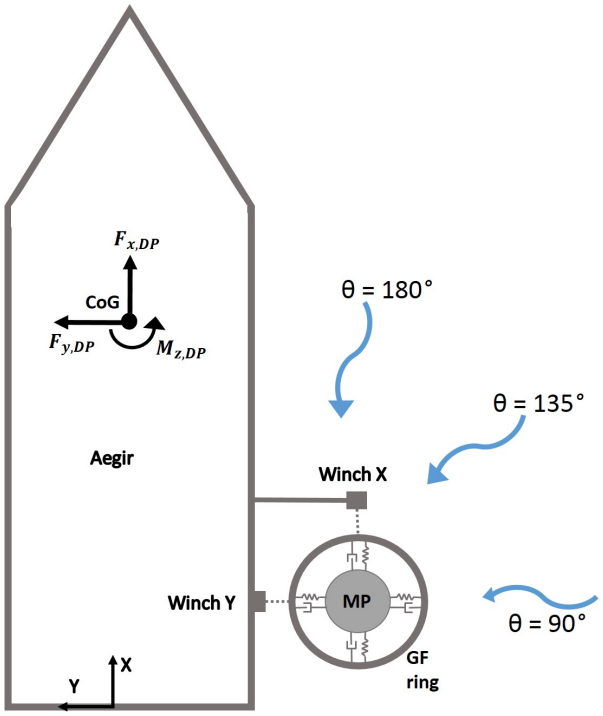

Figure 4.1: Top view of the model showing the wave directions, the global axes, the gripper frame ring connected to the vessel by winches and the monopile inside the ring. Two forces and a moment are applied as global loads at the CoG of the vessel, simulating the DP system of the vessel.

For every load case a simulation of 10800 s with a time step t_{step} of 0.1 s has been run. Every simulation has a build-up period of 300 s during which the wave dynamics and motions of the objects are smoothly increased to their full value to reduce the transient responses.

4.1. Varying k_P and k_D for a Perfect Control System

As described in the previous section, it it assumed that the winch wire always reaches the desired tension in the perfect control system case. In addition, the motion compensation of the vessel motions is perfect, so the vessel motions do not influence the monopile motions. The load cases for the simulations are given in Table A.1. Every load case consists of 15 individual simulations of 10800 s, each with a different proportional gain k_P. The minimum value of k_P is based on the minimum value described in the section 3.5. However, the presence of wave forcing requires a higher minimum than 392 kN/m and the minimum is set to 500 kN/m. Simulations show instability for a k_P larger than 200,000 kN/m, as a very high proportional gain leads to aggressive control. Increasing the k_P more than 100,000 kN/m does not significantly decrease the motions, as the values are going asymptotically to zero. Therefore,

the maximum k_P is set to a 100,000 kN/m.

The time trace of the simulation of load case 1.1 with a k_P of 3000 kN/m is given in Figure 4.2a for the period between t = 0-300 s as an example of one of the individual runs. The motion of the monopile and the resulting tension in the winch wire are plotted and, as shown in the latter figure, the tension opposes the monopile motion to correct the monopile inclination. In order to create a clear overview of the results and show the effect of changing k_P or k_D, the maximum value of each run is obtained instead of showing the 15 time traces of every load case. The results are shown in Figure A.1, Figure A.2 and Figure A.3. These plots show the maximums for every simulation of the load cases in Table A.1.

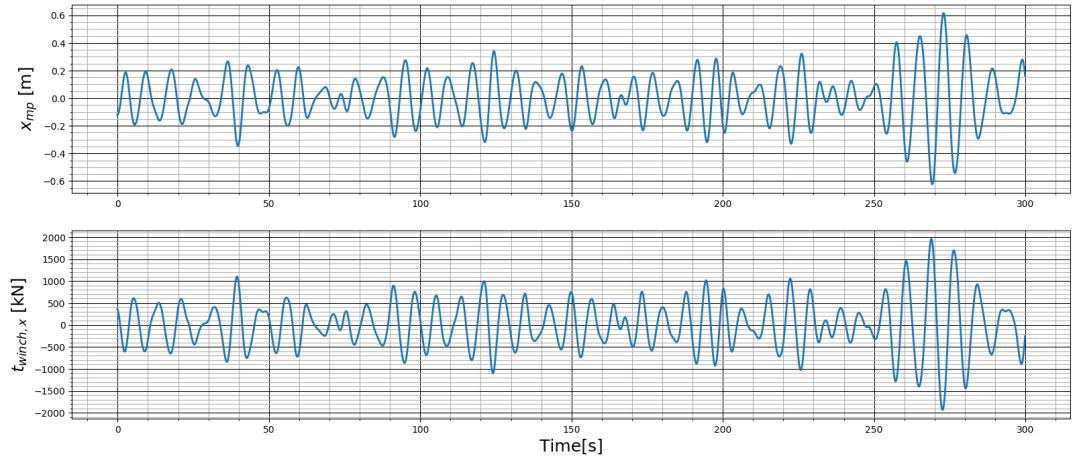

(a) A time trace of the results of load case 1.1 with a k_P of 3000 kN/m.

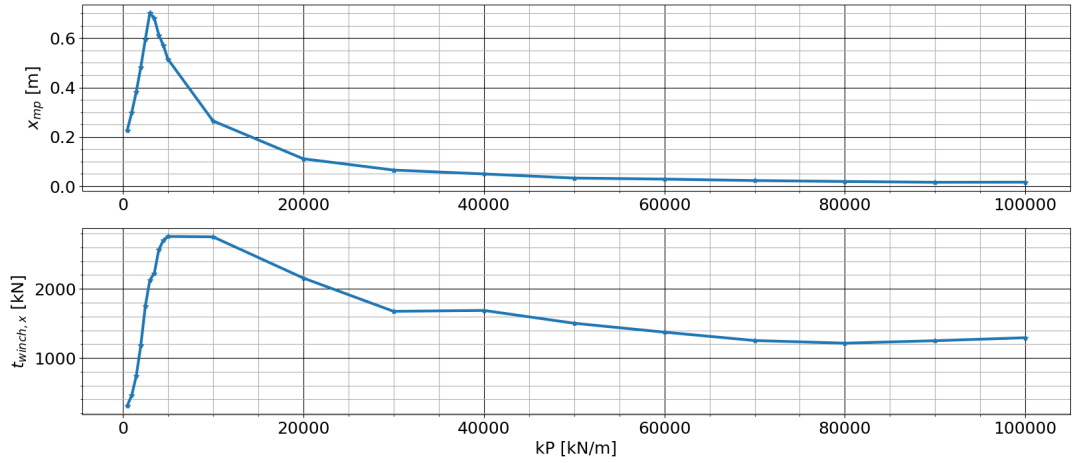

(b) The maximum values for varying proportional gain k_P.

Figure 4.2: The maximum values of the monopile motion and tension based on the individual runs from Table A.1

.

Depending on the wave direction θ the monopile motion is dominant in x- or y-direction. In head waves (180°) the x-motion dominates and the motions in the y-direction are negligible, while in beam waves (90°) the motion in y-direction dominates. For all six load cases there is a clear peak in the motion of the monopile for values of k_P around 3000 kN/m. This is to be expected based on Equation 3.5, since for this value of k_P the natural frequency of the system is close to the wave forcing frequency and, therefore, resonance occurs. Due to the increased monopile motion, the winch wire length and velocity show a peak as well. As a results of the increased velocity, the power required to keep the monopile stable increases as well. Even though the monopile motions are decreasing for k_P larger than 3000 kN/m, the tension still increases until a k_P of 8000 kN/m due to the fact that the k_P is increasing more rapidly than that the monopile motion is decreasing. Hence, the tension, given by the product of the error (offset of MP) and the value of k_P, is increasing. For higher values of k_P the motion of the

monopile is decreased significantly, as a small monopile motion is immediately adjusted with a high force due to the high value of k_P. As a result, all parameters are decreasing.

As described in section 3.2 the effect of adding k_D is most significant close to the resonance area. This is evident when looking at the results. The blue and orange line respectively correspond to a derivative gain of 1000 kNs/m and 2000 kNs/m. The load cases with a higher value of k_D result in less motions of the monopile close to a k_P of 3000 kN/m. Furthermore, the amount of tension in the winch and power required drop significantly as well. However, away from the resonance area the lines coincide and the effect of k_D is limited.

The Aegir hardly shows any motion for head waves as shown in Figure A.1. This direction minimises the area of the vessel perpendicular to the incoming waves and, therefore, the vessel shows limited motion. There is a slight increase in vessel motions when the monopile motions show a peak due to the increased loads on the vessel at this stage. For bow waves (θ = 135°), the vessel motion in y-direction is increased compared to head waves, since the waves are now impacting the side of the vessel. However, the vessel motions remain relatively small. Only beam waves (θ = 90°) result in large vessel motions in y-direction, as side of the vessel is fully exposed to the incoming waves. The resulting vessel motions do not result in a higher motion of the monopile, since the motion compensation ability is still assumed to be perfect.

Based on the results in Figure 4.2 the monopile motions and the resulting stroke, tension and power would be minimised for very high values of k_P. It is possible to have a stable system for these high values of k_P as the instantaneous position of the body is always known and responded to instantly by the PID controller. In reality, there is always a slight delay or inaccuracy in the system. Therefore, the influence of a lag in the system on the monopile motions is investigated in the next section.

4.2. Varying k_P and k_D With Lag

In the previous section it was assumed that the instantaneous position of the pile is always known and the required tension to keep the pile upright is always reached instantly. However, in the real world the control and actuator system are never perfect. Therefore, the coupled system is analysed for different values of lag in the system. It is assumed that the required tension, based on Equation 3.11, is exerted on the monopile with a time lag τ. This lag is implemented by feeding the error measured τ seconds before into the PID controller instead of the current error of the monopile. First of all, the effect of introducing lag on the stability of the monopile is investigated for the monopile only based on the model presented in section 3.2. This is then compared to the results obtained in the OrcaFlex model.

4.2.1. Introducing Lag in the Model: Analytical Solution

As the assumption of perfect motion compensation is still applied in this section, the monopile motions are not influenced by the vessel motions and, therefore, the model of only the monopile described in section 3.2 is applicable to the coupled model as well. In case of a time lag τ, the force applied by the PID controller to correct for the monopile inclination is not applied instantly. Instead the force is applied τ seconds later. The linearised PID force including the delay τ is then described by:

$$F_{PID} = k_P l_{gf} \sin(\theta(t-\tau)) + k_D l_{gf} \sin(\dot{\theta}(t-\tau)) \approx k_P l_{gf} \theta(t-\tau) + k_D l_{gf} \dot{\theta}(t-\tau) \tag{4.2}$$

When assuming a solution $\theta(t) = X_n e^{s_n t}$ and $\theta(t) = X_n e^{s_n (t-\tau)}$ the characteristic equation is complicated and solving for s_n is not straightforward. Therefore, another method is used [15]. The angle and angular velocity of the pile is expanded in series and linearising based on the assumption that the delay τ is relatively small compared to the period of the pile motion. This gives the following approximation of the delayed pile motion and angular velocity:

$$\theta(t-\tau) = \theta(t) - \dot{\theta}(t)\tau \tag{4.3}$$

$$\dot{\theta}(t-\tau) = \dot{\theta}(t) - \ddot{\theta}(t)\tau \tag{4.4}$$

Substitution of the two equations above (Equation 4.3 and Equation 4.4) into the Equation 4.2 yields the following equation of motion in case of a lag τ:

$$\left(I_{tot} - k_D l_{gf}^2 \tau\right) \ddot{\theta}(t) + \left(k_D - k_P \tau\right) l_{gf}^2 \dot{\theta}(t) + \left(k_P l_{gf}^2 - mgl_{\text{cog}}\right) \theta(t) = M_{env} \cos(\omega_f t) \tag{4.5}$$

Note that when the delay in the system is equal to zero Equation 4.5 is equal to the original equation of Equation 3.2. Furthermore, for increasing values of τ both the inertia and damping term are decreased.

In order to investigate the stability of the system for various values of lag, the equation of motion of the free vibration is investigated. In case of a free vibration there is no external forcing and the right hand side of Equation 4.5 is equal to zero, resulting in Equation 4.6.

$$\underbrace{\left(I_{tot} - k_D l_{gf}^2 \tau\right)}_{I} \ddot{\theta}(t) + \underbrace{\left(k_D - k_P \tau\right) l_{gf}^2}_{c} \dot{\theta}(t) + \underbrace{\left(k_P l_{gf}^2 - mgl_{\text{cog}}\right)}_{k} \theta(t) = 0 \tag{4.6}$$

The equation of motion above is rewritten in the form:

$$\ddot{x} + 2n\dot{x} + \omega_n^2 x = 0 \tag{4.7}$$

where n and ω_n are given by:

$$\omega_n^2 = \frac{k}{I} = \frac{k_P l_{gf}^2 - mgl_{\text{cog}}}{I_{tot} - k_D l_{gf}^2 \tau} \tag{4.8}$$

$$2n = \frac{c}{I} = \frac{k_D - k_P \tau}{I_{tot} - k_D l_{gf}^2 \tau} \tag{4.9}$$

Assuming the general solution of the second order equation:

$$x(t) = \sum_{n=1}^{2} X_n \exp\left(s_n t\right) \tag{4.10}$$

Substituting the assumed solution into the equation of motion and rewriting the equation using Equation 3.5 and Equation 3.6 gives the following characteristic equation:

$$s_n^2 + 2ns_n + \omega_n^2 = 0 \tag{4.11}$$

Then solving for the characteristic exponents s_n of the above equation:

$$s_1 = -n + \sqrt{n^2 - \omega_n^2}, \quad s_2 = -n - \sqrt{n^2 - \omega_n^2} \tag{4.12}$$

The general solution then becomes:

$$x(t) = X_1 \exp\left(s_1 t\right) + X_2 \exp\left(s_2 t\right) \tag{4.13}$$

The solution grows to infinity over time for any real value of s_n > 0. Hence, system is stable in case the real part of s_n < 0. When looking at Equation 4.5 the system becomes unstable in case the inertia, damping or stiffness term becomes negative. As shown in the latter equation, the delay τ does not influence the stiffness term in this case.

Figure 4.3 plots the real part of the solutions of the characteristic equations as a function of k_P for a k_D of 1000 kNs/m and various values of τ. As the damping (k_D) is relatively small compared to the 'spring' term k_P, the value of n is smaller than the value of ω_n. As a result, the real part of the solution only depends on n, since the value of $\sqrt{n^2 - \omega_n}$ is imaginary, and the real part of s_1 and s_2 is the same in this case. As depicted in the latter figure, for an increasing value of τ the system is unstable for a lower value of kP as the damping term c becomes negative for increasing values of τ, see Equation 4.6. For example, in case of a delay of τ = 0.1 s the system is unstable for a value of k_P > 10,000 as the real part of s_n is larger than zero in this case. Setting the damping term (k_D - $k_P\tau$) larger than zero, yields that the system is unstable for a $k_P > \frac{k_D}{\tau}$. Hence, if the value of k_D is increased the value of τ for which the system becomes unstable due to negative damping increases. This corresponds to the fact that

k_D increases the phase margin from a control point of view and, therefore, allows for higher values of lag before the controller is unstable. On the other hand, if the value of k_D is increased the inertia term I becomes smaller, see Equation 4.6 and the system is also unstable in case $I < 0$.

Whereas the value of k_P can be increased to values of 100,000 kN/m in case of a 'perfect' control system and a k_D of 1000 kNs/m, it is expected that the system shows instability for higher values of k_P in case of lag. In the next section the coupled model is tested for various values of lag and the results of the OrcaFlex model are compared to the results in this section.

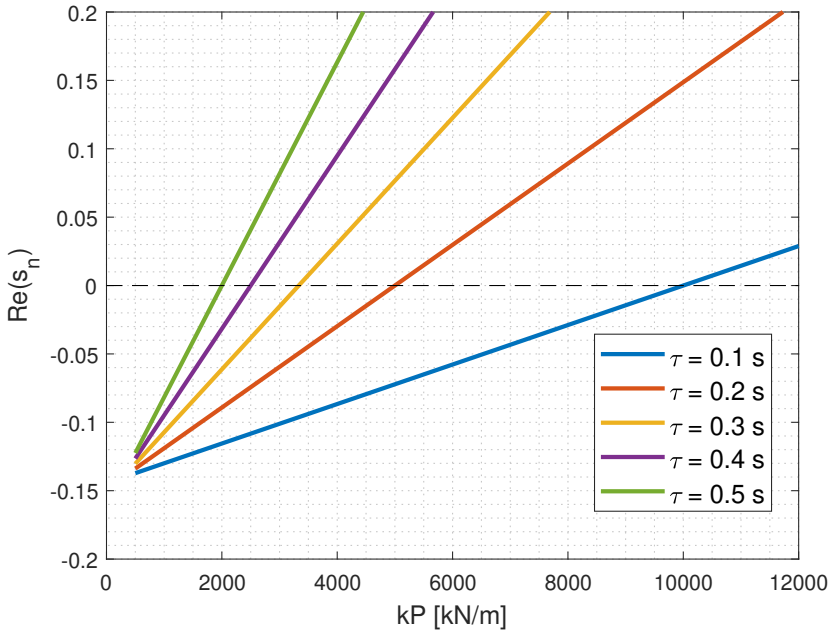

Figure 4.3: The solutions of the characteristic equation s_1 and s_2 in Equation 4.12 as function of the delay τ. The system is stable if the real part of the solution s_n is smaller than 0.

4.2.2. Introducing Sensor Lag in the Model: OrcaFlex Model

Based on the findings presented in subsection 4.2.1 the model is expected to show instability for increasing values of k_P when a delay τ is introduced. The value for which the system is unstable depends on the value of k_D and delay τ. In this section the value of k_D is equal to 1000 kNs/m and the system is tested for various values of k_P and delay τ. The amount of lag per load case is given in Table 4.3. The motion compensation of the vessel motions is still assumed to be perfect.

The delay is implemented by changing the external function of the PID controller that controls the winch wire tension (the green block in Figure 3.6). The monopile motions are saved and based on the value of τ the error $e(t-\tau)$ is obtained. Figure 4.4 illustrates the effect of adding lag. It shows the actual position of the monopile in blue and the position of the monopile that is fed into the PID controller in orange in case of a delay of 0.1 s. As depicted in the figure, the monopile motion that is fed into the PID controller is slightly delayed compared to the actual position of the monopile. For an increase in lag the orange line is shifted further to the right since $\theta(t-\tau)$.

LC	Wave	PID settings ring controller	Lag
2.1 a-e	JONSWAP, H_s = 1 m, T_p = 7 s, θ = 180°	range 1: k_P = 500-5000 kN/m (Δk_P = 500) range 2: k_P = 1e4-10e4 kN/m (Δk_P = 1e4) k_I = 0 kN/ms k_D = 1000 kNs/m	τ = 0.1-0.5 s with $\Delta\tau$ = 0.1 s

Table 4.3: Load cases for varying values of lag τ.

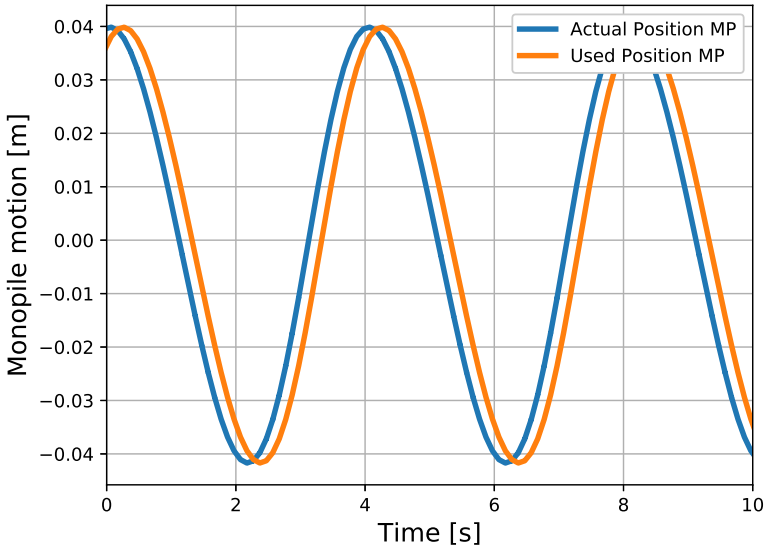

Figure 4.4: The effect of adding a delay of 0.1 s. The position of the monopile that is fed into the PID controller is delayed compared to the actual monopile position represented by the blue and orange line, respectively.

As expected based on results in the previous section the system shows instability for much lower values of k_P now that the control system is not perfect anymore. This is shown in Figure B.2 and Figure B.3. A time trace of the monopile motion x_{mp} and y_{mp} is shown in Figure B.1. The motion of the monopile is increasing and at some point the monopile falls over. Note that the monopile motions and winch wire tension are extremely high in this case. Figure B.2 and Figure B.3 also show that the pile motion and tension in the winch wire are increasing drastically for higher values of k_P in case of lag.

For larger values of τ the maximum value of k_P before the monopile is falls over is decreased. Table 4.4 shows the k_P for which the system is still stable, for any higher values the monopile falls over. The results of the OrcaFlex model correspond to the findings presented in Figure 4.3. Only for a lag of τ = 0.1 s the results do not match, as the system is still stable for a k_P of 11,000 kN/m, while the analytical solution shows instability for a k_P > 10,000 kN/m. However, this simulation shows a pile motion over 5.6 m at gripper frame level and a tension in the winch wire of 60,000 kN. The pile does not fall over due to the increase in drag force as a result of the high velocity of the pile, which adds damping to the pile. This is neglected in the analytical solution in subsection 4.2.1 and is justified for smaller pile motions. However, even though the pile does not fall over the position and winch wire tension are unrealistically high in practice.

Lag τ [s]	Maximum k_P [kN/m] before instability of monopile for k_D = 1000 kNs/m
0.1	11000
0.2	5000
0.3	3000
0.4	2500
0.5	2000

Table 4.4: The maximum value of k_P for which the system is still stable when a lag is introduced for a kD of 1000 kNs/m.

In conclusion, for a system with perfect control virtually any value of k_P and k_D may be chosen. However, when simulating a more realistic system with lag involved the choice of parameters is more critical. A high value of k_P leads to instability when lag is present in the system if the value of k_D is not high enough to ensure a positive total damping term.

4.3. Selecting Suitable Values of Proportional and Derivative Gain

In previous sections the effects of changing k_P and k_D for a system with perfect motion compensation and a perfect PID controller was shown. Furthermore, it has been shown that the system becomes unstable for high values of k_P in case of lag and that this instability may be avoided by increasing the derivative gain. In this section, a final choice of the proportional and derivative gain is made based on the findings in previous sections. The system is then tested for the perfect system in different conditions, with lag in the system and with imperfect motion compensation to determine if the values selected are suitable.

Choosing the right parameters is always a trade-off. On the one hand, a high k_P leads to lower monopile motions and lower forces if the control system is working well. On the other, in case of imperfections in the system, such as a delay, a high k_P increases the monopile motion and can even lead to instability of the monopile (it falls over). A higher k_D reduces the instability due to lag. However, adding damping to the system means the energy in the system has to be dissipated, which increases the complexity and costs of the system. Therefore, the aim is to select a k_P which limits the monopile motions, but at the same time does not require an extreme amount of derivative gain to cope with lag in the system.

The system should be stable for all wave periods that are expected during the installation, which is in the range of T_p = 4-10 s. As discussed in section 3.2 the system is expected to show resonance for a k_P around 6000 kN/m without the ring. Including the mass moment of inertia of the gripper frame ring, resonance is expected for a value of 7000 kN/m. Hence, to avoid resonance of the pile a high k_P should be selected. One could argue that a very low value of k_P could work in case of low wave periods, as the low values of k_P are away from the resonance peak as well. However, when hammering the monopile into the soil, the soil stiffness is increased, leading to resonance for a low value of k_P as well at some point in time. Based on the fact that for the lowest peak period resonance is expected at 7000 kN/m, a k_P of 10,000 kN/m is selected.

Furthermore, the pile motions should be limited to 0.25°, as this is the installation tolerance. In order to limit the pile motion to this particular value, a k_D of 3700 kNs/m is required for the perfect control system based on experience and previous results. However, it is likely that with lag, imperfect motion compensation and higher wave heights, a higher k_D should be selected. Therefore, simulations are also performed for a k_D of 11,000 kNs/m. The two settings are presented in Table 4.5. Both settings are tested for the perfect system, the sensor lag and the imperfect motion compensation and the results are presented in subsection 4.3.1, subsection 4.3.3 and subsection 4.3.4.

	kP [kN/m]	kD [kNs/m]
Setting 1	10,000	3700
Setting 2	10,000	11,000

Table 4.5: The two settings for k_P and k_D.

To determine whether the selected values are adequate settings for the system a few criteria the system should meet are set up:

1. The maximum pile inclination may be ±0.25°, which is equal to a motion of ±0.22 m at a gripper frame level of 51 m.
2. The maximum tension or compression in the winch wire should be ±3000 kN/m, as this is a reasonable limit for industry actuators.
3. The maximum stroke should be less than ±2.5 m, which is the stretched length of the winch and the distance between the gripper frame ring and the vessel. A very long stroke of the actuators is unfavourable from a structural point of view, as a larger gripper frame requires a stronger and heavier design. On the other hand, the stroke should be sufficienctly large to adequately compensate for the vessel and monopile motions.

Furthermore, a reasonable maximum velocity of the actuators is around 0.2-0.3 m/s. However, based on the load cases in previous section the velocity is not an issue if the pile motions are within the limit and not presented in the results of this chapter.

4.3.1. Analysis Perfect System

Firstly, the perfect system is analysed for two different wave directions. The vessel shows movement of 1.4 m in sway direction for beam waves (θ = 90°) with a period of 7 s and a wave height of only 1 m, as shown in Figure A.3. Thus, it is not desirable to install the monopile with the vessel perpendicular to the waves as this yields large vessel motions. Shielding effects are not taken into account, so it is assumed waves from 135° or 215° yield the same results. Therefore, head waves (180°) and bow waves (135°) are simulated. The wave height is initially set to 1 meter and a peak period of 4 s is selected, as this value gives a resonance area closest to the selected value of k_P and, thus, the highest monopile motions. The load cases are represented in Table 4.6 and the a and b correspond to setting 1 and setting 2, respectively.

LC and PID settings		Wave Spectrum
3.1	a) Setting 1 b) Setting 2	JONSWAP, H_s = 1 m, T_p = 4 s, θ = 180°
3.2	a) Setting 1 b) Setting 2	JONSWAP, H_s = 1 m, T_p = 4 s, θ = 135°

Table 4.6: Load cases for the perfect system.

The results are presented in Table 4.7 to Table 4.10 as the mean, maximum, minimum and standard deviation. As the motions are harmonic the minimum and the maximum are the same order of magnitude, however, depending on the wave direction either the minimum or maximum value is critical. The results of the motion of the monopile and the winch tension in both x- and y-direction are presented graphically in Figure 4.5. The red line corresponds to the maximum allowable value described in the criteria in the beginning of this section. As shown in Figure 4.5 the maximum and minimum motion of the monopile do not exceed the value of 0.22 m for a k_D of 3700 kNs/m. For the values of k_D 11,000 kNs/m the values are even smaller.

In conclusion, for waves of the JONSWAP spectrum with a peak period of 4 s and a significant wave height of 1 m both settings shown in Table 4.5 meet all criteria mentioned at the beginning of this section. In the next section the system is subject to higher peak periods and wave heights.

Variables	Unit	Mean	Max	Min	Std
x_{mp}	m	-0.00	0.216	-0.204	0.041
y_{mp}	m	-0.00	0.002	-0.002	0.000
$t_{winch,x}$	kN	5.71	2456.444	-2657.865	499.528
$t_{winch,y}$	kN	0.07	22.093	-20.192	3.023
x_{Aegir}	m	-0.03	0.023	-0.223	0.028
y_{Aegir}	m	0.03	0.125	-0.013	0.019
$R_{z,Aegir}$	°	-0.03	0.013	-0.115	0.018

Table 4.7: Results of load case 3.1a.

Variables	Unit	Mean	Max	Min	Std
x_{mp}	m	-0.00	0.075	-0.092	0.015
y_{mp}	m	-0.00	0.000	-0.000	0.000
$t_{winch,x}$	kN	2.97	1722.162	-1825.141	333.927
$t_{winch,y}$	kN	0.03	5.594	-3.836	0.601
x_{Aegir}	m	-0.02	0.039	-0.167	0.020
y_{Aegir}	m	0.02	0.059	-0.003	0.009
$R_{z,Aegir}$	°	-0.01	0.003	-0.054	0.008

Table 4.8: Results of load case 3.1b

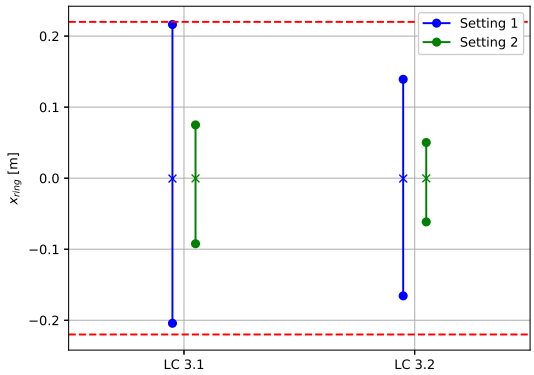

(a) The x-motion of the monopile for both settings in load cases 3.1 and 3.2.

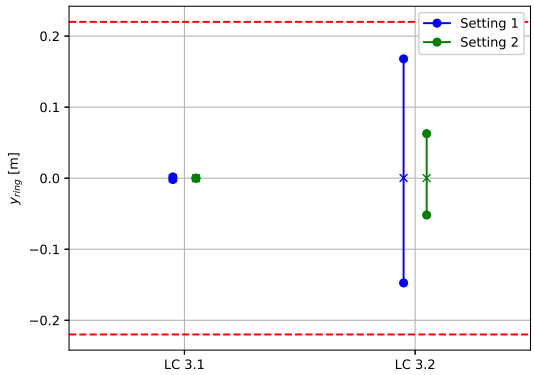

(b) The y-motion of the monopile for both settings in load cases 3.1 and 3.2.

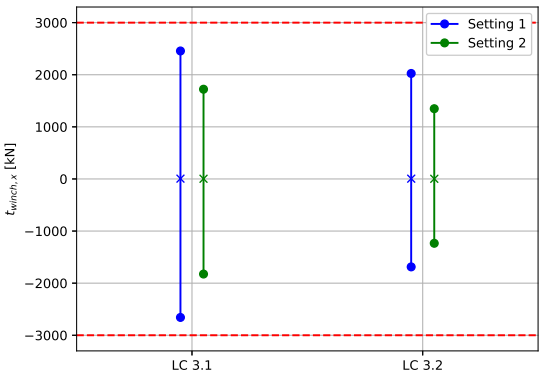

(c) The maximum tension in the winch wire in x-direction $t_{winch,x}$ for both load cases 3.1 and 3.2.

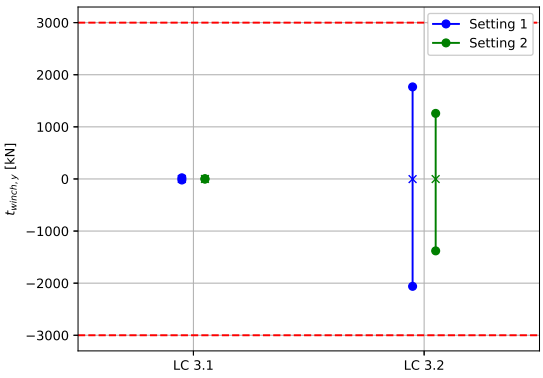

(d) The maximum tension in the winch wire in y-direction $t_{winch,x}$ for both load cases 3.1 and 3.2.

Figure 4.5: Graphical representation of the results of load cases 3.1 and 3.2.

Variables	Unit	Mean	Max	Min	Std
x_{mp}	m	-0.00	0.139	-0.166	0.029
y_{mp}	m	0.00	0.168	-0.147	0.029
$t_{winch,x}$	kN	5.03	2024.793	-1687.751	351.800
$t_{winch,y}$	kN	-2.91	1766.954	-2060.839	356.171
x_{Aegir}	m	-0.04	0.140	-0.233	0.035
y_{Aegir}	m	0.07	0.492	-0.264	0.072
$R_{z,Aegir}$	°	-0.06	0.210	-0.185	0.057

Table 4.9: Results of load case 3.2a

Variables	Unit	Mean	Max	Min	Std
x_{mp}	m	-0.00	0.050	-0.062	0.011
y_{mp}	m	0.00	0.063	-0.052	0.011
$t_{winch,x}$	kN	2.29	1348.371	-1234.852	235.669
$t_{winch,y}$	kN	-1.90	1258.481	-1380.275	237.322
x_{Aegir}	m	-0.02	0.181	-0.160	0.036
y_{Aegir}	m	0.04	0.388	-0.399	0.083
$R_{z,Aegir}$	°	-0.03	0.337	-0.198	0.076

Table 4.10: Results of load case 3.2b

4.3.2. Analysis Perfect System for Increasing Wave Height and Period

In order to determine if the perfect system still meets the criteria in case of larger wave height and period, the system is subject to wave spectra with larger peak period and wave heights. The system is tested for the upper and lower peak period corresponding to a significant wave height of 2 m according to Equation 2.1, which results in the load cases presented in Table 4.11.

The results have been represented graphically in Figure 4.6. For all the load cases, setting 1 does not satisfy the criteria. For load case 4.4, the individual motions in the x- and y-direction are within the limits. However, when taking into account the total displacement using Pythagoras term ($\sqrt{x^2 + y^2}$), the total motion exceeds the maximum of 0.22 m. Therefore, the tables showing the results of setting 1 have been put in Appendix C and in this section only the results of setting 2 are discussed. The monopile motions are within the limit for all four load cases, but the maximum force is exceed in case of head waves with a peak period T_p of 5.1 s (load case 4.1). In bow waves the load on the monopile is divided over both actuators in x- and y-direction and, as a result, the maximum force is within the limits for load case 4.2b, see Figure 4.6c and Figure 4.6d. Hence, bow waves allow a higher significant wave height compared to head waves. As shown in Table 4.13, vessel motions are significantly increased for bow waves due to the increase in area of the vessel hull that is exposed to the incoming waves. This is illustrated in Figure 2.12 as well, since the limiting wind speed is much higher in case of a wind direction of 0° compared to a wind direction of 45°.

For a higher period the forcing frequency is lower and further away from the natural frequency and, as a result, the motion and forces are lower compared to a wave period of 7 s. This is shown when comparing load cases 4.1 and 4.3 or 4.2 and 4.4 in Figure 4.6. Whereas the monopile motions are decreasing, the vessel motions are increasing in the direction of the wave height. When comparing the results of the wave period of 5.1 s in Table 4.14 to a wave period of 7 s in Table 4.15, the vessel motions in the direction of the incoming wave (135°) are increased. This is shown by the increased minimum in the x-direction and the increased maximum of the y-direction. The rotation of the vessel is smaller, since the rotation is mainly due to the gripper frame force at the side of the vessel and the tension is lower for the 7 s wave period.

LC and PID settings		Wave Spectrum
4.1	a) Setting 1 b) Setting 2	JONSWAP, H_s = 2 m, T_p = 5.1 s, θ = 180°
4.2	a) Setting 1 b) Setting 2	JONSWAP, H_s = 2 m, T_p = 5.1 s, θ = 135°
4.3	a) Setting 1 b) Setting 2	JONSWAP, H_s = 2 m, T_p = 7 s, θ = 180°
4.4	a) Setting 1 b) Setting 2	JONSWAP, H_s = 2 m, T_p = 7 s, θ = 135°

Table 4.11: Load cases for higher significant wave height.

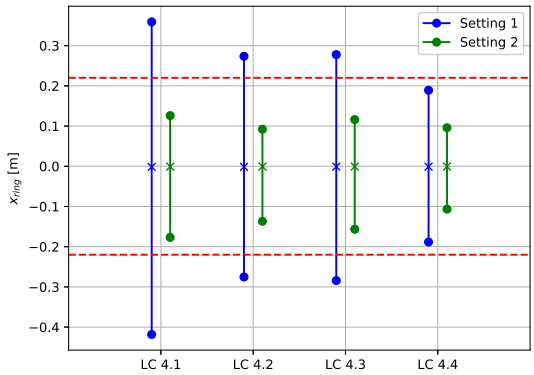

(a) The x-motion of the monopile for both settings in load cases 4.1 to 4.4.

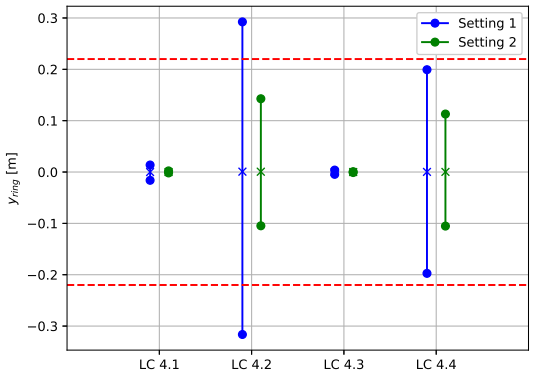

(b) The y-motion of the monopile for both settings in load cases 4.1 to 4.4.

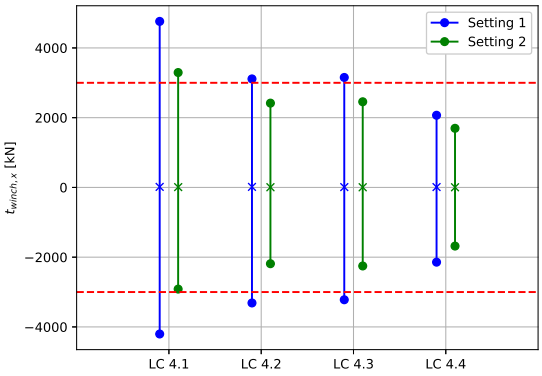

(c) The maximum tension in the winch wire in x-direction $t_{winch,x}$ for both load cases 4.1 to 4.4.

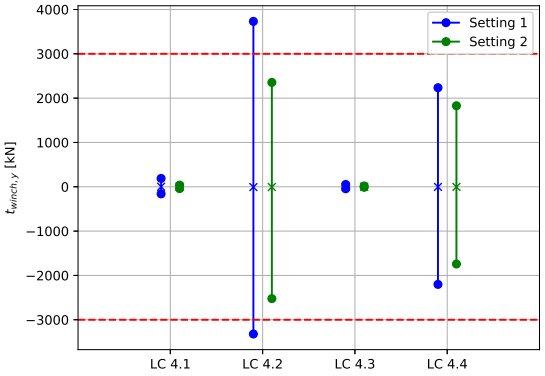

(d) The maximum tension in the winch wire in y-direction $t_{winch,x}$ for both load cases 4.1 to 4.4.

Figure 4.6: Graphical representation of the results of load cases 4.1 to 4.4.

Variables	Unit	Mean	Max	Min	Std
x_{mp}	m	-0.00	0.126	-0.177	0.035
y_{mp}	m	-0.00	0.002	-0.002	0.000
$t_{winch,x}$	kN	8.80	3294.582	-2915.373	652.366
$t_{winch,y}$	kN	0.15	38.343	-40.985	3.994
x_{Aegir}	m	-0.05	0.208	-0.709	0.105
y_{Aegir}	m	0.05	0.218	-0.073	0.033
$R_{z,Aegir}$	deg	-0.04	0.069	-0.202	0.031

Table 4.12: Results of load case 4.1b.

Variables	Unit	Mean	Max	Min	Std
x_{mp}	m	-0.00	0.092	-0.137	0.025
y_{mp}	m	0.00	0.143	-0.105	0.025
$t_{winch,x}$	kN	7.22	2417.122	-2187.679	458.824
$t_{winch,y}$	kN	-5.46	2354.783	-2523.259	471.693
x_{Aegir}	m	-0.05	0.734	-0.692	0.177
y_{Aegir}	m	0.09	1.618	-1.755	0.418
$R_{z,Aegir}$	deg	-0.07	1.498	-1.282	0.375

Table 4.13: Results of load case 4.2b.

Variables	Unit	Mean	Max	Min	Std
x_{mp}	m	-0.00	0.116	-0.157	0.036
y_{mp}	m	-0.00	0.001	-0.001	0.000
$t_{winch,x}$	kN	6.02	2456.392	-2252.371	595.842
$t_{winch,y}$	kN	0.20	18.872	-11.659	2.367
x_{Aegir}	m	-0.04	0.233	-0.474	0.088
y_{Aegir}	m	0.03	0.113	-0.017	0.018
$R_{z,Aegir}$	deg	-0.03	0.016	-0.104	0.017

Table 4.14: Results of load case 4.3b.

Variables	Unit	Mean	Max	Min	Std
x_{mp}	m	-0.00	0.096	-0.107	0.025
y_{mp}	m	0.00	0.113	-0.105	0.026
$t_{winch,x}$	kN	5.47	1695.116	-1681.702	419.378
$t_{winch,y}$	kN	-2.66	1828.065	-1742.117	425.740
x_{Aegir}	m	-0.03	0.431	-0.772	0.131
y_{Aegir}	m	0.05	2.135	-0.830	0.311
$R_{z,Aegir}$	deg	-0.03	0.954	-0.729	0.222

Table 4.15: Results of load case 4.4b.

4.3.3. Analysis Sensor Lag

Both settings of the system are tested for various values of lag. Following the same procedure as described in subsection 4.2.1 the values of the characteristic exponents s_1 and s_2 are plotted in Figure 4.7. For setting 1 the value of n remains smaller than ω_n and the roots s_1 and s_2 are complex, comparable to subsection 4.2.1. For setting 2 the value of n becomes larger than ω_n for increasing values of τ, as the inertia term I is decreasing faster due to the high value of k_D. The value of ω_n is proportional to $\sqrt{I^{-1}}$, while the value of n is proportional to I^{-1}. As a result, the value of n is increasing more rapidly than the value of ω_n and the roots s_1 and s_2 are real for increasing values of τ. As a result, the real part of s_1 and s_2 is no longer equal, as shown in Figure 4.7b. At the moment the values of the roots are real, the damping term is higher than the critical damping $c_{crit} = 2\sqrt{kI}$ and the system is critically damped.

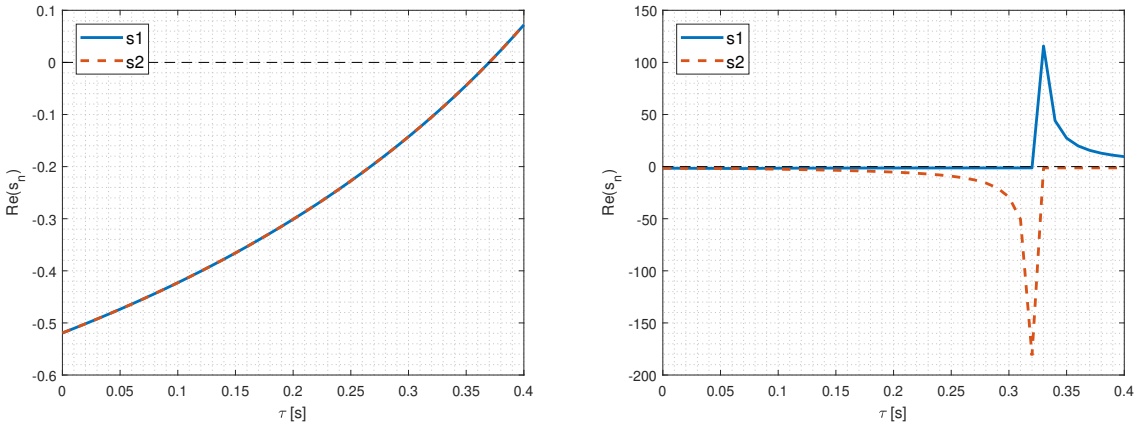

(a) The real part of the characteristic exponents s_n for setting 1.

(b) The real part of the characteristic exponents s_n for setting 2.

Figure 4.7: The real part of the characteristic exponents s_n for both settings.

In case the case of setting 2, numerical instability is observed in the OrcaFlex simulations if the Young's Modulus, a measure of the monopile stiffness, is equal to the standard value of 212 GPa. This numerical instability is solved when assuming a rigid monopile by increasing the Young's Modulus to an

unrealistically high value of 1e6 GPa. The cause of the numerical instability has not been identified, but numerical instability is only observed for setting 2 and is related to the fact that the inertia term I is much smaller compared to the damping term. For the other cases (load case 2.1, 5.1a and 5.2a) the system is unstable for increasing values of τ due to the fact that the total damping term becomes negative. In case of setting 2, it is the total inertia term instead of the damping term that becomes negative for increasing values of τ, which leads to instability. To ensure the rigidity of the monopile does not influence the results, the response of the rigid monopile is compared to the response of the monopile with the standard Young's modulus. In Figure 4.8 the response of the rigid and non-rigid monopile in an arbitrary sea state is plotted. The latter figure shows the monopile response is the same for a rigid and non-rigid pile. Hence, to avoid numerical instability the rigid monopile is used for simulations of setting 2 in this subsection.

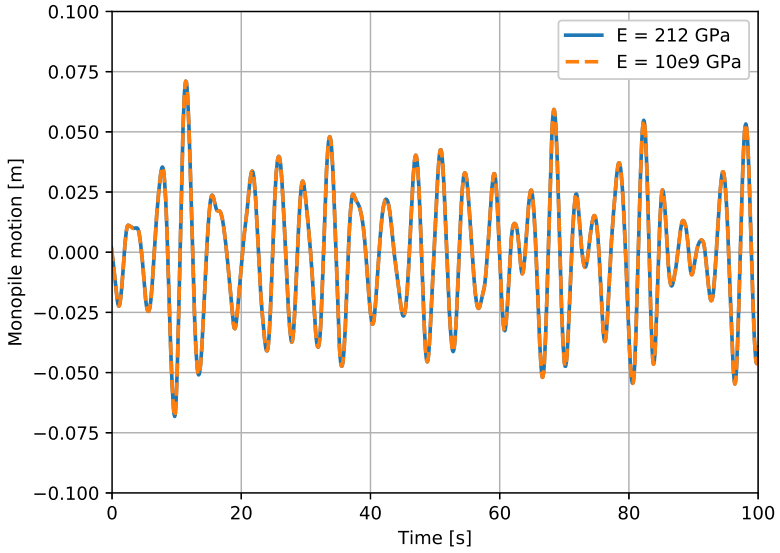

Figure 4.8: Comparing the response of the rigid monopile (E = 10e6 GPa) to that of a non-rigid monopile (E = 212 GPa.

Based on the analytical results it is expected that the OrcaFlex model shows instability for values of τ > 0.3 s for both settings. The environmental conditions are the same as load case 3.1, see Table 4.6. This yields the load case presented in Table 4.16. The results are shown graphically in Figure 4.9 and the tables with the results are presented in Appendix D.

For both settings in both environments the monopile is unstable, meaning it falls over, for a lag τ larger than 0.3 s, which is expected based on the analytical solution. The results show a similar trend as the results in subsection 4.2.2 and the motions of the pile and tension in the winch are increasing for larger values of τ. It should be noted that even though the pile does not fall over for a τ of 0.3 s, the values of the monopile motion and winch tension exceed the realistic values for setting 1. Furthermore, setting 1 does not meet the criteria for any value of lag for both load cases. For a lag of 0.1 s already results in monopile motions exceeding the first criterion regarding the maximum motion of the pile for both load case 5.1 and 5.2. For the latter load case the maximum motion is exceeded when taking the total motion by $\sqrt{x_{mp} + y_{mp}}$, even though the individual motions in x- and y-direction are within the limits.

For setting 2 an increase in monopile motions and winch tension is observed as well. Setting 2 meets the criteria for all load cases, except for load case 5.1 with τ = 0.3 s. In this case, the minimum winch tension in the x-direction is exceeded, see Figure 4.9c. As expected based on the analytical results, the monopile falls over in case of a lag exceeding 0.3 s for setting 2 as well. In case of head waves the maximum allowable lag is 0.2 s. For bow waves the maximum lag is 0.3 s, as the force is distributed over both actuators in this case.

LC and PID settings		Wave	Lag
5.1	a) Setting 1 b) Setting 2	JONSWAP, H_s = 1 m, T_p = 4 s, θ = 180°	τ = 0.1-0.4 s with $\Delta\tau$ = 0.1 s
5.2	a) Setting 1 b) Setting 2	JONSWAP, H_s = 1 m, T_p = 4 s, θ = 135°	τ = 0.1-0.4 s with $\Delta\tau$ = 0.1 s

Table 4.16: Load cases for lag for both settings.

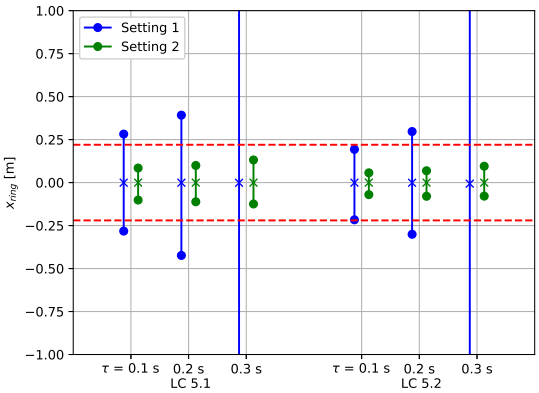

(a) The x-motion of the monopile for both settings in load cases 5.1 and 5.2.

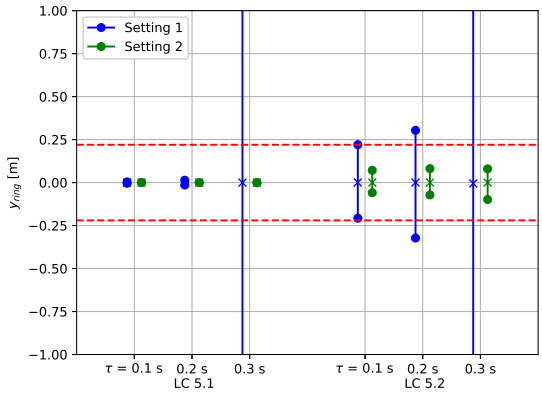

(b) The y-motion of the monopile for both settings in load cases 5.1 and 5.2.

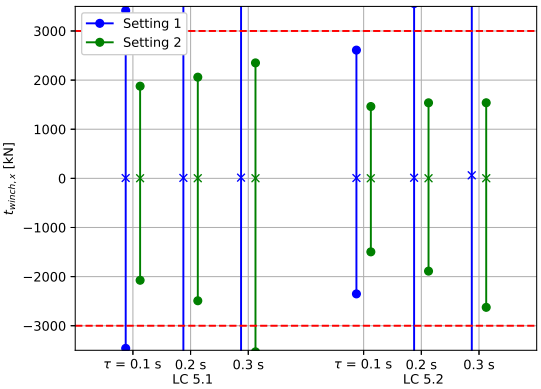

(c) The maximum tension in the winch wire in x-direction $t_{winch,x}$ for both load cases 5.1 and 5.2.

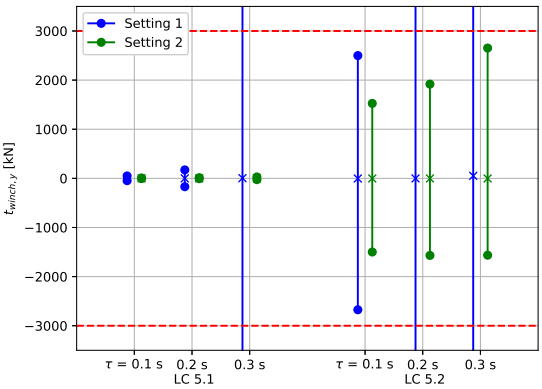

(d) The maximum tension in the winch wire in y-direction $t_{winch,x}$ for both load cases 5.1 and 5.2.

Figure 4.9: Graphical representation of the results of load cases 5.1 and 5.2.

4.3.4. Analysis Imperfect Motion Compensation

Both settings shown in Table 4.5 have been tested in various wave conditions for the perfect control system and in case of lag. In this section the model is expanded to include imperfect motion compensation. In case of imperfect motion compensation it is assumed the actuators, modelled by the winches, cannot fully compensate for the vessel motions. When the vessel moves the actuators do not adequately adjust their length and the gripper frame ring is forced to follow the vessel motion to a certain extent. Consequently, an additional force t_mc is introduced on the gripper frame ring and the vessel. This force depends on the stiffness of the actuators and the efficiency of the motion-compensation, see

Equation 4.14.

$$t_{mc} = \Delta x_v k_{act} \beta \tag{4.14}$$

where:

- Δx_v is the change of vessel in x-direction with respect to the previous time step. For Winch Y x_v is replaced by the change of vessel motion in y-direction Δy_v.
- k_{act} represents the actuator stiffness which is assumed to be 50,000 kN/m in consultation with HES.
- β represents the amount of lack of motion compensation and is equal to 1-E. Meaning with 70% motion compensation β = 0.3.

For example, if the vessel moves 0.2 m during one time step, such that Δx_v = 0.2 m, and assuming $\beta = 0.1$, then the actuator moves 0.18 m instead of the required 0.2 m to fully compensate the motion. This lack of motion compensation then results in a force t_{mc} of 0.2*50,000*0.1 = 1000 kN.

The total tension is then given by the tension due to the motion of the monopile and the imperfect motion compensation. Adding Equation 3.11 and Equation 4.14 gives the equation of the total winch tension in case of imperfect motion compensation as shown in Equation 4.15.

$$t_{\mathrm{w}} = t_{mp} + t_{mc} = k_p e + k_I \frac{1}{2} dt \left(e + e_{\mathrm{prev}}\right) + k_D \frac{e - e_{\mathrm{prev}}}{dt} + \Delta x_v k_{act} \beta \tag{4.15}$$

This is also represented in Figure 4.10, where the block diagram has been extended with an imperfect motion compensation block to include tension in the winch wire due to the vessel motions. The winch tension now depends on both the motion of the monopile and the motion of the vessel. The imperfect motion compensation block adds additional tension to the winch wire based on the change in vessel motion per time step Δx_v. Every time step the change in vessel motion is calculated by subtracting the previous vessel position $x_{v,prev}$ from the current vessel position x_v. This yields the change in vessel position Δx_v. The resulting tension due to the imperfect motion compensation is then determined in the block $KD_a(S)$ according to Equation 4.14 and fed into the monopile block.

The load cases are presented in Table 4.17 and the results are presented in Table 4.18 to Table 4.21 and graphically in Figure 4.11.

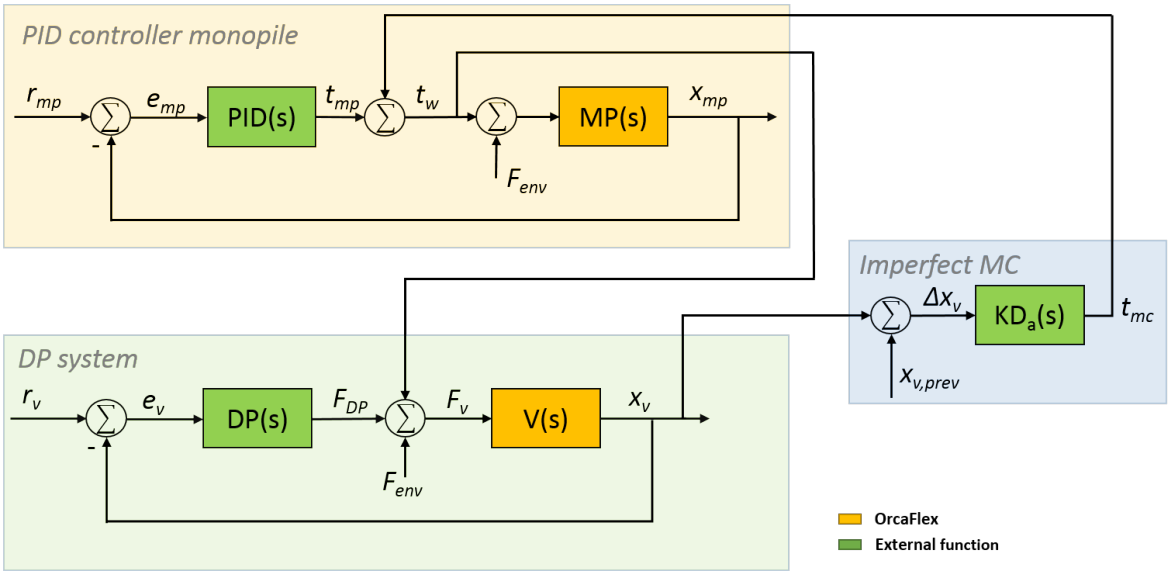

Figure 4.10: A block diagram of the entire system.

LC and PID settings		Wave	Efficiency
6.1	a) Setting 1 b) Setting 2	JONSWAP, H_s = 1 m, T_p = 4 s, θ = 180°	0.7
6.2	a) Setting 1 b) Setting 2	JONSWAP, H_s = 2 m, T_p = 7 s, θ = 135°	0.7

Table 4.17: Load cases for the imperfect motion compensation of the vessel.

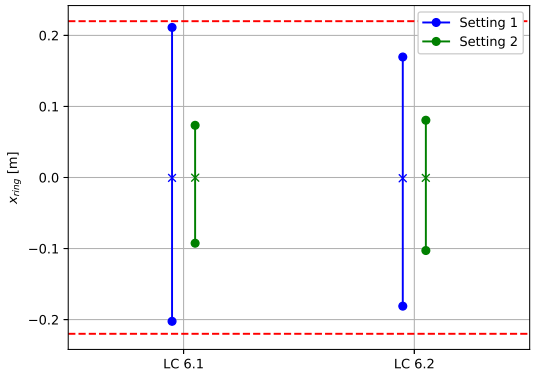

(a) The x-motion of the monopile for both settings in load cases 6.1 and 6.2.

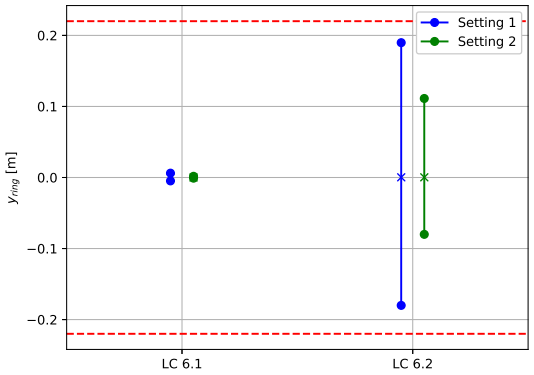

(b) The y-motion of the monopile for both settings in load cases 6.1 and 6.2.

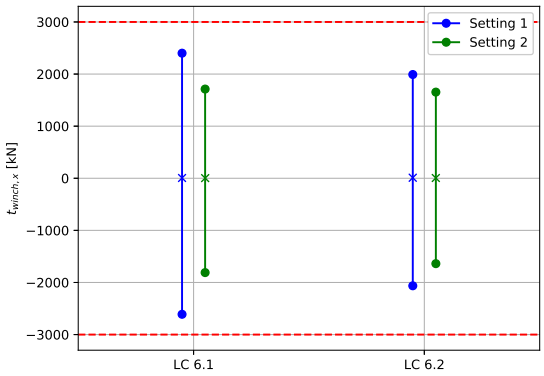

(c) The maximum tension in the winch wire in x-direction $t_{winch,x}$ for both load cases 6.1 and 6.2.

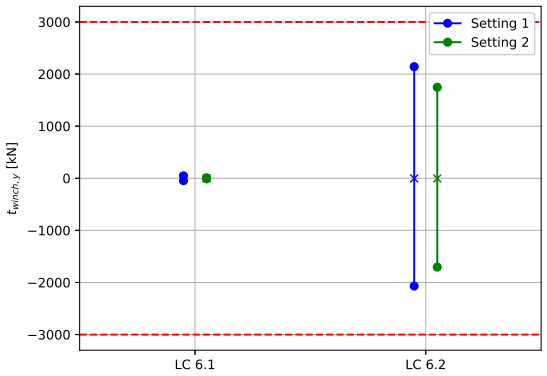

(d) The maximum tension in the winch wire in y-direction $t_{winch,x}$ for both load cases 6.1 and 6.2.

Figure 4.11: Graphical representation of the results of load cases 6.1 and 6.2.

The results of load case 6.1 show the movement of the pile in x-motion and y-motion is virtually the same compared to load case 3.1, even though an additional force on the monopile is exerted based on only 70% of the vessel motions being compensated. The motion in x-direction is even decreased compared to the perfect motion compensation system shown in Table 4.18. This is explained when looking at Figure 4.12b. As shown, the vessel motions are very small compared to the monopile motions due to the fact that the vessel is in head waves. Therefore, the contribution of $t_{mc,x}$ to the total tension in the winch $t_{winch,x}$ is negligible compared to the contribution of $t_{PID,x}$. Furthermore, the vessel motion and monopile motions in x-direction are 180 degrees out of phase and, as a result, the monopile is pushed and pulled back to its position by the vessel moving in the opposite direction. Therefore, it has

Variables	Unit	Mean	Max	Min	Std
x_{mp}	m	-0.00	0.211	-0.202	0.040
y_{mp}	m	-0.00	0.006	-0.005	0.001
$t_{winch,x}$	kN	5.58	2400.834	-2610.520	489.514
$t_{winch,y}$	kN	0.06	46.904	-46.007	9.494
x_{Aegir}	m	-0.03	0.024	-0.223	0.028
y_{Aegir}	m	0.03	0.124	-0.017	0.020
$R_{z,Aegir}$	deg	-0.03	0.016	-0.114	0.018

Table 4.18: Results of load case 6.1a.

Variables	Unit	Mean	Max	Min	Std
x_{mp}	m	-0.00	0.073	-0.093	0.015
y_{mp}	m	-0.00	0.002	-0.001	0.000
$t_{winch,x}$	kN	2.95	1712.238	-1810.227	331.473
$t_{winch,y}$	kN	0.03	10.237	-10.804	2.116
x_{Aegir}	m	-0.02	0.041	-0.168	0.021
y_{Aegir}	m	0.02	0.061	-0.004	0.009
$R_{z,Aegir}$	deg	-0.01	0.004	-0.056	0.008

Table 4.19: Results of load case 6.1b.

Variables	Unit	Mean	Max	Min	Std
x_{mp}	m	-0.00	0.170	-0.181	0.049
y_{mp}	m	0.00	0.190	-0.180	0.050
$t_{winch,x}$	kN	9.87	1991.433	-2063.482	560.743
$t_{winch,y}$	kN	-2.99	2142.107	-2068.710	569.973
x_{Aegir}	m	-0.06	0.409	-0.800	0.134
y_{Aegir}	m	0.10	2.196	-0.758	0.314
$R_{z,Aegir}$	deg	-0.07	0.899	-0.771	0.210

Table 4.20: Results 6.2a

Variables	Unit	Mean	Max	Min	Std
x_{mp}	m	-0.00	0.081	-0.103	0.024
y_{mp}	m	0.00	0.111	-0.080	0.024
$t_{winch,x}$	kN	5.28	1653.630	-1638.616	411.706
$t_{winch,y}$	kN	-2.75	1747.034	-1704.703	414.728
x_{Aegir}	m	-0.03	0.445	-0.786	0.135
y_{Aegir}	m	0.05	2.172	-0.852	0.319
$R_{z,Aegir}$	deg	-0.03	0.973	-0.756	0.227

Table 4.21: Results 6.2b

a stabilising effect. There is a very slight increase in the monopile motions in y-direction compared to the perfect motion compensation case. This is due to the fact that the monopile and vessel are moving in phase in this instance, meaning the pile is pulled and pushed out of position by the vessel in case of imperfect motion compensation. The extra tension is however negligible due to small vessel motions.

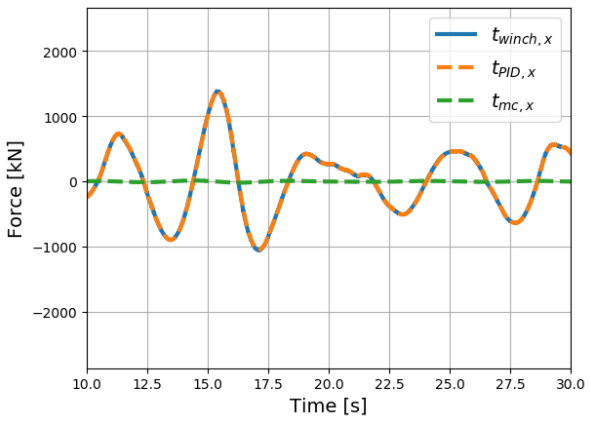

(a) The total tension in the winch wire in x-direction $t_{winch,x}$ and its two components $t_{PID,x}$ and $t_{mc,x}$.

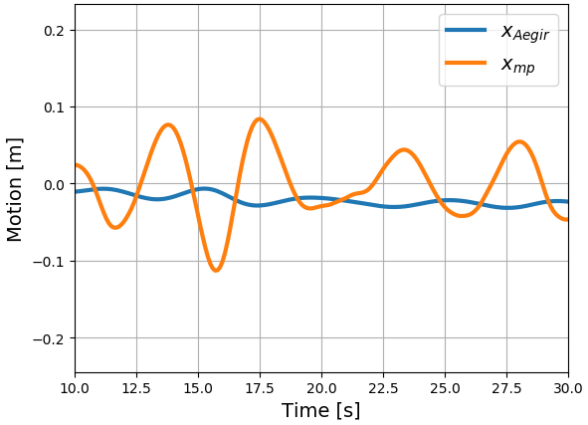

(b) The motion of the Aegir and monopile in x-direction. Note that the motions are out of phase.

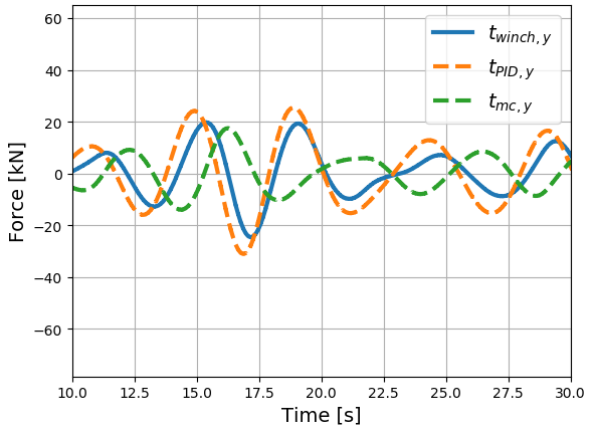

(c) The total tension in the winch wire in y-direction t_winch,y and its two components $t_{PID,y}$ and $t_{mc,y}$.

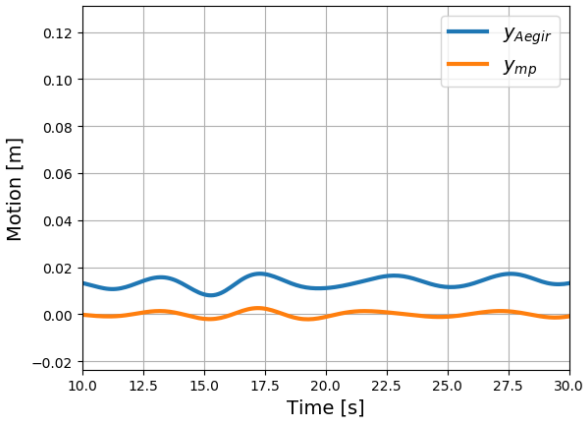

(d) The motion of the Aegir and monopile in y-direction. Note that the motions are in phase.

Figure 4.12: The time trace of the force in the winch wire in x- and y-direction and Aegir and monopile motion of load case 4.1a

For load case 6.1 the vessel motions are small compared to the monopile motions. To investigate the effect of imperfect motion compensation for larger vessel motions the significant wave height and peak period are increased for load case 6.2. Note that the environmental conditions are the same as in load case 4.4. The results are shown in Figure 4.11 and Table 4.20 and Table 4.21. The results remain virtually the same compared to the same load case of perfect motion compensation, see Figure 4.6 or Table C.4 and Table 4.15. The slight decrease in monopile motions is due to the fact that the pile motion and vessel motion are out of phase, as described in the previous paragraph.

Figure 4.13a shows the time trace of the tension in the winch and the contribution of the PID controller $t_{PID,x}$ and additional load due to the imperfect motion compensation $t_{mc,x}$ for load case 6.2b. Figure 4.13b shows the monopile and Aegir motion of load case 6.2b and load case 4.4b to compare the imperfect and perfect motion compensation system. As the monopile moves in positive x-direction, the vessel is moving in the negative x-direction, see Figure 4.13b. To keep the monopile from falling over the winch should go in compression if the monopile is moving in the positive x-direction (see Figure 4.1), meaning the winch tension should be negative. As shown in the latter figure, the total winch tension is smaller due to the negative contribution of the vessel $t_{mc,x}$. As a result, the monopile motion is smaller due to the imperfect motion compensation compared to the perfect motion compensation, see the blue

and orange line in Figure 4.13a respectively. In the y-direction similar results are observed. However, the change in vessel motion remains relatively small in both directions and the tension contribution of the vessel motions $t_{mc,x}$ remains small compared to the contribution of the PID controller $t_{PID,x}$, see Figure 4.13a. This is also depicted in Figure 4.13b when comparing the monopile and Aegir motions in case of 70% motion compensation and perfect motion compensation (E = 1), see the solid and dashed line.

In conclusion, the vessel motions are slowly varying compared to the monopile motions. As a result, the effect of not adequately adjusting the length of the actuators based on the vessel motions, leading to imperfect motion compensation, is not very substantial. In case the vessel and monopile motion are opposing, imperfect motion can have a stabilising effect on the monopile.

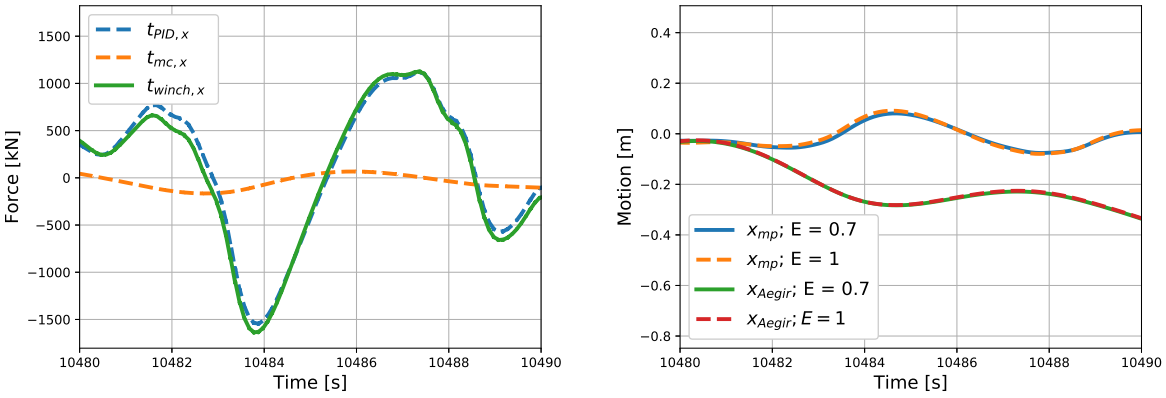

(a) The total tension in the winch wire in x-direction $t_{winch,x}$ and its two components $t_{PID,x}$ and $t_{mc,x}$.

(b) The motion of the Aegir and monopile in x-direction. Note that the motions are out of phase.

Figure 4.13: Time trace of load case 6.2b showing the winch tension and motion of the monopile in x-direction.

4.3.5. Overview of Results

The coupled system is evaluated for these two control settings for various cases in this section and Table 4.22 gives an summary of the results. A check mark in the table means the controller setting meets all three criteria described at the beginning of section 4.3 regarding the maximum monopile motion, maximum winch wire tension (corresponding to a maximum force in the actuators) and maximum stretched length of the winch (corresponding to a maximum stroke of the actuators). An x mark indicates that either one of the criteria has not been met and the setting is unsatisfactory in this case.

Based on the results setting 1 is not recommended, since the forces and motions are exceeded in case of a significant wave height of 2 m. Furthermore, both the monopile motions and tension exceed the limit in case of lag for setting 2. As shown in Table 4.22, setting 2 in bow waves is the only setting that always meets the criteria. Compared to head waves the vessel motions increase for bow waves, however, the wave force is distributed over both actuators. Therefore, based on the results presented it is recommended to select setting 2, especially in case of significant wave heights exceeding 1 m.

	Perfect Control System		**Perfect Control System H_s = 2 m**				**Lag**		**Imperfect MC**	
	H_s = 1 m, T_p = 4 s		**T_p = 5 s**		**T_p = 7 s**		**H_s = 1 m, T_p = 4 s, τ = 0.3 s**		**H_s = 1 m, T_p = 4 s, E = 0.7**	
	Head	Bow	Head	Bow	Head	Bow	Head	Bow	Head	Bow
Setting 1	✓	✓	×	×	×	×	×	×	✓	✓
Setting 2	✓	✓	×	✓	✓	✓	×	✓	✓	✓

Table 4.22: Overview of the results of the different load cases. A check mark indicates all three criteria have been met. In case of a cross at least one criteria has not been met for that particular load case..

In case of setting 2 in bow waves, the system can still operate in case of a significant wave height of 2 m with a peak period of 5.1 s, which is the minimum peak period according to [8]. Higher wave periods are less critical, since the monopile motion are decreased due to the lower forcing frequency, further away from the natural frequency of the system. The maximum lag in case of head waves is 0.2 s, while the maximum lag is 0.3 s for bow waves due to the distribution of the force over both winches in this case. The effects of imperfect motion compensation are limited due to the slow variation of the vessel motions and, as a result, both settings meet the criteria in this case.

4.4. Fixed Monopile and Imperfect Motion Compensation.

Once the monopile has been hammered into the soil and the monopile has almost reached the desired penetration depth, the soil stiffness is so large at some point it could be approximated as a rigidly clamped pile. To determine what the loads are on the pile in case it is rigidly clamped at the bottom, the system is tested with 70% motion compensation in a 1 meter wave with a peak period of 4 seconds, see Table 4.23. The settings of the PID controller have been omitted since the error of the pile motion is equal to zero, meaning the tension in the winch wire due to the PID controller of the monopile motions is always equal to zero.

For the fixed pile and 70% motion compensation an additional force is exerted on the monopile. The magnitude of the force depends on the vessel motions, hence, on the direction of the waves. As expected, the forces are largest in case of a beam waves and relatively small for head waves. However, even for a worse case scenario of beam waves, the force is relatively small compared to the wave forcing. A force of -272 kN results in a overturning moment of 13.8 MNm, while the OrcaFlex simulations show a overturning moment of 31 MNm for a fixed pile in Airy waves of 1 m with a period of 4 s. Therefore, based on these results and the results in the previous paragraph a lack of motion compensation does not lead to extreme forces or instability in these conditions.

LC	Wave	Efficiency
7.1	JONSWAP, H_s = 1 m, T_p = 4 s, θ = 180°	E = 0.7
7.2	JONSWAP H_s = 1 m T_p =4 s θ = 135 °	E = 0.7
7.3	JONSWAP H_s = 1 m T_p = 4 s θ = 90°	E = 0.7

Table 4.23: Load cases for the fixed monopile.

Variables	Unit	Mean	Max	Min	Std
x_{mp}	m	0.0	0.000	0.000	0.000
y_{mp}	m	0.0	0.000	0.000	0.000
$t_{winch,x}$	kN	0.0	8.422	-10.386	1.463
$t_{winch,y}$	kN	-0.0	1.554	-1.285	0.257
x_{Aegir}	m	0.0	0.024	-0.090	0.012
y_{Aegir}	m	0.0	0.007	-0.011	0.002
$R_{z,Aegir}$	deg	-0.0	0.012	-0.009	0.002

Table 4.24: Results of load case 7.1

Variables	Unit	Mean	Max	Min	Std
x_{mp}	m	0.0	0.000	0.000	0.000
y_{mp}	m	0.0	0.000	0.000	0.000
$t_{winch,x}$	kN	0.0	14.991	-19.089	2.840
$t_{winch,y}$	kN	0.0	50.315	-55.146	10.124
x_{Aegir}	m	0.0	0.113	-0.056	0.017
y_{Aegir}	m	-0.0	0.261	-0.291	0.046
$R_{z,Aegir}$	deg	0.0	0.416	-0.127	0.066

Table 4.25: Results of load case 7.2

Variables	Unit	Mean	Max	Min	Std
x_{mp}	m	0.0	0.000	0.000	0.000
y_{mp}	m	0.0	0.000	0.000	0.000
$t_{winch,x}$	kN	0.0	9.730	-14.459	1.696
$t_{winch,y}$	kN	-0.0	251.046	-272.397	51.574
x_{Aegir}	m	0.0	0.050	-0.070	0.013
y_{Aegir}	m	-0.0	0.699	-0.198	0.087
$R_{z,Aegir}$	deg	0.0	0.237	-0.154	0.039

Table 4.26: Results of load case 7.3

5

Conclusion and Recommendations

5.1. Conclusion

Due to the increasing size of the offshore wind turbines the monopile are increasing in size and weight as well. The crane capacity of the jack-up vessel, the conventional monopile installation vessel, is limited and, therefore, these vessels are becoming less suitable for monopile installation. One of the solutions to this problem is installing monopiles using DP floating vessels, as these generally have a larger crane capacity. Another advantage of floating vessels is that they can operate in larger water depths as well, which is another limiting factor of the jack-up vessel. In order to successfully install the monopile, it should be held vertical over the course of the installation. In addition, the motions of the vessel should not impose large forces on the monopile. To solve this problem HMC and HES are working together to develop a motion compensated gripper frame.

It is assumed the monopile has just been lowered to the seabed and can be modelled as an inverted pendulum hinged at the seabed with no soil stiffness. As a first approximation, the monopile is modelled in the frequency domain as an inverted pendulum held vertically by a spring and dashpot, which represent the proportional gain k_P and derivative gain k_D of the controller, respectively. The frequency domain calculations clearly show an increase in monopile motions and the force applied on the monopile, in case the value of k_P is chosen such that the natural frequency of the pile matches the forcing frequency; in other words, resonance occurs. Adding damping in the form of k_D can greatly reduce the monopile motion in case of resonance. Outside the resonance area this effect is limiting.

To model the dynamics of the coupled system, composed of the monopile, vessel and gripper frame, an OrcaFlex model is set-up. The coupled model is analysed for different values of proportional and derivative gain in various sea states and the results presented in chapter 4 match the findings of the frequency domain calculations in earlier chapters. In case of a perfect system, where the force exerted by the gripper frame based on the monopile motion is instantly applied, a very high value of k_P gives low monopile motions and forces. However, in reality the monopile motion cannot be corrected for instantly. Therefore, a sensor lag is introduced in section 4.2 to simulate imperfections in the system. In case of lag it is shown that high values of k_P lead to instability in case k_D is not high enough, as the damping term becomes negative for increasing values of τ. However, increasing k_D to very high values leads to instability as well, as the effective inertia term becomes negative. Based on these results a final selection of the value of k_P and k_D is proposed.

Choosing a low value of k_P results in low monopile motions and relatively low forces for shorter wave periods. However, due to the increasing soil stiffness when hammering the monopile into the soil, resonance will occur during the installation for larger penetration depths. To avoid resonance during the entire installation, a high value of k_P (10,000 kN/m) is selected. This value of k_P is simulated for two different values of derivative gain, k_D equal to 3700 kNs/m and 11,000 kNs/m, in various sea states. Both settings are tested for the perfect system and in case of imperfections, such as lag and imperfect motion compensation. The results are compared to the three criteria. First of all, the maximum force

in the actuators, represented by the winch tension, should not exceed 3000 kN/m. Furthermore, the maximum monopile motion should be limited to 0.22 m at gripper frame level (corresponding to a maximum angle of 0.25°). Lastly, the maximum stroke of the actuators is 2.5 m (distance between vessel and monopile). It is assumed these criteria should be met to successfully install the monopile. Taking all the results into account, the research question of this work can be answered:

What values of the gripper frame parameters - e.g. control setting: k_P, k_I and k_D – minimise the pile inclination and the gripper frame force exerted on the monopile and are these parameters feasible in practice?

Setting 2 (k_P = 10,000 kN/m and k_D = 11,000 kNs/m) is the recommended setting when taking into account all the results of the load cases presented in chapter 4. The most favourable wave direction is bow waves compared to head waves, despite the increase in vessel motions, because the force on the actuators is distributed more evenly. The shortest wave periods introduce the largest monopile motions, as the forcing frequency is closest to the natural frequency of the monopile and gripper frame combination for the selected settings.

How sensitive is the system to system and sensor inaccuracies such as a delay in the controller or imperfect motion compensation?

The monopile motions and winch tension significantly increase in case of a sensor lag. The monopile falls over in case the sensor lag exceeds 0.3 s for both settings. The effect of imperfect motion compensation is limited due to the slow variation of the vessel motions.

In conclusion, the monopile motions are limited for higher values of k_P and k_D and the proposed values are k_P = 10,000 and k_D = 11,000. This setting meets the criteria regarding the maximum monopile motions, force exerted on the monopile and maximum actuator stroke and, therefore, it is assumed these values are feasible in practice. The translation from the theoretical model to industry hardware is outside the scope of this work. Introducing a sensor lag results in instability of the monopile for values larger than 0.3 s for this particular setting. However, the response time of industry actuators is well within these limits. Not fully compensating the vessel motions introduces an additional force on the monopile, the effects of which are limited due to the fact that the motions are slowly varying. It should be noted that this is not the only possible setting and recommendations for future work is discussed in section 5.2.

5.2. Recommendations

In reality, the system is much more complicated than the system modelled in OrcaFlex. For example, the actuators moving the gripper frame ring are extremely simplified and modelled as a winch which exerts a force on the monopile and vessel. In reality a hydraulic fluid is moving the piston rod, which then moves the gripper frame ring and eventually exerts a force on the monopile and vessel. This part could be modelled in more detail.

In subsection 4.3.3 numerical instability is observed and the monopile shows bending in the second mode for some cases if the pile is not assumed rigid. The effect of sensor lag on the bending of the monopile should be investigated in more detail to determine if this is merely a numerical error or if this behaviour is likely to occur in reality.

The criteria to asses suitability of the two different settings in section 4.3 are based on reasonable maximum values of the actuator force and stroke according to industry standards. However, the practical implementation of the system has not been studied in detail. The translation from the theoretical model to hardware is not considered. However, this is an important factor that determines the feasibility of the motion compensated gripper frame. For example, how should the monopile angle be measured and what is the accuracy of the sensors? Another issue that has not been considered is noise in the signal. The derivative gain k_D tends to amplify noise in a signal, which may limit the maximum value of k_D.

The interface between the monopile and gripper frame ring is modelled as a rigid connection. Varying the stiffness and damping of this interface could be of interest. In case of a much smaller stiffness, the monopile is able to move within the ring. This design option could be considered to investigate if the

monopile motions and the force exerted on the monopile remain within the tolerances.

Another design option to be considered is rotating the current set-up of the gripper frame ring by 45°, such that the actuators are at an angle of 135° and 45° with the side of the vessel. In this configuration, the force on the actuators would be distributed in case of head waves. This would provide the benefit of limited vessel motion and, at the same time, distribute the load on the actuator.

A

Results Perfect Control System

LC	Wave	PID settings ring controller
1.1	JONSWAP, H_s = 1 m, T_p = 7 s, θ = 180°	range 1: k_P = 500-5000 kN/m (Δk_P = 500) range 2: k_P = 1e4-1e5 kN/m (Δk_P = 1e4). k_I = 0 kN/ms k_D = 1000 kNs/m
1.2	JONSWAP H_s = 1 m T_p = 7 s θ = 180 °	range 1: k_P = 500-5000 kN/m (Δk_P = 500) range 2: k_P = 1e4 - 10e4 kN/m (Δk_P = 1e4) k_I = 0 kN/ms k_D = 2000 kNs/m
1.3	JONSWAP, H_s = 1 m, T_p = 7 s, θ = 135 °	range 1: k_P = 500-5000 kN/m (Δk_P = 500) range 2: k_P = 1e4-1e5 kN/m (Δk_P = 1e4). k_I = 0 kN/ms k_D = 1000 kNs/m
1.4	JONSWAP H_s = 1 m T_p = 7 s θ = 135 °	range 1: k_P = 500-5000 kN/m (Δk_P = 500) range 2: k_P = 1e4 - 10e4 kN/m (Δk_P = 1e4) k_I = 0 kN/ms k_D = 2000 kNs/m
1.5	JONSWAP, H_s = 1 m, T_p = 7 s, θ = 90 °	range 1: k_P = 500-5000 kN/m (Δk_P = 500) range 2: k_P = 1e4-1e5 kN/m (Δk_P = 1e4). k_I = 0 kN/ms k_D = 1000 kNs/m
1.6	JONSWAP H_s = 1 m T_p = 7 s θ = 90 °	range 1: k_P = 500-5000 kN/m (Δk_P = 500) range 2: k_P = 1e4 - 10e4 kN/m (Δk_P = 1e4) k_I = 0 kN/ms k_D = 2000 kNs/m

Table A.1: Load cases for simulations of the perfect controller system. The system is subject to an irregular wave produced using the JONSWAP spectrum with a significant wave height of 1 m and a peak period of 7 s for two different wave directions. Various values of k_P are simulated. The difference between load case 1.1 and 1.2 is the value of the derivative gain k_D.

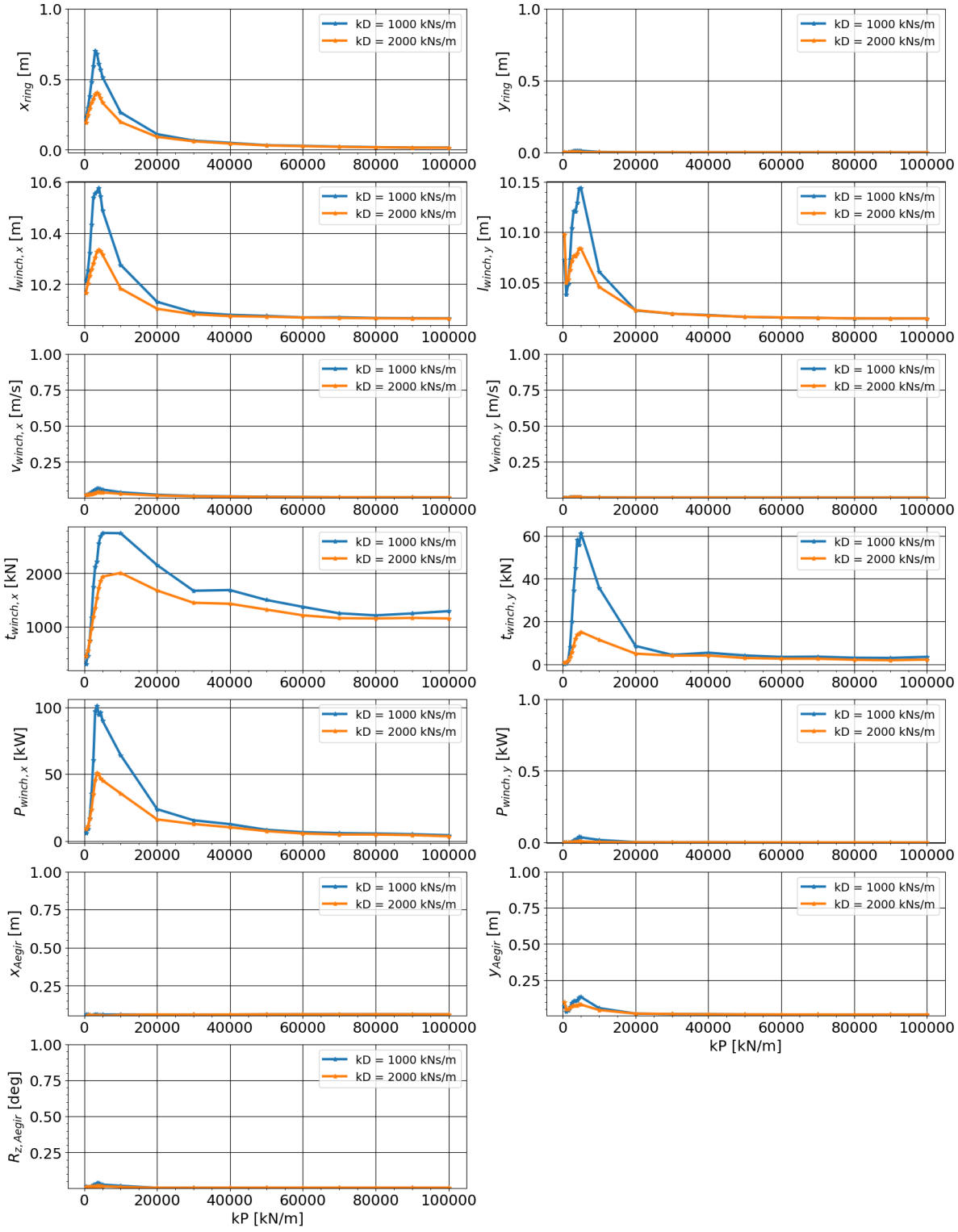

Figure A.1: The results of load case 1.1 and 1.2 combined in one plot represented by the blue and orange line, respectively.

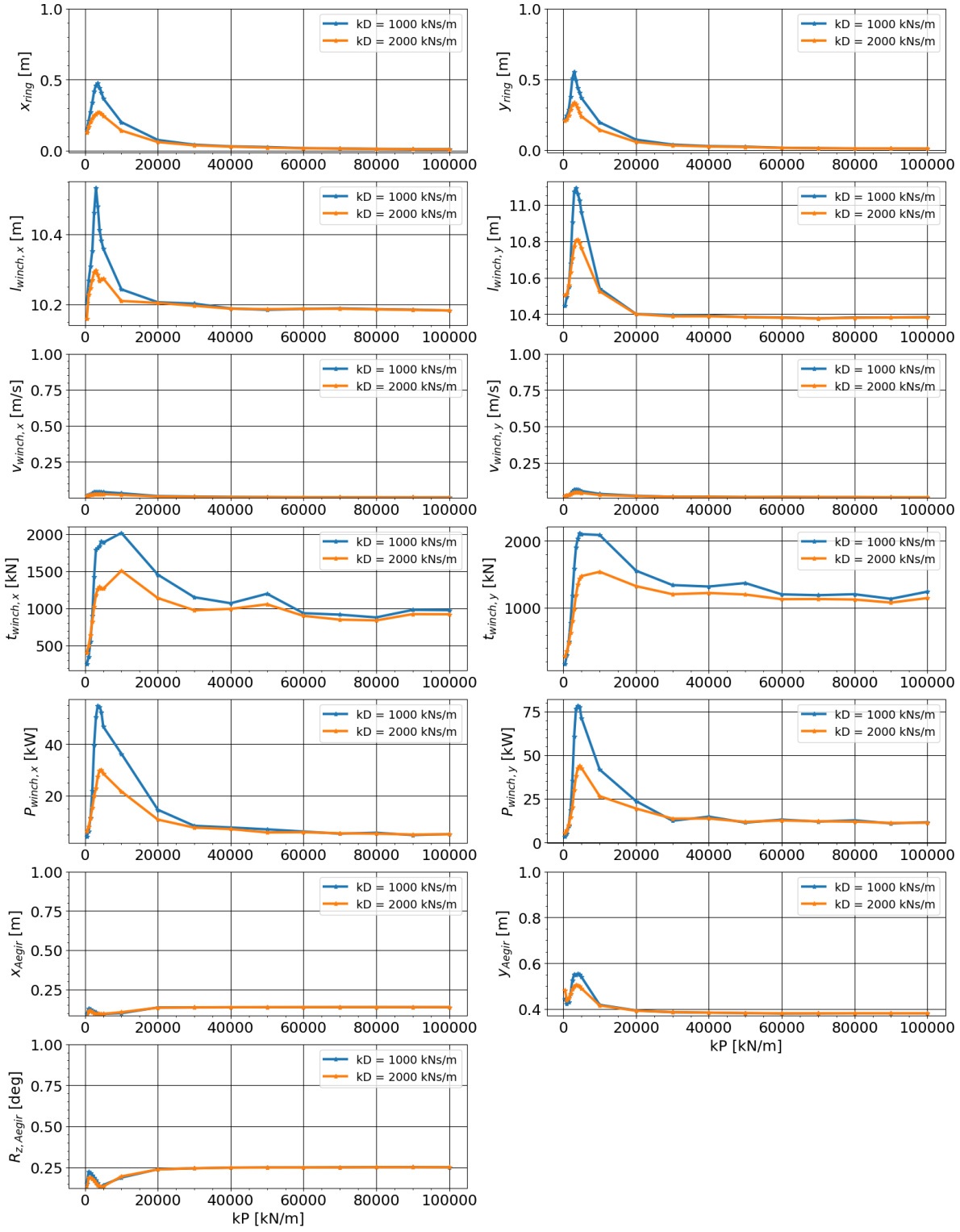

Figure A.2: The results of load case 1.3 and 1.4 combined in one plot represented by the blue and orange line, respectively.

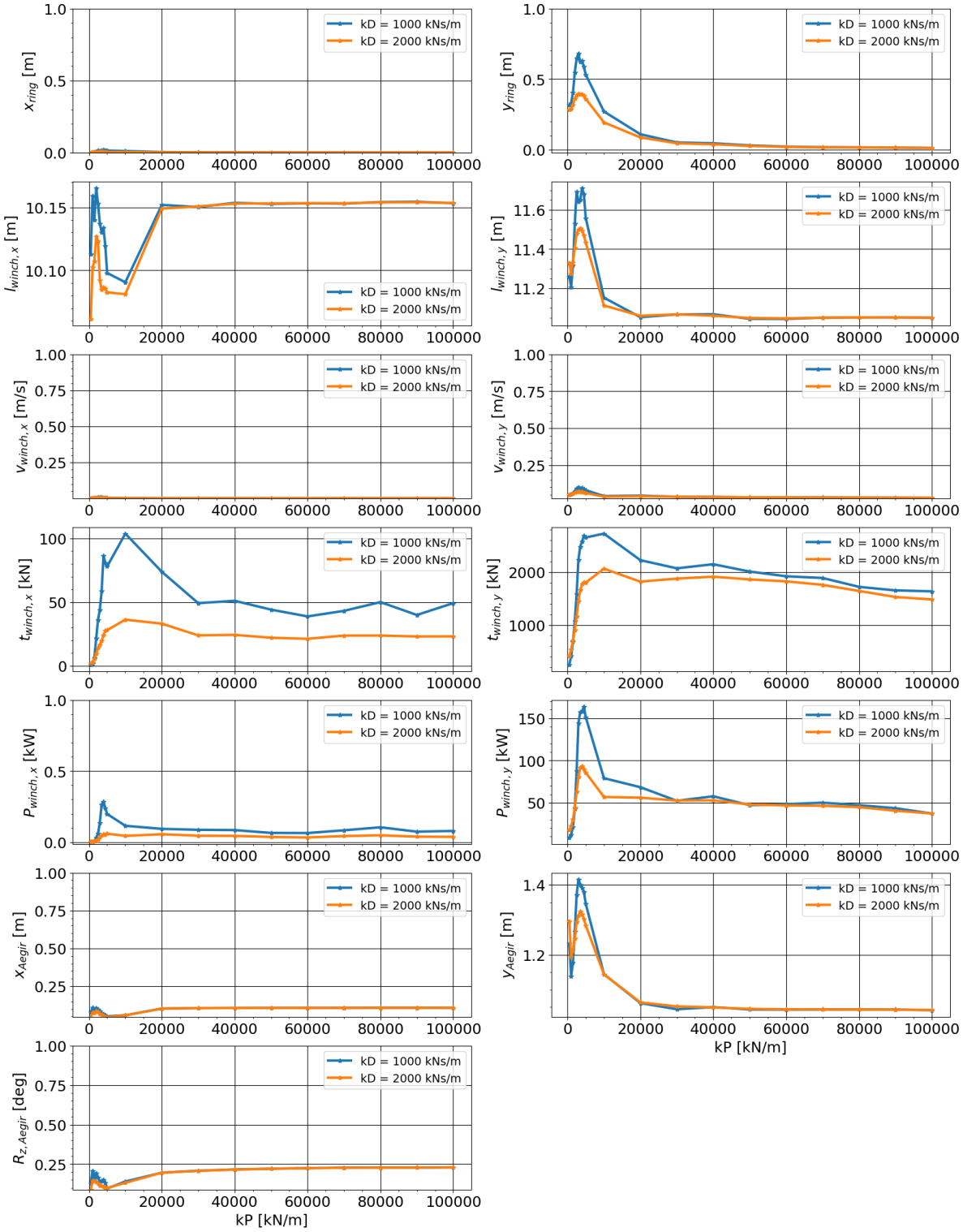

Figure A.3: The results of load case 1.5 and 1.6 combined in one plot represented by the blue and orange line, respectively.

B

Results Sensor Lag

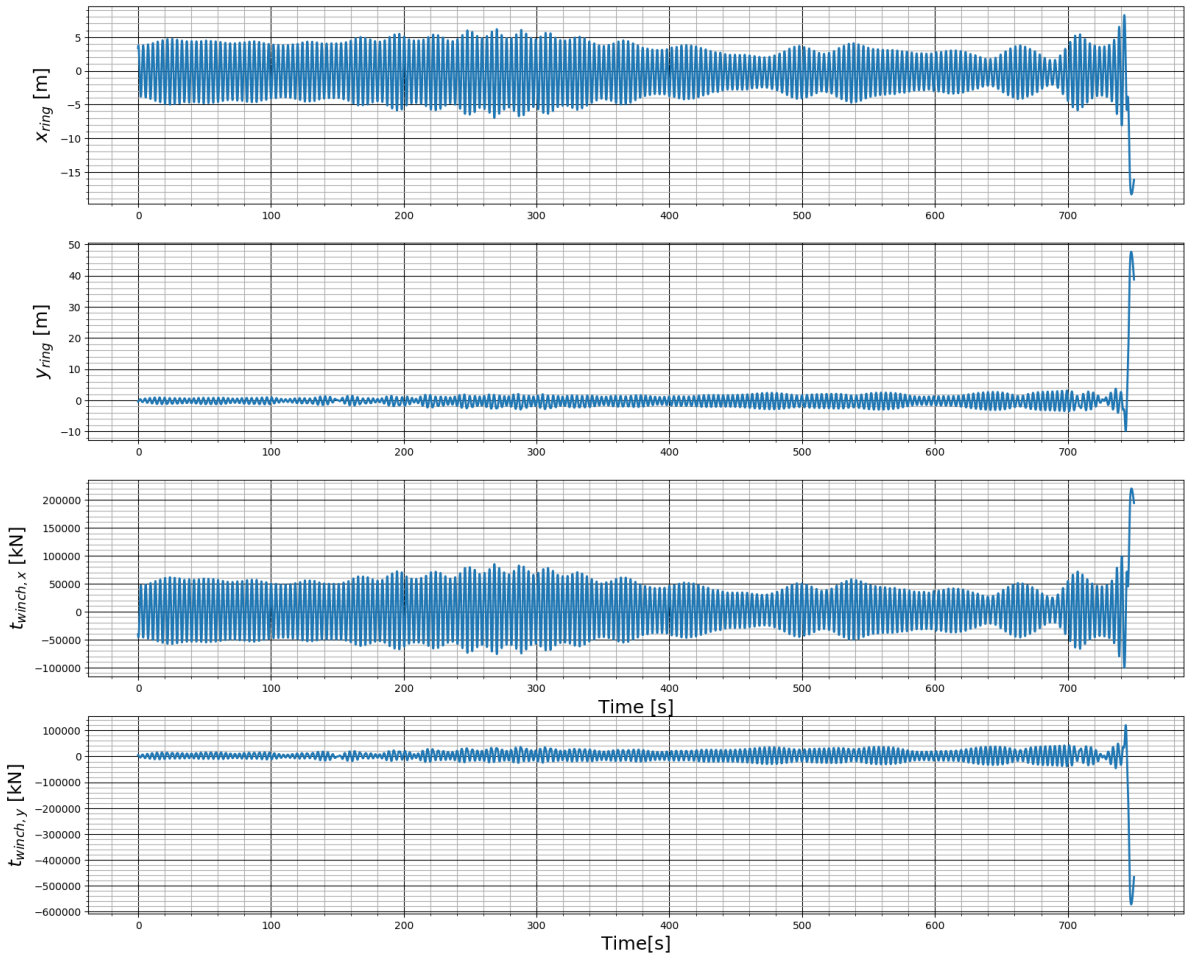

Figure B.1: Time trace of load cases 2.1a with a k_P of 12000 showing instability.

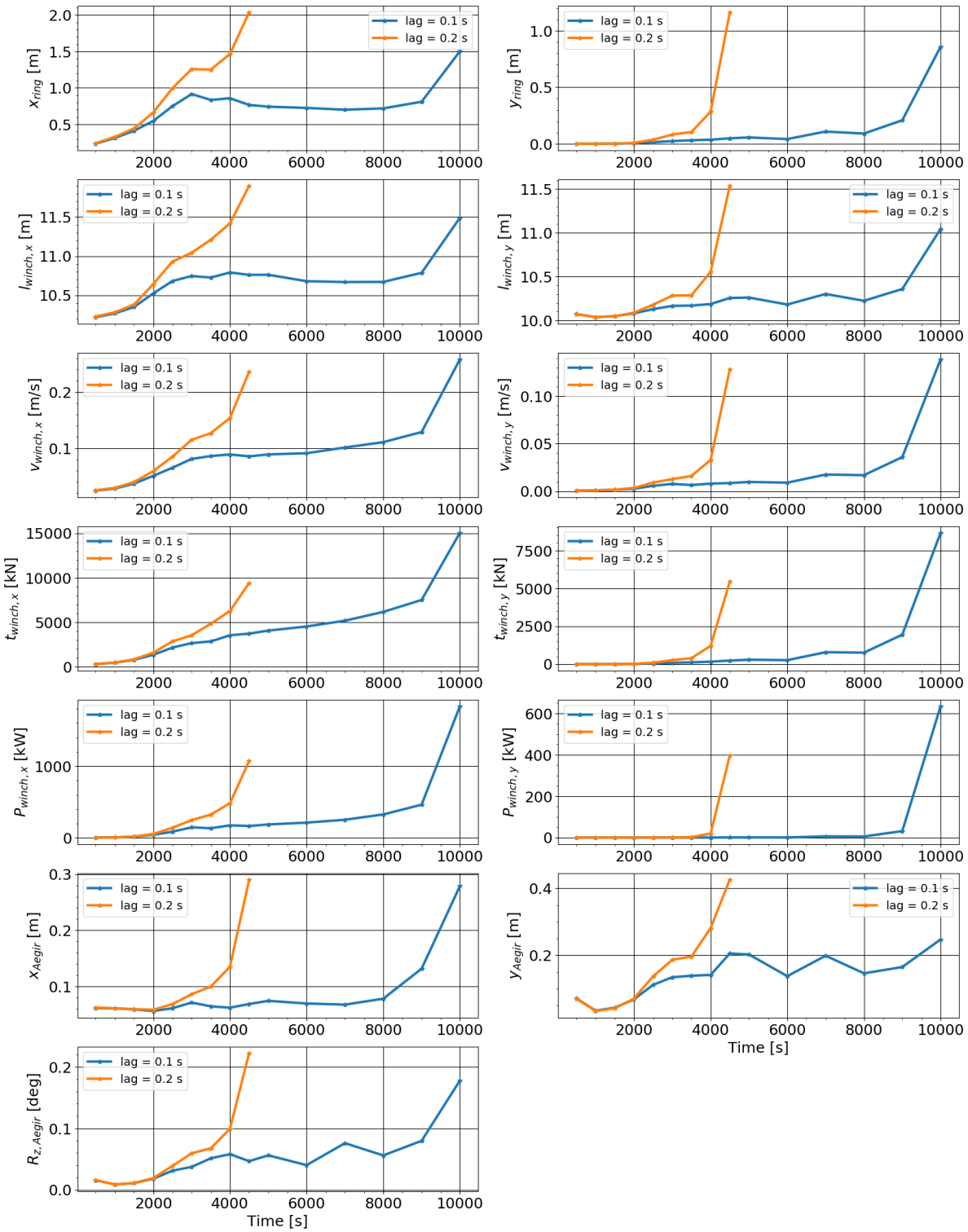

Figure B.2: Load cases 2.1a and 2.1b show that introducing a lag of just 0.1 or 0.2 seconds leads to instability of the system for higher proportional gain.

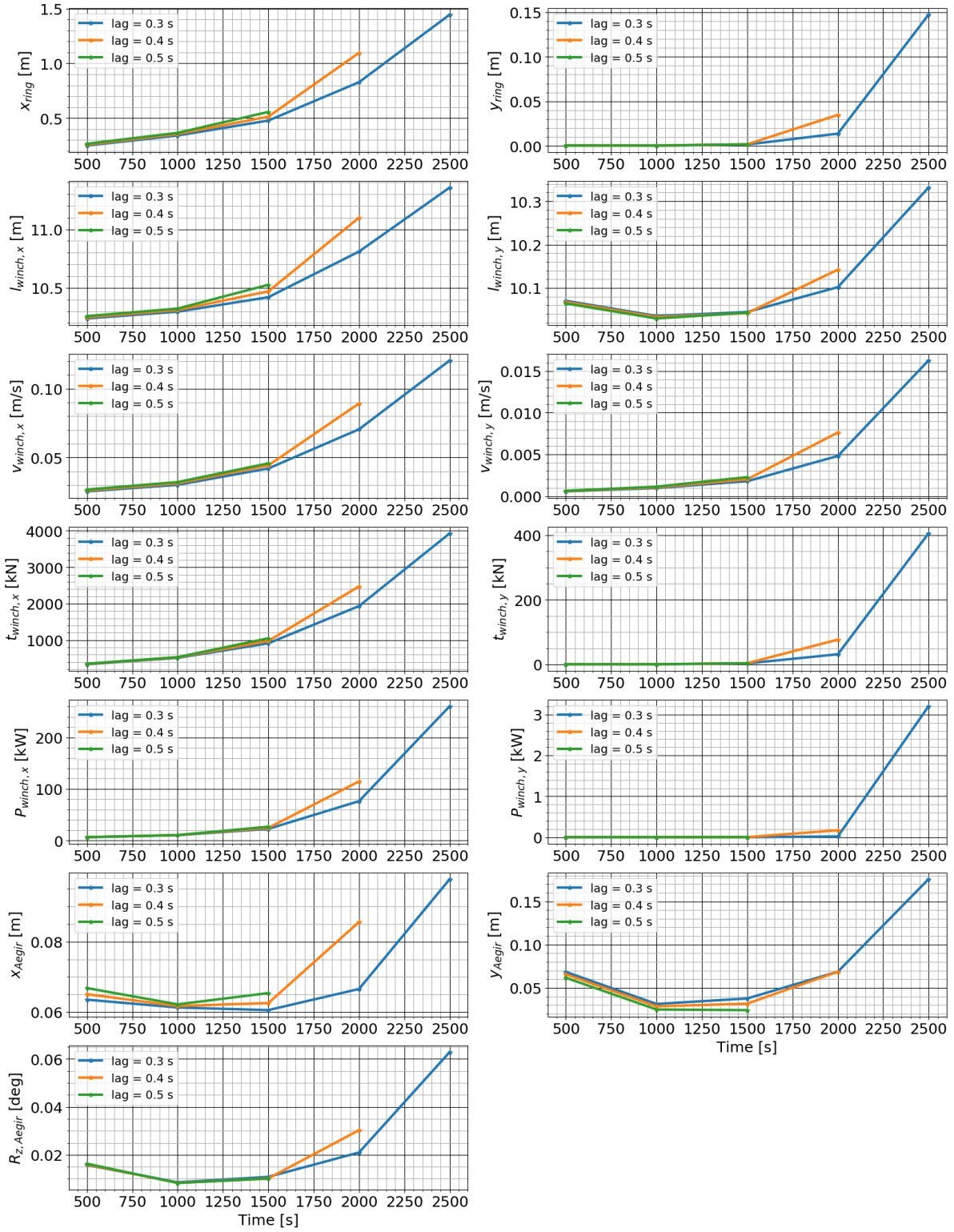

Figure B.3: Results of load cases 2.1c, 2.1d and 2.1e.

C

Results Increased Wave Height Perfect Control System Setting 1

Variables	Unit	Mean	Max	Min	Std
x_{mp}	m	-0.00	0.359	-0.418	0.085
y_{mp}	m	-0.00	0.014	-0.016	0.001
$t_{winch,x}$	kN	15.67	4761.469	-4203.134	980.292
$t_{winch,y}$	kN	0.37	188.442	-159.663	17.086
x_{Aegir}	m	-0.09	0.189	-0.885	0.120
y_{Aegir}	m	0.09	0.416	-0.144	0.058
$R_{z,Aegir}$	deg	-0.08	0.137	-0.384	0.054

Table C.1: Results of load case 4.1a

Variables	Unit	Mean	Max	Min	Std
x_{mp}	m	-0.00	0.273	-0.275	0.059
y_{mp}	m	0.00	0.292	-0.316	0.063
$t_{winch,x}$	kN	15.32	3111.808	-3313.142	682.289
$t_{winch,y}$	kN	-6.83	3731.776	-3321.294	725.587
x_{Aegir}	m	-0.10	0.652	-0.880	0.175
y_{Aegir}	m	0.18	1.932	-1.532	0.393
$R_{z,Aegir}$	deg	-0.15	1.204	-1.182	0.325

Table C.2: Results of load case 4.2a.

Variables	Unit	Mean	Max	Min	Std
x_{mp}	m	-0.00	0.278	-0.284	0.073
y_{mp}	m	-0.00	0.004	-0.005	0.001
$t_{winch,x}$	kN	9.46	3153.836	-3221.119	825.047
$t_{winch,y}$	kN	0.38	52.931	-44.019	7.452
x_{Aegir}	m	-0.06	0.212	-0.493	0.091
y_{Aegir}	m	0.05	0.152	-0.024	0.026
$R_{z,Aegir}$	deg	-0.05	0.023	-0.141	0.025

Table C.3: Results of load case 4.3a.

Variables	Unit	Mean	Max	Min	Std
x_{mp}	m	-0.00	0.189	-0.188	0.051
y_{mp}	m	0.00	0.199	-0.197	0.053
$t_{winch,x}$	kN	10.22	2069.335	-2143.144	577.913
$t_{winch,y}$	kN	-2.61	2235.381	-2202.316	595.528
x_{Aegir}	m	-0.06	0.396	-0.781	0.130
y_{Aegir}	m	0.10	2.150	-0.736	0.306
$R_{z,Aegir}$	deg	-0.07	0.889	-0.749	0.207

Table C.4: Results of load case 4.4a.

D

Results Lag kPspecific

Variables	Unit	Mean	Max	Min	Std
x_{mp}	m	-0.00	0.282	-0.282	0.055
y_{mp}	m	-0.00	0.004	-0.004	0.001
$t_{winch,x}$	kN	7.20	3415.318	-3460.195	672.222
$t_{winch,y}$	kN	0.13	49.518	-46.393	7.144
x_{Aegir}	m	-0.04	0.024	-0.258	0.032
y_{Aegir}	m	0.04	0.159	-0.018	0.026
$R_{z,Aegir}$	deg	-0.04	0.017	-0.147	0.024

Table D.1: Result load case 5.1a with τ = 0.1 s

Variables	Unit	Mean	Max	Min	Std
x_{mp}	m	-0.00	0.392	-0.424	0.086
y_{mp}	m	-0.00	0.014	-0.014	0.002
$t_{winch,x}$	kN	9.51	5105.033	-4813.653	1044.509
$t_{winch,y}$	kN	0.34	172.314	-170.157	25.913
x_{Aegir}	m	-0.05	0.027	-0.319	0.042
y_{Aegir}	m	0.05	0.212	-0.029	0.038
$R_{z,Aegir}$	deg	-0.05	0.028	-0.195	0.035

Table D.2: Result load case 5.1a with τ = 0.2 s

Variables	Unit	Mean	Max	Min	Std
x_{mp}	m	-0.00	1.710	-1.734	0.288
y_{mp}	m	-0.00	2.425	-2.464	0.175
$t_{winch,x}$	kN	14.40	21672.744	-20848.031	3539.910
$t_{winch,y}$	kN	4.59	29830.197	-30336.639	2158.317
x_{Aegir}	m	-0.07	0.522	-0.712	0.110
y_{Aegir}	m	0.07	1.041	-0.987	0.133
$R_{z,Aegir}$	deg	-0.06	0.859	-0.795	0.119

Table D.3: Result load case 5.1a with τ = 0.3 s

Variables	Unit	Mean	Max	Min	Std
x_{mp}	m	-8.01	46.385	-32.541	5.724
y_{mp}	m	42.72	50.580	-43.094	18.023
$t_{winch,x}$	kN	80093.10	325936.719	-471992.719	57289.033
$t_{winch,y}$	kN	-427243.51	431330.625	-505805.031	180249.558
x_{Aegir}	m	113937.39	236789.207	-358.018	69726.275
y_{Aegir}	m	-724138.69	1861.839	-1686253.115	529393.678
$R_{z,Aegir}$	deg	3659.80	5619.073	-460.601	1082.930

Table D.4: Result load case 5.1a with τ = 0.4 s.

Variables	Unit	Mean	Max	Min	Std
x_{mp}	m	-0.00	0.085	-0.101	0.017
y_{mp}	m	-0.00	0.000	-0.000	0.000
$t_{winch,x}$	kN	3.39	1875.093	-2061.240	381.107
$t_{winch,y}$	kN	0.03	8.467	-5.853	0.886
x_{Aegir}	m	-0.02	0.036	-0.172	0.021
y_{Aegir}	m	0.02	0.065	-0.002	0.009
$R_{z,Aegir}$	deg	-0.02	0.002	-0.059	0.009

Table D.5: Result load case 5.1b with τ = 0.1 s.

Variables	Unit	Mean	Max	Min	Std
x_{mp}	m	-0.00	0.100	-0.112	0.019
y_{mp}	m	-0.00	0.000	-0.001	0.000
$t_{winch,x}$	kN	3.82	2059.902	-2491.501	455.305
$t_{winch,y}$	kN	0.04	13.926	-7.024	1.405
x_{Aegir}	m	-0.02	0.034	-0.177	0.021
y_{Aegir}	m	0.02	0.070	-0.003	0.010
$R_{z,Aegir}$	deg	-0.02	0.002	-0.064	0.009

Table D.6: Result load case 5.1b with τ = 0.2 s.

Variables	Unit	Mean	Max	Min	Std
x_{mp}	m	-0.00	0.132	-0.124	0.024
y_{mp}	m	-0.00	0.001	-0.001	0.000
$t_{winch,x}$	kN	4.32	2350.692	-3531.209	615.518
$t_{winch,y}$	kN	0.06	28.922	-25.775	3.716
x_{Aegir}	m	-0.02	0.033	-0.183	0.021
y_{Aegir}	m	0.02	0.074	-0.002	0.011
$R_{z,Aegir}$	deg	-0.02	0.002	-0.068	0.010

Table D.7: Result load case 5.1b with τ = 0.3 s.

Variables	Unit	Mean	Max	Min	Std
x_{mp}	m	49.38	50.999	-4.775	8.731
y_{mp}	m	1.54	36.578	-4.704	1.605
$t_{winch,x}$	kN	-493804.11	140949.656	-604600.312	87730.167
$t_{winch,y}$	kN	-15430.41	152282.625	-599010.562	16703.357
x_{Aegir}	m	-678127.92	0.327	-1382912.497	404642.710
y_{Aegir}	m	-13302.98	6845.687	-26330.259	8002.938
$R_{z,Aegir}$	deg	5059.64	10133.744	-1894.025	3188.693

Table D.8: Result load case 5.1b with τ = 0.4 s.

Variables	Unit	Mean	Max	Min	Std
x_{mp}	m	-0.00	0.193	-0.216	0.039
y_{mp}	m	0.00	0.220	-0.207	0.040
$t_{winch,x}$	kN	7.00	2610.583	-2351.791	472.460
$t_{winch,y}$	kN	-2.92	2499.149	-2674.750	481.331
x_{Aegir}	m	-0.05	0.121	-0.272	0.037
y_{Aegir}	m	0.09	0.547	-0.195	0.070
$R_{z,Aegir}$	deg	-0.07	0.147	-0.196	0.048

Table D.9: Result load case 5.2a with τ = 0.1 s.

Variables	Unit	Mean	Max	Min	Std
x_{mp}	m	-0.00	0.297	-0.301	0.060
y_{mp}	m	0.00	0.304	-0.323	0.062
$t_{winch,x}$	kN	11.53	3557.500	-3667.865	731.343
$t_{winch,y}$	kN	-1.30	3894.983	-3647.391	756.272
x_{Aegir}	m	-0.06	0.096	-0.342	0.043
y_{Aegir}	m	0.12	0.625	-0.087	0.075
$R_{z,Aegir}$	deg	-0.09	0.069	-0.227	0.041

Table D.10: Result load case 5.2a with τ = 0.2 s.

Variables	Unit	Mean	Max	Min	Std
x_{mp}	m	-0.01	2.402	-2.417	0.307
y_{mp}	m	-0.01	4.478	-4.710	0.440
$t_{winch,x}$	kN	62.60	29234.914	-30201.285	3776.447
$t_{winch,y}$	kN	51.29	56289.391	-56381.547	5414.237
x_{Aegir}	m	-0.09	0.726	-0.928	0.147
y_{Aegir}	m	0.14	1.793	-1.596	0.296
$R_{z,Aegir}$	deg	-0.12	1.386	-1.343	0.245

Table D.11: Result load case 5.2a with τ = 0.3 s.

Variables	Unit	Mean	Max	Min	Std
x_{mp}	m	-0.17	50.644	-47.978	5.432
y_{mp}	m	0.14	49.574	-50.814	5.649
$t_{winch,x}$	kN	1693.84	482993.344	-510765.562	54577.080
$t_{winch,y}$	kN	-1450.37	516097.062	-506270.250	56742.942
x_{Aegir}	m	1507.49	6217.676	-2984.600	1394.307
y_{Aegir}	m	1257.14	4854.288	-585.581	1178.121
$R_{z,Aegir}$	deg	106991.13	328261.820	-3220.236	106841.568

Table D.12: Result load case 5.2a with τ = 0.4 s.

Variables	Unit	Mean	Max	Min	Std
x_{mp}	m	-0.00	0.057	-0.070	0.012
y_{mp}	m	0.00	0.071	-0.059	0.012
$t_{winch,x}$	kN	2.67	1462.573	-1496.239	269.026
$t_{winch,y}$	kN	-2.10	1525.623	-1499.334	271.242
x_{Aegir}	m	-0.02	0.178	-0.163	0.036
y_{Aegir}	m	0.04	0.400	-0.388	0.082
$R_{z,Aegir}$	deg	-0.03	0.326	-0.200	0.075

Table D.13: Result load case 5.2b with τ = 0.1 s.

Variables	Unit	Mean	Max	Min	Std
x_{mp}	m	-0.00	0.069	-0.080	0.014
y_{mp}	m	0.00	0.081	-0.072	0.014
$t_{winch,x}$	kN	3.14	1538.126	-1888.436	321.166
$t_{winch,y}$	kN	-2.26	1918.042	-1568.793	324.168
x_{Aegir}	m	-0.03	0.175	-0.170	0.036
y_{Aegir}	m	0.05	0.412	-0.379	0.081
$R_{z,Aegir}$	deg	-0.04	0.316	-0.205	0.074

Table D.14: Result load case 5.2b with τ = 0.2 s.

Variables	Unit	Mean	Max	Min	Std
x_{mp}	m	-0.00	0.095	-0.079	0.017
y_{mp}	m	0.00	0.080	-0.099	0.017
$t_{winch,x}$	kN	3.86	1538.964	-2625.378	435.172
$t_{winch,y}$	kN	-2.26	2653.030	-1564.141	438.025
x_{Aegir}	m	-0.03	0.173	-0.176	0.036
y_{Aegir}	m	0.05	0.424	-0.375	0.081
$R_{z,Aegir}$	deg	-0.04	0.311	-0.215	0.074

Table D.15: Result load case 5.2b with τ = 0.3 s.

Variables	Unit	Mean	Max	Min	Std
x_{mp}	m	46.93	51.000	-3.955	11.166
y_{mp}	m	-10.89	33.150	-15.515	3.211
$t_{winch,x}$	kN	-469293.51	140605.484	-829361.875	111723.897
$t_{winch,y}$	kN	108890.06	172931.484	-540368.750	36120.120
x_{Aegir}	m	-510220.90	1.528	-1074325.728	324022.936
y_{Aegir}	m	120545.69	258827.082	-75.973	80470.328
$R_{z,Aegir}$	deg	3593.50	7627.330	-1193.087	2724.184

Table D.16: Result load case 5.2b with τ = 0.4s.

Bibliography

[1] Wilson Ivan Guachamin Acero. *Assessment of marine opertions for offshore wind turbine installation with emphasis on response-based operational limits*. Number December. 2016. ISBN 9788232620128.

[2] P. Albers. *Motion control in offshore and dredging*. 2010. ISBN 9789048188024. doi: 10.1007/978-90-481-8803-1.

[3] Ampelmann. A-type Enhanced Performance - Ampelmann - Motion Compensated Gangway. URL https://www.ampelmann.nl/systems/a-type-enhanced-performance.

[4] L.G. Buitendijk. Floating installation of offshore wind turbine foundations, Van Oord. (December): 1–8, 2016.

[5] Olivier Cadet. Introduction to Kalman Filter and its use in Dynamic Positioning Systems. In *Proceedings of Dynamic Positioning …*, pages 1–33, 2003. URL http://www.dynamic-positioning.com/dp2003/design_cadet.pdf.

[6] Panagiotis K. Chaviaropoulos, Anand Natarajan, and Peter Hjuler Jensen. Key performance indicators and target values for multi-megawatt offshore turbines. *European Wind Energy Association Conference and Exhibition 2014, EWEA 2014*, (January), 2014.

[7] Claire Smith. Offshore piles on the straight and narrow - New Civil Engineer, 12 2013. URL https://www.newcivilengineer.com/archive/offshore-piles-on-the-straight-and-narrow-20-12-2013/.

[8] DNV (Det Norske Veritas). Design of Offshore Wind Turbine Structures; Offshore Standard. *Design of Offshore Wind Turbine Structures*, (January):214, 2013.

[9] EEW Group. Monopiles / XL Monopiles / Transition Pieces, 2016. URL http://www.eew-group.com/portfolio/structural-pipes/monopiles/.

[10] O.M. Faltinsen. *Sea Loads on Ships and Offshore Structures. Cambridge University Press*. 1993. ISBN 9780521458702. doi: 9780521458702. URL https://books.google.com/books?hl=zh-CN&lr=&id=qZq4Rs2DZXoC&oi=fnd&pg=PP9&dq=Faltinsen+O.+Sea+loads+on+ships+and+offshore+structures.+Cambridge+University+Press%3B+1993.&ots=68ptYooUoq&sig=8nXbglfkXm3KIXi1E7uUkOqlmMc.

[11] Forfatter Forfattersen and Erin Elizabeth Bachynski. *Design and Dynamic Analysis of Tension Leg Platform Wind Turbines (electronic version)*. 2014. ISBN 978-82-326-0096-0.

[12] Gene F Franklin, J David Powell, and Abbas Emami-Naeini. *Feedback Control of Dynamic Systems Seventh Edition*. 2015. ISBN 9781292068909. URL https://lccn.loc.gov/2017032553.

[13] F.W.B. Gerner, J. van der Tempel, R. Zoontjes, and H. de Groot. Motion Compensated Float-Over Installation with the Use of Ampelmann Systems. 2007. doi: 10.4043/18640-ms.

[14] Andrew R. Henderson. Offshore wind in Europe: The current state of the art. *Refocus*, 3(2):14–17, 2002. ISSN 14710846. doi: 10.1016/S1471-0846(02)80021-X.

[15] J.M.J Journée and W.W Massie. OFFSHORE HYDROMECHANICS (lecture notes). (January):1–558, 2008. URL http://www.shipmotions.nl/DUT/LectureNotes/OffshoreHydromechanics.pdf.

[16] A Kielkiewicz, A Marino, C Vlachos, F J L Maldonado, and I Lessis. The practicality and challenges of using XL monopiles for offshore wind turbine substructures, 2015. URL http://www.esru.strath.ac.uk/EandE/Web_sites/14-15/XL_Monopiles/index.html.

[17] Ivan Komusanac, Daniel Fraile, Guy Brindley, Colin Walsh, and Ivan Pineda. Wind energy in Europe in 2018. *Wind Europe*, 2019.

[18] G. Kovacs. Environmental conditions and environmental testing. *INTELEC, International Telecommunications Energy Conference (Proceedings)*, 2(October):92–99, 1993. ISSN 02750473. doi: 10.1109/INTLEC.1993.388591.

[19] Lin Li. *Dynamic Analysis of the Installation of Monopiles for Offshore Wind Turbines*. 2016. ISBN 9788232616169.

[20] Lin Li, Zhen Gao, and Torgeir Moan. Numerical simulations for installation of offshore wind turbine monopiles using floating vessels. In *Proceedings of the International Conference on Offshore Mechanics and Arctic Engineering - OMAE*, volume 8, pages 1–11, 2013. ISBN 9780791855423. doi: 10.1115/OMAE2013-11200.

[21] Lin Li, Zhen Gao, and Torgeir Moan. Response analysis of a nonstationary lowering operation for an offshore wind turbine monopile substructure. *Journal of Offshore Mechanics and Arctic Engineering*, 137(5), 2015. ISSN 1528896X. doi: 10.1115/1.4030871. URL https://asmedigitalcollection.asme.org/offshoremechanics/article-pdf/137/5/051902/6245621/omae_137_05_051902.pdf.

[22] Hatim Machrafi. *Green Energy and Technology*. 2012. ISBN 9781608054220. doi: 10.2174/97816080528511120101.

[23] Alan MacLeay. Monopile Installation on DP, 2019.

[24] Amir R. Nejad, Lin Li, Wilson Ivan Guachamin Acero, and Torgeir Moan. A systematic design approach of gripper's hydraulic system utilized in offshore wind turbine monopile installation. In *Proceedings of the International Conference on Offshore Mechanics and Arctic Engineering - OMAE*, volume 11A, pages 1–10, 2018. ISBN 9780791851326. doi: 10.1115/OMAE2018-77228.

[25] Orcina Ltd. *OrcaFlex Manual - Online Documentation*. 2020. URL https://www.orcina.com/webhelp/OrcaFlex/.

[26] R. H. Rogers. *Fluid Mechanics.* McGraw-Hill Education, 1978. ISBN 0710086814.

[27] DJC SALZMANN. *Development of the Access System for Offshore Wind Turbines*. PhD thesis, 2010. URL http://repository.tudelft.nl/assets/uuid:28576ef7-dee4-4ab4-a824-36f7b94ab21f/Cerda_2010_-_Ampelmann_PhD_thesis.pdf.

[28] Arunjyoti Sarkar and Ove T. Gudmestad. Study on a new method for installing a monopile and a fully integrated offshore wind turbine structure. *Marine Structures*, 33:160–187, 2013. ISSN 09518339. doi: 10.1016/j.marstruc.2013.06.001. URL http://dx.doi.org/10.1016/j.marstruc.2013.06.001.

[29] M. L.A. Segeren and K. W. Hermans. Experimental investigation of the dynamic installation of a slip joint connection between the monopile and tower of an offshore wind turbine. *Journal of Physics: Conference Series*, 524(1), 2014. ISSN 17426596. doi: 10.1088/1742-6596/524/1/012080.

[30] Robert H Stewart. Physical oceanography. *Deep Sea Research Part B. Oceanographic Literature Review*, 34(8):629–645, 1987. ISSN 01980254. doi: 10.1016/0198-0254(87)95466-5.

[31] A. Svendsen and Ivar G. Jonsson. *Hydrodynamics of Coastal Regions*. Den Private Ingeniorfond Technical University Denmark, 1982. ISBN 87-87245-57-4.

[32] The Nautical Institute. What Is Dynamic Instability ? URL https://web.archive.org/web/20130125101320/http://www.nautinst.org/en/dynamic-positioning/what-is-dynamic-positioning/index.cfm.

[33] TWD. Installation of Monopile Gripper Frame, 2014. URL https://twd.nl/installation-of-the-monopile-gripper-frame/.

[34] Martijn Wittingen. Offshore Wind Turbine Monopile Foun- dation Installation with a Dynamic Positioned Vessel. 2018.